



HAL
open science

Design of an Integrated Bioimpedance Measurement System for Chronic Monitoring of Biological Tissue Composition

Achraf Lamlih

► **To cite this version:**

Achraf Lamlih. Design of an Integrated Bioimpedance Measurement System for Chronic Monitoring of Biological Tissue Composition. Optics / Photonic. Université Montpellier, 2018. English. NNT : 2018MONT070 . tel-02138957

HAL Id: tel-02138957

<https://theses.hal.science/tel-02138957>

Submitted on 24 May 2019

HAL is a multi-disciplinary open access archive for the deposit and dissemination of scientific research documents, whether they are published or not. The documents may come from teaching and research institutions in France or abroad, or from public or private research centers.

L'archive ouverte pluridisciplinaire **HAL**, est destinée au dépôt et à la diffusion de documents scientifiques de niveau recherche, publiés ou non, émanant des établissements d'enseignement et de recherche français ou étrangers, des laboratoires publics ou privés.

**THÈSE POUR OBTENIR LE GRADE DE DOCTEUR
DE L'UNIVERSITE DE MONTPELLIER**

En Systèmes Automatiques et Microélectroniques (SYAM)

École doctorale : Information, Structures, Systèmes

Unité de recherche : LIRMM

**Conception d'un système intégré de mesure de
bioimpédance pour le suivi long terme de la composition
des tissus biologiques**

Présentée par Achraf LAMLIH.

Le 26-11-2018

Sous la direction de Serge Bernard

Devant le jury composé de

BRAGOS Ramon, Associate Professor , UPC Barcelona
ROMAIN Olivier, Professeur, Université de Cergy - ETIS
YUFERA GARCIA Alberto, Professor, Universidad de Sevilla - IMSE-CNM
BERNARD Serge, Directeur de Recherche, LIRMM - CNRS
KERZERHO Vincent, Chargé de Recherche, LIRMM - CNRS
ROUYER Tristan, Chercheur, MARBEC - IFREMER
RENOVELL Michel, Directeur de Recherche, CNRS-LIRMM
SOULIER Fabien, Maître de Conférences, LIRMM - UM
BONHOMMEAU Sylvain, Chercheur, IFREMER - DOI

Rapporteur
Président du jury/Rapporteur
Examineur
Directeur
Co-encadrant
Co-encadrant
Invité
Invité
Invité



**UNIVERSITÉ
DE MONTPELLIER**

UNIVERSITY OF MONTPELLIER

DOCTORAL THESIS

Design of an Integrated
Bioimpedance Measurement
System for Chronic Monitoring of
Biological Tissue Composition

Author:

Achraf LAMLIH

Supervisors:

Serge BERNARD

Vincent KERZÉHO

Fabien SOULIER

Tristan ROUYER

Sylvain BONHOMMEAU

*A thesis submitted in fulfillment of the requirements
for the degree of Doctor of Philosophy*

in the

SYAM - I2S

LIRMM - IFREMER

“The most exciting phrase to hear in science, the one that heralds the most discoveries, is not ‘Eureka!’ but ‘That’s funny. . . ’ ”

Isaac Asimov

Acknowledgements

I would like to take this opportunity to thank all those who have contributed to the achievement of this work. In particular I would like to express my gratitude to the following persons.

Special mention goes to my enthusiastic supervisor, Serge Bernard. My PhD has been an amazing experience and I thank Serge wholeheartedly, not only for his tremendous academic support and thought-provoking ideas but also for giving me so many wonderful opportunities. Similar, profound gratitude goes to Vincent Kerzérho and Fabien Soulier, who have been truly dedicated to their role as my secondary supervisors. I am particularly indebted to Vincent and Fabien for their passionate participation and their invaluable guidance and advises in our weekly meetings. I am also hugely appreciative to Tristan Rouyer and Sylvain Bonhommeau, especially for sharing their expertise in fisheries science and marine ecology so willingly. Their insightful comments improved the quality of the manuscript and other publications.

I would like to thank Prof. Ramon Bragos, Prof. Olivier Romain and Prof. Alberto Yufera Garcia, for being my thesis examiners and for their constructive criticism and invaluable suggestions that have improved this thesis.

Special thanks goes to Philippe Freitas. The integrated circuit prototype would not have been sent to fabrication without his expertise and tremendous efforts. I thank Philippe not only for that, but also for his ever-present sense of humour. I would also like to extend my thanks to Stéphane David-Grignot for generously sharing his expertise in signal processing. Without his contributions, the study on sine wave harmonic cancellation would not have been so elaborated. Besides, I thank Stéphane for all the stimulating conversations we had about blockchain. Special mention goes to Moez Belhadj, his efforts and expertise in flexible electrodes development were crucial for the specification of the integrated circuit architecture. My thanks go also to Jérémie Salles, who so generously assisted in the design and layout of the circuit. I also wish to thank Mohan Julien, for all the stimulating late night discussions and brain-storming sessions we had in the lab which helped solve various problems. Guys, I have learned a lot working with you. I would also like to express my sincere gratitude to Michel Renovell who reviewed my work multiple times. I am gratefully indebted to Michel not only for his very valuable comments on my presentations and this thesis manuscript, but also for all the book recommendations and the interesting conversations we had about history, economy and religions.

For all the team, it will be difficult to forget all the meals, coffee breaks, and interesting conversations we have shared. For making this years memorable, from the bottom of my heart I say thank you.

Achraf

Contents

Acknowledgements	3
Abstract	17
Résumé	19
1 Thesis Introduction : Context and Objectives	25
1.1 Research Project Background: case study	26
1.2 Research goals and methodology	27
1.3 Thesis content and outline	30
2 Biological Tissue Composition assessment	31
2.1 Introduction	31
2.2 Tissue composition analysis techniques	32
2.2.1 Introduction	32
2.2.2 Micro-wave propagation	32
2.2.3 Near Infrared Spectroscopy	34
2.2.4 Ultrasound	35
2.2.5 Bioimpedance Spectroscopy	37
2.2.6 Comparative status	38
2.3 Bioimpedance spectroscopy : From electrical properties of tissue to its electrical impedance	40
2.3.1 Introduction	40
2.3.2 Cell electrical properties	40
2.3.3 Cell electrical model	41
2.3.4 Dispersion regions	44
2.3.5 Single frequency vs spectroscopy analysis	46
2.3.6 Biological vs. bioimpedance correlation approaches	46
2.4 Conclusion	48
3 Design challenges	49
3.1 Introduction	49
3.1.1 Methodology	49
3.1.2 Research questions	50
3.1.3 Chapter content	51
3.2 Experimentation resources	51
3.2.1 Electrodes	52
3.2.2 The handheld AD5933 measurement system	52
3.2.3 The MFIA impedance analyzer	54
3.3 Frequency range	54

3.4	Current vs voltage stimulation	56
3.4.1	Voltage excitation system	56
3.4.2	Current excitation system	57
3.5	Electrode configuration	57
3.6	Electrode-tissue impedance range	59
3.7	Non-linearity investigation	60
3.7.1	Motivation	60
3.7.2	Experiments	60
3.7.3	Results and conclusion	62
3.8	Measurement environment related errors	63
3.9	Summary of system specifications	66
4	Architecture definition	69
4.1	Introduction	69
4.1.1	Methodology and research questions	69
4.2	Specifications impact on the architecture	70
4.3	Design constraints	70
4.3.1	Constraints	70
4.4	State of the art of BIS architectures	73
4.4.1	Frequency sweep excitation architectures	74
4.4.2	Wideband simultaneous excitation architectures	75
4.5	Proposed hybrid architecture	76
4.5.1	Wideband simultaneous excitation	76
4.5.2	Frequency sweep excitation	77
4.5.3	Hybrid architecture	78
4.6	Design status of the integrated bioimpedance measurement system	80
4.7	Conclusion	82
5	Stimuli generation	83
5.1	Introduction	83
5.2	Sine-wave construction	84
5.2.1	Introduction	84
5.2.2	Basic principle and constraints of harmonic cancellation techniques	86
5.2.3	Fixed phase-shifts and adjustable amplitudes of square-waves	86
5.2.4	Fixed amplitudes and adjustable phase-shifts of square-waves	88
5.2.5	Adjustable amplitudes and adjustable phase-shifts of square-waves	91
5.2.6	Conclusion on harmonic cancellation techniques	92
5.2.7	Hardware implementation	93
5.2.8	Robustness study	96
5.2.9	Conclusion	99
5.3	Composite signal generation	100
5.3.1	Introduction	100
5.3.2	Signal quality metrics and comparison setup	102
5.3.3	Multitone excitation techniques comparison	103

5.3.4	Proposed multitone excitation technique	107
5.3.5	Conclusion	113
5.4	Chapter conclusion	116
6	Current driver for BioImpedance Spectroscopy	119
6.1	Introduction	119
6.2	Design constraints of current drivers for BIS	120
6.3	State of the art of current drivers for BIS	122
6.4	Optimization of the Current driver's architecture	123
6.4.1	Proposed architecture	123
6.4.2	Output impedance increasing	126
6.4.3	Maximization of the output voltage swing	129
6.5	Simulation Results	130
6.5.1	Output impedance	131
6.5.2	Output voltage swing	133
6.5.3	Comparison table with existing architectures	133
6.6	Conclusion	136
	Conclusion and perspectives	137
	Bibliography	141

List of Figures

1	Principe de fonctionnement d'un système de marque pour poisson	20
2	Processus biologiques non-qualifiés des poissons dans leur milieu sauvage	21
1.1	Operating principle of electronic tags for large pelagic fish . . .	26
1.2	Unqualified fish biological processes in the wild	27
1.3	Scope of the thesis research work	28
2.1	Design of the portable device propagating microwaves, reproduced from (Kent, 1990)	33
2.2	Correlation between total body water and the fat rate for Atlantic herring (Kent, 1990)	33
2.3	Photo-electric conversion circuit	35
2.4	An ultrasound probe components, reproduced from (<i>Basix principle of medical ultrasonic probes</i>)	36
2.5	Bioimpedance analysis operating principle	38
2.6	Cell components	41
2.7	Bilayer lipid membrane	41
2.8	Fricke's Electrical Equivalent Model	42
2.9	Low frequency current path	43
2.10	high frequency current path	43
2.11	Dispersions of biological tissue (Schwan, 1957)	44
3.1	Methodology	50
3.2	First generation of electrodes	52
3.3	flexible Electrodes	53
3.4	AD5933 Hand-held bioimpedance measurement system	53
3.5	AD5933 system function blocks diagram	54
3.6	The MFIA impedance analyzer	54
3.7	Structure of a : (a) current excitation system (b) voltage excitation system	56
3.8	2-electrode configuration	58
3.9	4-electrodes configuration	58
3.10	4-electrode measurements on bluefin tuna using the MFIA impedance analyzer	59
3.11	2-electrode measurements on bluefin tuna using the MFIA impedance analyzer	60
3.12	Experimentation setup	61
3.13	modified portable BIA device schematic	61
3.14	Data processing algorithm	62
3.15	Frequency content of the response signals at 10KHz	63

3.16	BIS and EMG electrodes implanted on the gilt-head bream . . .	64
3.17	Bioimpedance module of a gilt-head bream during different swimming speeds	65
3.18	Bioimpedance phase of sea bream during different swimming speeds	65
4.1	Constraints summary for each BIS measurement approach . . .	73
4.2	Wideband simultaneous excitation bioimpedance spectroscopy architecture	77
4.3	Frequency sweep bioimpedance spectroscopy architecture	77
4.4	Hybrid bioimpedance spectroscopy architecture	79
4.5	Layout of the first generation integrated circuit measurement system	81
5.1	Excitation signal generation block	83
5.2	Sine wave construction block	84
5.3	Symmetry of sine-wave signal generated by summing square-wave signals	87
5.4	Sine-wave signal generated using square-wave signals with various amplitudes for five signals ($M = 5$)	88
5.5	Spectrum of sine-wave signal generated using square-wave signals with various amplitudes for five signals ($M = 5$)	89
5.6	Sine-wave signal generated using square-wave signals with various phase shifts for six signals $M = 6$ with $[\varphi_1; \varphi_2; \varphi_3] = [0.2037; 0.4701; 0.9784]rad$	90
5.7	Spectrum of sine-wave signal generated using square-wave signals with various phase shifts for six signals $M = 6$	91
5.8	THD ratio variations due to varying phase-shift error Monte-Carlo results for a sine-wave signal generated using square-wave signals with various phase shifts for six signals $M = 6$	92
5.9	Comparison of harmonic cancellation techniques	93
5.10	THD of a sine-wave generated using square-wave signals with approximated amplitudes with fraction with denominator d . . .	94
5.11	SFDR of a sine-wave generated using square-wave signals with approximated amplitudes with iteration on continued fraction .	95
5.12	THD up to harmonic 11 of a sine-wave generated using square-wave signals with approximated amplitudes with n iterations on continued fractions	96
5.13	SFDR of a sine-wave generated using square-wave signals with approximated amplitudes with n iterations on continued fractions	97
5.14	Spectrum of a sine-wave signal affected by amplitude error and/or jitter on the square-wave signals for sine-wave signal generated using square-wave signals with various amplitudes five signals $M = 5$	98
5.15	Total Harmonic distortion ratio of a sine-wave generated using square-wave signals with various amplitudes deviations and affected by various level of jitter	99
5.16	Multitone excitation signal generation block	100
5.17	Bioimpedance magnitude of bluefin tuna using the MFIA impedance analyzer and the flexible electrodes (4-electrode measurements) .	101

5.18	Square-wave signal in time and frequency domain	104
5.19	Linear feedback shift register based pseudo random generation .	105
5.20	Frequency components of the BMS excitation technique	106
5.21	Frequency components of the BMS excitation technique after filtering	107
5.22	Functional diagram of a sigma delta modulator	108
5.23	Frequency components of a classic sigma delta based multitone excitation	110
5.24	Customized loop filter bode diagram	112
5.25	Nyquist diagram of the customized transfer function	113
5.26	Signal transfer function of the proposed excitation	114
5.27	Noise transfer function of the proposed excitation	114
5.28	Frequency components of the proposed excitation	115
5.29	Frequency components of the proposed excitation after filtering	116
6.1	Current driver position in the integrated circuit architecture . .	119
6.2	current source model	121
6.3	Output impedance vs load impedance illustration	121
6.4	Saturation voltage illustration	122
6.5	OTA architectures : (a) Simple OTA (b) Telescopic OTA (c) Miller OTA (d) Symmetrical OTA (e) Folded cascode OTA . . .	123
6.6	Current driver architecture	126
6.7	Current mirror structures: (a) Simple current mirror(b) cascode (c) high swing cascode (d) gain boosted cascode (e) regulated cascode	127
6.8	Improved regulated cascode architecture	128
6.9	Layout of the current drive	130
6.10	Current driver bandwidth	131
6.11	Output impedance of the current driver	131
6.12	Improved regulated cascode (NMOS) stability check	132
6.13	Impedance magnitude of the electrode-tissue-interface of bluefin tuna in a 2 electrodes configuration	133
6.14	Output current vs output voltage characteristic of the high swing cascode, the regulated cascode and the improved regulated cascode for an input current of 300 μ A	134
6.15	monte carlo simulation of the DC output level	134

List of Tables

2.1	Optical parameters of muscle and fat tissue, reproduced from (Song et al., 2009)	34
2.2	Comparative status on the studied techniques	39
5.1	local SNR's for the binary multi-frequency excitation	107
5.2	local SNR's for a classic sigma delta excitation	110
5.3	local SNR's for the proposed excitation	113
6.1	Comparison of amplifier architectures	124
6.2	Current mirror performances comparison	128
6.3	Results comparison with existing architectures	135

*To my family,
for their patience and their faith*

Abstract

Biologging consists in attaching data-recording devices to animals to collect data on their environment and infer information about their biology and ecology. In the last decades, advances in science and engineering, especially in microelectronics, biotechnology, and materials have fueled the development of sophisticated devices, which resulted in smaller species being tagged for longer periods and in different types of environment (terrestrial, aquatic or aerial). This allowed researchers to address a diverse panel of scientific questions related to the behavior and ecology of wild species. Current technology provides a description of the physical environment of animals, but no device allows to describe their physiological aspects over relevant time scales. Therefore, physiological parameters tracking is on the rise as it offers extremely valuable information to answer key questions such as the response of individuals to climate change. The miniaturization of silicon electronics has benefited the development of implantable devices that opened up new opportunities for the long-term monitoring of physiological states. In that respect, a promising line of research is to use tissue composition to infer information on physiological states of animals.

The ultimate goal of this research work is to design an integrated measurement system capable of assessing biological tissue composition. This research work intends to be an exploratory work aiming to bring to the scientific community tools that are capable of measuring changes in a wide range of physiological processes. Thus, this measurement system will be adjustable to a large scope of physiological variables and long-term monitoring applications. The research work presented in this thesis is part of the POP-up Satellite Tag for Advancing Research in marine ecology (POPSTAR) project which aims at developing a new generation of tagging devices for fish. The main goal of the project is to enhance our understanding of fish behavior by linking the analysis of the environment in which the fish travels and lives to its physiological states. the POPSTAR project will be used to validate research hypotheses and narrow down the specifications of the integrated measurement system.

After comparing several tissue composition techniques, bioimpedance spectroscopy has been chosen as the technique to be used for the design of the integrated measurement system. Since the electrical impedance of the biological tissue is a function of physiological processes, variations in the composition of the biological tissue are expected to change its electrical properties, which by extension can be seen as variations of the electrical impedance of the tissue.

After defining bioimpedance spectroscopy as the technique to be used, we have identified the design challenges of such measurement system by using an in-depth literature review of the existing bioimpedance measurement systems as well as the bioimpedance theoretical concepts. Because design challenges are very application dependent, we also took into account the constraints related

to the measurement environment and configuration. Given that the majority of bioimpedance measurements on fishes that can be found in the literature use single frequency, we have conducted several bioimpedance spectroscopy experiments on fish species such as bluefin tuna, sea bass, sardine or sea bass in order to assess the missing parameters. Following this methodology we have been able to narrow down as much as possible the integrated circuit specifications, which layed the foundation of the integrated circuit design guidelines.

The integrated circuit design guidelines being defined, we have demonstrated that the constraints ruling the design of the measurement system could be categorized depending on the frequency band of excitation. In order to break the trade-off between short measurement durations and precision, we have decided to use a wideband simultaneous excitation approach for the low and the nominal frequency bands, and a frequency sweep excitation for the high frequency band. A hybrid architecture providing fast measurements while maximizing precision has therefore been proposed. It has been defined for the POPSTAR project as a special research context, and for biological tissue electrical properties exploration over a wide frequency range as a general research context.

As the excitation signal generation blocks are critical and their performances affect the whole architecture performances, the second part of this research focuses on the design and optimization of the signal generation part of the architecture which is composed of stimuli generation blocks and a current driver that transforms the voltage stimuli to an excitation current. In the stimuli generation part of the architecture, two stimuli generators have been designed, one for frequency sweep excitation and one for wideband simultaneous excitation. For the frequency sweep excitation, we compared on-chip sine wave construction techniques. This techniques are used to generate sine-wave signals by summing digital signals in order to cancel low-order harmonics. We first compared several approaches and analytically proven that for a given number of square-wave generators, an approach allows to cancel a higher number of harmonics compared to the others. The sine-wave constructor implementation that suits our research context has been discussed. For the wideband simultaneous excitation, several techniques have been compared, and key parameters defining their performances presented. A novel multitone generation technique based on a delta sigma modulator has thus been proposed. Finally, a simple implementation of the multitone generator has been presented.

These two signal generation approaches have a common block, which is the current driver of the architecture. The current driver transforms the voltage optimized stimuli to a proportional current signal. A current driver architecture optimized for bioimpedance measurements has been proposed. It uses an improved regulated cascode to enhance the output impedance, enabling accurate measurements of transfer impedances at low and high frequencies. The current driver uses a common-mode feedback compensation technique capable of accurately setting the output common mode voltage independently of process variations. The proposed architecture therefore offers a high output swing for a given supply voltage. A first prototype chip containing the critical blocks of the architecture has been successfully designed and simulated in a 0.18 μm AMS (Austria MicroSystems) CMOS process operating at 1.8 V power supply.

Résumé

Le biologging consiste à attacher des dispositifs à des animaux dans le but d'enregistrer des données liées à leur état biologique ou à leur environnement. Au cours des dernières décennies, les progrès de la science et de l'ingénierie en microélectronique, en biotechnologie et en science des matériaux, ont aidé au développement de dispositifs évolués, ce qui a permis de marquer des espèces de petite taille pour des périodes de plus en plus longues dans des environnements différents (terrestre, marin ou aérien). Cette évolution a donné aux chercheurs les outils nécessaires pour traiter un large panel de questions scientifiques liées au comportement et à l'écologie d'espèces sauvages.

Le suivi de paramètres physiologiques est de plus en plus utilisé car il permet d'obtenir des informations extrêmement utiles sur les espèces en question. La miniaturisation de l'électronique intégrée a favorisé le développement de dispositifs implantables qui ont ouvert de nouvelles opportunités pour le suivi à long terme de l'état physiologique de plusieurs espèces. L'un des indicateurs physiologiques les plus intéressants à suivre est la composition des tissus. Les techniques d'évaluation de la composition des tissus biologiques permettent de mieux comprendre les processus physiologiques et leur impact global sur l'état biologique des sujets expérimentaux.

Les techniques d'évaluation de la composition tissulaire varient en précision mais aussi en types de tissus qu'ils sont capables de mesurer. Historiquement, ces techniques étaient difficiles à intégrer. Des techniques telles que l'absorptiométrie à rayons X à double énergie (DEXA), la résonance magnétique nucléaire (RMN) ou la conductivité électrique totale du corps offrent des performances élevées, mais nécessitent des équipements de grande taille qui les rendent impropres à des mesures *in vivo*. Grâce aux améliorations technologiques continues, de plus en plus de travaux de recherche visent à fournir à la communauté scientifique des outils et des techniques hautement intégrés qui répondent au besoin de suivi continu des paramètres physiologiques.

Le but principal de ce travail de recherche est de concevoir un système de mesure intégré capable d'évaluer la composition des tissus biologiques. Ce travail de recherche se veut être un travail exploratoire visant à apporter à la communauté scientifique des outils capables de mesurer un large éventail de biomarqueurs. Ainsi, ce système de mesure pourra être adapté à une large gamme d'applications de suivi à long terme de variables physiologiques. Néanmoins, les travaux de recherche présentés dans cette thèse font partie du projet POPSTAR, qui vise à développer une génération innovante de systèmes de marquage de poissons. L'objectif principal du projet est d'améliorer notre compréhension du comportement des poissons en analysant non seulement l'environnement dans lequel les poissons se déplacent et vivent, mais aussi les poissons eux-mêmes.

Le projet POPSTAR servira de cas d'étude afin de valider des hypothèses scientifiques et d'affiner les spécifications du système de mesure intégré.

Les systèmes de biologging disponibles dans le commerce aujourd'hui pour tagger des poissons utilisent des circuits électroniques pour enregistrer des paramètres environnementaux tels que la lumière, la température ou la pression. Après une durée préétablie, le système est libéré du poisson et émerge à la surface de l'eau grâce à une flottabilité légèrement positive. Les données enregistrées sont ensuite transmises à un satellite et récupérées pour être analysées (voir figure 1.1).

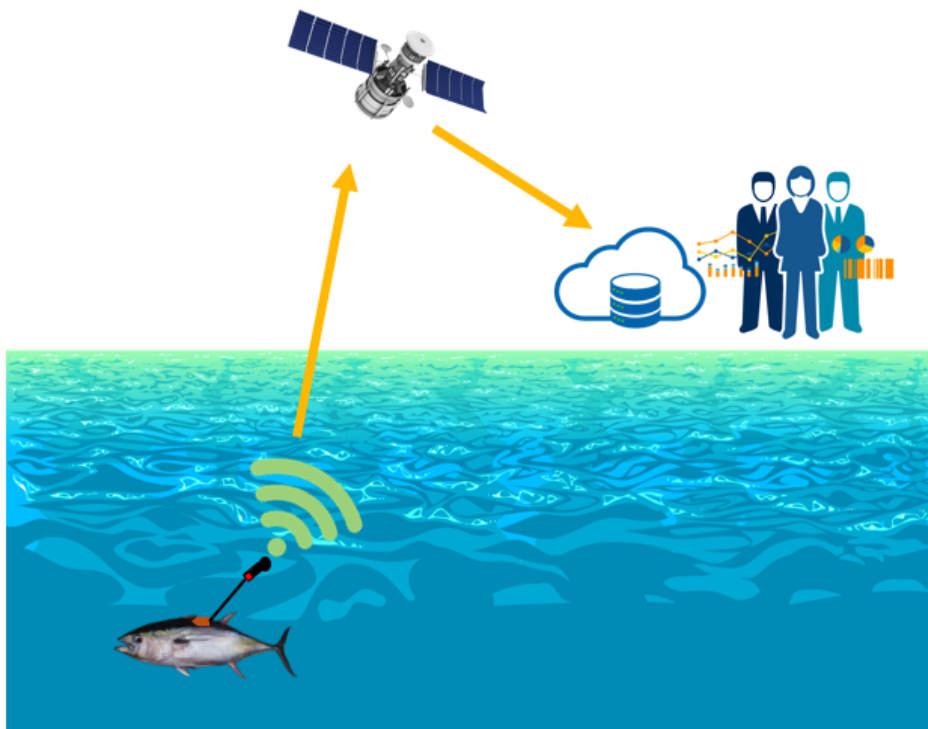


FIGURE 1: Principe de fonctionnement d'un système de marquage pour poisson

Bien que ces systèmes de marquage aient permis de mieux comprendre l'environnement dans lequel évoluent les poissons, ils ne fournissent pas d'informations sur les poissons eux-mêmes. Par conséquent, les informations scientifiques nécessaires pour conserver et gérer efficacement le poisson font actuellement défaut. Une des solutions possibles pour améliorer notre compréhension des espèces marines consiste à utiliser des capteurs implantables pour surveiller les paramètres physiologiques liés aux principaux processus biologiques tels que l'alimentation et le frai. En effet, de tels processus offrent des informations significatives sur une foule de paramètres démographiques clés tels que la croissance, la survie ou la reproduction (voir figure 1.2). Par exemple, un paramètre physiologique clé est la teneur en graisse musculaire. La variation de ce paramètre dans l'espace et le temps est en effet liée aux processus mentionnés précédemment, tels que l'alimentation, qui peut se traduire en une accumulation des

réserves en gras, ou la reproduction pendant laquelle le poisson va puiser dans ses réserves de gras.

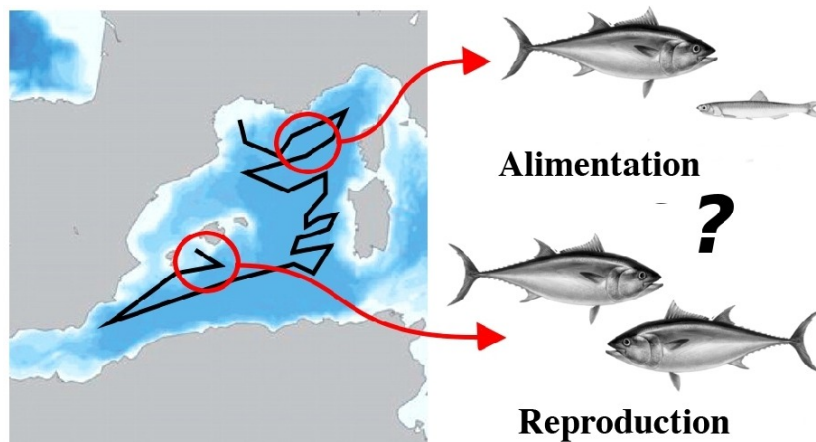


FIGURE 2: Processus biologiques non-qualifiés des poissons dans leur milieu sauvage

Suivre l'état physiologique des poissons dans leur environnement naturel est une première mondiale. Il va donc de soi que nous n'avons pas d'informations précises sur la pertinence d'un paramètre biologique en particulier. Partant de ce constat, les travaux de recherche présentés dans cette thèse visent à concevoir un système de mesure intégré capable d'explorer un large éventail de variables physiologiques. L'objectif est de fournir à la communauté scientifique un outil de suivi continu fournissant des informations sur l'état physiologique des espèces sauvages dans leur environnement naturel.

Après avoir comparé plusieurs techniques d'estimation de la composition tissulaire, la spectroscopie de bioimpédance a été choisie comme technique à utiliser pour la conception du système de mesure intégré. Étant donné que l'impédance électrique du tissu biologique est fonction des processus physiologiques, les modifications de la composition du tissu biologique se traduisent en une modification de ses propriétés électriques, ce qui par extension, se traduit en une variation de l'impédance électrique du tissu.

Concevoir un système de mesure intégré capable de mesurer une large gamme de biomarqueurs sur de longues périodes est un défi majeur. En effet, en adaptant le système pour explorer un large éventail de variables physiologiques, la conception d'un tel système devient rapidement régie par de fortes contraintes telles que la bande passante, la précision, le temps de mesure ou la sûreté de fonctionnement. Le choix entre différentes architectures de système potentielles devient une tâche difficile. En outre, certains blocs d'architecture sont critiques et il convient de veiller à optimiser leur conception.

Après avoir défini la spectroscopie de bioimpédance comme la technique à utiliser, nous avons identifié les défis de conception d'un tel système de mesure intégré en utilisant une analyse bibliographique approfondie des systèmes de mesure de bioimpédance existants ainsi que des concepts théoriques de bioimpédance. Les défis de conception étant dépendant des applications, nous avons également pris en compte les contraintes liées à l'environnement de mesure et à la configuration. Étant donné que la majorité des mesures de bioimpédance sur

les poissons que l'on peut trouver dans la littérature utilisent une mesure mono-fréquence (à 50 kHz, nous avons mené plusieurs expériences de spectroscopie de bioimpédance sur des espèces de poissons telles que le thon rouge, le bar, la sardine ou le bar. En suivant cette méthodologie, nous avons pu affiner autant que possible les spécifications du circuit intégré, ce qui a permis de définir les lignes directrices de conception du circuit de mesure.

Les lignes directrices pour la conception du circuit intégré étant définies, nous avons démontré que les contraintes régissant la conception du système de mesure pouvaient être classées en fonction de la bande de fréquence de l'excitation. Afin de rompre le compromis entre une durée de mesure courte et la précision de mesure, nous avons décidé d'utiliser une approche d'excitation simultanée à large bande pour les bandes de fréquences basses et nominales et une excitation en balayage de fréquences pour la bande haute fréquence. Une architecture hybride permettant des mesures rapides tout en maximisant la précision a donc été proposée. Cette architecture a été défini pour le projet POPSTAR comme contexte de recherche particulier et pour l'exploration des propriétés électriques des tissus biologiques sur une large gamme de fréquences en tant que contexte de recherche général.

Les blocs de génération du signal d'excitation de l'architecture proposée sont critiques car leurs performances affectent les performances de l'ensemble de l'architecture. L'accent a ainsi été mis sur la conception et l'optimisation de ces blocs. De l'optimisation de la création des stimuli à l'aide de techniques de traitement du signal numérique à l'amélioration des performances de la source de courant pour laquelle nous avons proposé une nouvelle architecture analogique.

Pour la partie génération de stimuli de l'architecture, deux générateurs de stimuli ont été conçus, le premier sert à injecter dans le tissu biologique un signal sinusoïdal mono-fréquentiel, le deuxième générateur permet l'excitation du tissu biologique avec un signal multi-fréquentiel.

Pour la génération mono-fréquentielle, nous avons comparé les techniques de construction sur puce intégrée d'un signal sinusoïdal. Ces techniques sont utilisées pour générer des signaux sinusoïdaux en sommant des signaux numériques afin d'annuler les harmoniques de faible ordre.

Plusieurs approches sont possibles. Dans cette partie nous avons d'abord comparé les différentes approches possibles. Ensuite, nous avons prouvé de manière analytique que pour un nombre donné de signaux carrés, une approche en particulier permet d'annuler un nombre plus élevé d'harmoniques par rapport aux autres. Finalement, l'implémentation du générateur sinusoïdal qui convient à notre contexte de recherche a été discutée.

Pour l'excitation multi-fréquentielle, les techniques de génération d'un signal composite ont été comparées et les paramètres clés définissant leurs performances ont été présentés. Une nouvelle technique de génération d'un signal multi-fréquentiel basée sur un modulateur delta sigma a été proposée. Enfin, une implémentation simple de ce générateur a été présentée.

La source de courant est l'un des blocs les plus critiques de l'architecture. Ce bloc étant commun aux deux approches de mesure, il doit opérer sur une large gamme de fréquence (de 8 Hz à 8 MHz).

Les paramètres clés définissant ses performances ont d'abord été énumérés et discutés. Un de ces paramètres clé d'une source de courant est l'impédance de sortie. L'impédance de sortie détermine non seulement la plage de fréquence de fonctionnement mais également la plage d'impédance de charge pour laquelle la source de courant est capable de maintenir un courant de sortie constant. Un autre paramètre clé est l'amplitude maximale de la tension de sortie, qui détermine la plage d'impédance de charge dans laquelle la source de courant est capable de maintenir ses performances de linéarité. Ce paramètre est d'autant plus critique quand la tension d'alimentation est basse et l'amplitude de courant de sortie élevée (nécessaire pour faciliter l'analyse de la réponse). Partant de ce constat, nous avons cherché à optimiser l'architecture en fonction de ces contraintes majeures.

Différentes architectures de sources de courant pour la spectroscopie de bioimpédance ont donc été comparées, et finalement une nouvelle architecture analogique présentant des performances supérieures par rapport à l'état de l'art a été présentée. Une puce contenant les blocs critiques de l'architecture a été conçue et simulée avec succès avec un process CMOS AMS (Austria MicroSystems) 0.18 μm fonctionnant sous une alimentation de 1,8 V.

Chapter 1

Thesis Introduction : Context and Objectives

Biologging consists in attaching data-recording devices to animals to collect data on their environment and infer information about their biology and ecology. Biologging found its beginnings in the marine environment. In fact, this technique has first been introduced by Pers Scholander who had the idea of attaching a capillary depth gauge onto a freshly harpooned whale in the objective of studying the maximum immersion depth of the cetacean (Ropert-Coudert et al., 2010).

In the last decades, advances in science and engineering, especially in microelectronics, biotechnology, and materials have fueled the development of sophisticated devices, which resulted in smaller and smaller species being tagged for longer periods and in different types of environment (terrestrial, aquatic or aerial), thus allowing researchers to address a diverse panel of scientific questions related to the behavior and ecology of wild species.

In the process of widening our understanding of wild species, physiological parameters tracking is on the rise as it offers extremely valuable informations. The mass adoption of consumer electronics as well as the rise of open source software and hardware in the past decade have permitted the development of cheap and miniaturized sensors. The miniaturization of silicon electronics has benefited the development of implantable devices which opens up new opportunities for physiological states long-term monitoring. One of the most interesting physiological indicators is tissue composition. Tissue composition assessment techniques are used to help better comprehend physiological processes and their overall impact on the biological state of the experiments subjects.

The tissue composition assessment techniques vary in precision and in the target tissue of interest. Historically, these techniques were difficult to integrate. Techniques such as Dual-energy X-ray absorptiometry, Nuclear Magnetic Resonance (NMR) or Total Body Electrical Conductivity, offer high performances but need large size equipments which make them unsuitable for in-vivo measurements. Thanks to continuous technology improvements more and more research studies are aiming to provide the scientific community with highly integrated tools and techniques that satisfies the need for continuous monitoring of physiological parameters.

From this perspective, the research work presented in this thesis intents to design an integrated measurement system capable of exploring a wide range of physiological variables. The goal is to provide the scientific community with a

continuous monitoring tool that provides valuable informations related to the physiological state of wild species in their natural environment.

1.1 Research Project Background: case study

The research work presented in this thesis has been equally funded by the LabEx NUMEV and IFREMER. LabEx NUMEV is an Excellence Laboratory created in 2011 in the framework of the French Program of Investments to the Future. NUMEV seeks to harmonize hard and computational sciences approaches with life sciences and pave the way for emerging interdisciplinary groups with an international profile.

IFREMER has a research project named POP-up Satellite Tag for Advancing Research in marine ecology (POPSTAR), which is the result of a close collaboration between several research units from IFREMER and LIRMM. In particular, this PhD project has been funded and yearly evaluated by IFREMER and LabEx NUMEV.

POPSTAR aims at developing an innovative generation of electronic tags for large pelagic fish (e.g. tunas and billfishes). The main goal of the project is to improve our understanding of fish behavior through the joint analysis of the evolution of its physical environment and physiological state.

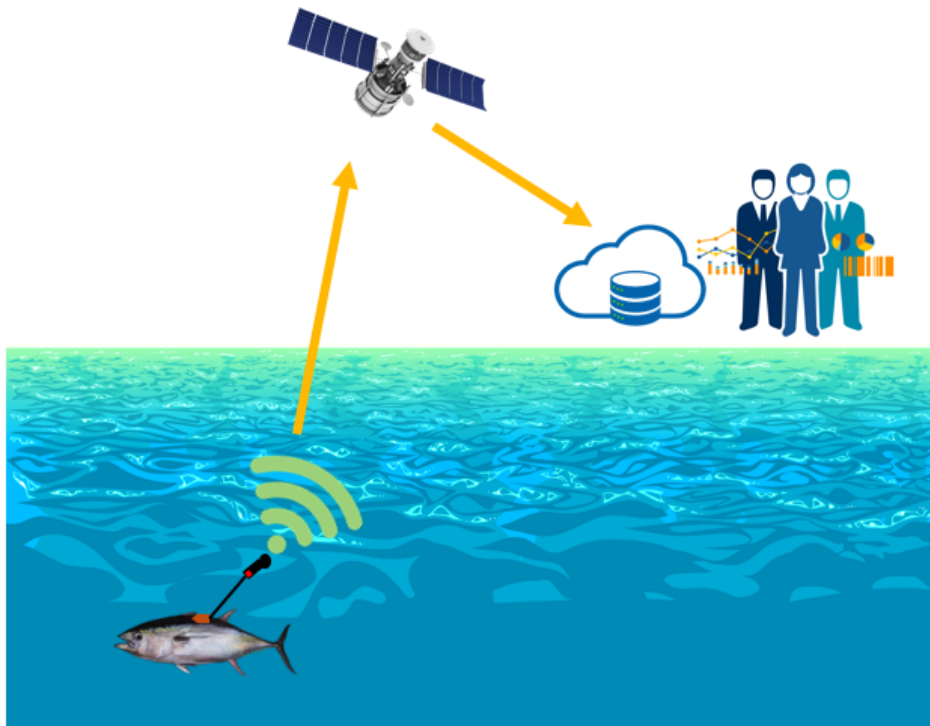


FIGURE 1.1: Operating principle of electronic tags for large pelagic fish

Electronic tags currently available on the market use electronic circuits to record environmental parameters, typically light, temperature and pressure.

The tag is programmed to be released after a given duration and floats up to the surface thanks to its slightly positive buoyancy. The recorded data are then transmitted through the ARGOS system, and retrieved in order to be analyzed (see figure 1.1).

Although these electronic tags have allowed a better understanding about the environment in which large pelagics evolve, they generally do not provide any information about their physiological state across time scales consistent with their large geographical movements. Thus, key scientific information to conserve and manage fish efficiently is currently lacking. A way to improve our understanding of marine species is to use implantable sensors for monitoring physiological parameters related to key biological processes such as feeding and spawning. Indeed, such processes offer significant insights into a host of key population parameters such as growth, survival, and reproduction. One key physiological parameter is muscle fat content. The variation of this parameter in space and time can indeed be related to the previously mentioned processes as fish feed to accumulate reserves, which are then used during reproduction (see figure 1.2).

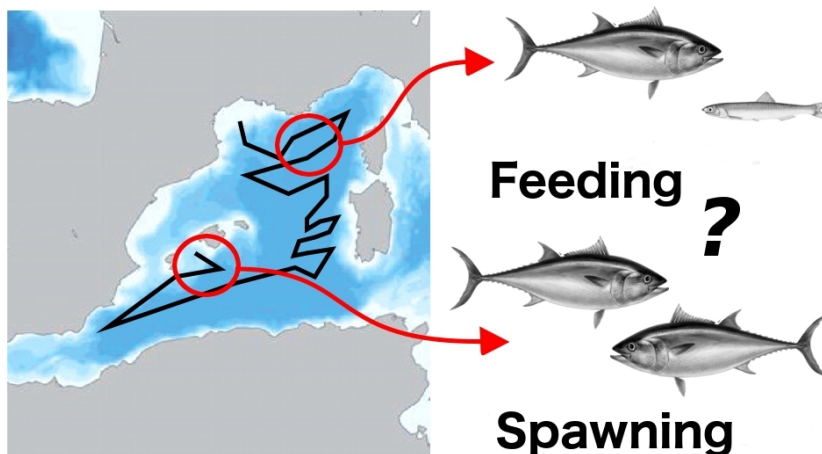


FIGURE 1.2: Unqualified fish biological processes in the wild

POPSTAR is a multi-disciplinary project that brings several improvements to existing tag technology. It intends to decrease the size and cost of currently available tags on the market. It also aims at improving the transmission system efficiency. However, the most outstanding innovation of the POPSTAR project is the *in situ* collection of data related to biological processes of the fish. For the first time, it will be possible to jointly analyze the physiological state of the fish in their natural environment and their geolocation. The recorded data will provide new scientific insights to the scientific community.

1.2 Research goals and methodology

As previously noted, POPSTAR is a multi-disciplinary project that brings several improvements to current state of the art in tag technology. Other than the collection of data related to biological processes, it aims to improve the ratio of

the acquired vs lost transmitted data by improving data transmission technology. The project aims also to improve the mechanics of the tagging system and to develop the interface between the biological tissue and the electronic system.

The ultimate goal of the present research work is to design an integrated measurement system capable of assessing biological tissue composition. This thesis focuses on the choice of the tissue composition technique, the integrated circuit design as well as signal processing. The other innovations previously enumerated are out of the scope of this work (see figure 1.3). The POPSTAR project will thus serve as a case study in order to validate research hypotheses and narrow down the specifications of the integrated measurement system. To do so, this research work has also been backed up by experimentations conducted using a hand-held measurement system for in the field operations as well as a high precision tool for in-lab measurements. The experiments specifically targeted bluefin tuna, but they were also conducted on other species that are easier to handle for lab experiments such as sea bream, sardine and sea bass. The large size of bluefin tuna, up to 4m and 650kg, makes it unsuitable for most of lab experiments and warrants the use of more lab-friendly alternative animal models.

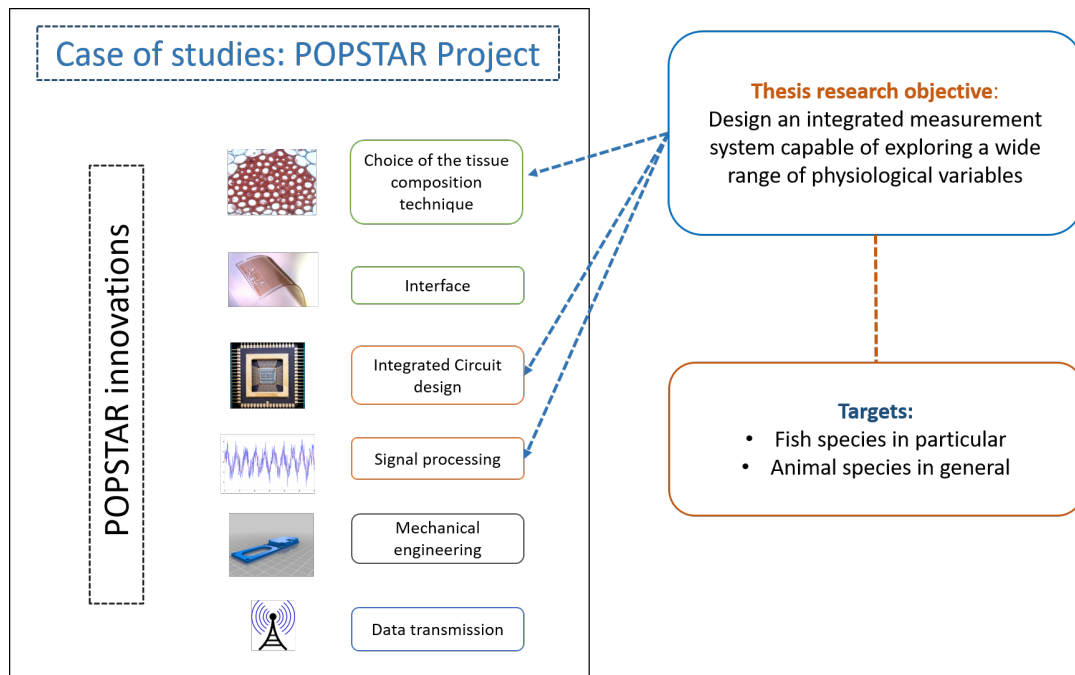


FIGURE 1.3: Scope of the thesis research work

Given that the measurement device is intended to be used to improve our understanding of wild species, the research and development process was not restricted to one particular physiological parameter. Instead, the present work intends to be exploratory in order to provide the scientific community with tools capable of measuring a wide range of physiological processes. Thus, this measurement system will be adjustable to a large scope of physiological variables for long time monitoring applications and the technique chosen for tissue composition analysis must be capable of assessing a wide range of biomarkers. From this perspective, several tissue composition assessment techniques

were first compared and the most suitable was chosen for the design of the integrated measurement system.

Designing such a system is an outstanding challenge. Indeed, by tailoring the system to explore a large scope of physiological states, the design of such system becomes rapidly ruled by strong constraints such as bandwidth, precision, measurement time and safety. An overview of the design challenges of the integrated measurement system was therefore laid out.

Due to the nature of the constraints, the choice between various potential system architectures becomes a difficult task. To address this issue, the existing integrated circuit architectures have been studied and a novel architecture suitable for the exploration of biological variables has been proposed.

Given that the excitation signal generation blocks are critical and their performances affect the whole architecture performances, care must be taken in order to optimize their design. therefore, emphasis has been placed on the signal generation part of the architecture. The stimuli creation have been optimized for different generation scenarios and a novel analog current driver architecture has been proposed in order to enhance its performances. The presented research aims to provide improved circuit blocks that can be used in Integrated Circuit (IC) architectures for physiological parameters assessment applications specifically, and biomedical/healthcare applications generally.

Taking into consideration the aforementioned aspects, the following research questions need to be answered :

- Research Question 1 : What is the most suitable biological tissue composition assessment technique in the context of our research project ?
- Research Question 2 : What are the design challenges of an integrated measurement system within the context of our research project ?
- Research Question 3 : Taking into consideration these challenges, what is the most suitable integrated circuit architecture for the measurement system ? How can the measurement system adapt itself to different sources of errors ?

As the emphasis has been placed on the blocks of the architecture responsible for the generation of the stimulation signal, the following research questions are related to this part of the architecture:

- Research Question 4 :For the signal generation part of the architecture, what are the metrics defining the quality of the signal ? What is the most optimized stimuli with regards to those metrics ? What is the most efficient circuit implementation of a stimuli generator ?
- Research Question 5 : What are the analog topologies for the current driver of the architecture? What are their limitations in terms of performance ?
- Research Question 6 : How can an integrated design overcome performance limitations of the current drivers ?

1.3 Thesis content and outline

This thesis is structured as follows :

Chapter 1 presents the context of the present research work, the research goals and methodology as well as the key research questions that this work is aiming to answer.

Chapter 2 deals with the biological tissue composition assessment techniques, it begins by a comparison of several well-adopted techniques. The result is the choice of the technique to be used for this research work. In its second part, this chapter presents a theoretical background for the chosen technique from a single cell electrical properties to the correlation methods used to link the electrical parameter with physiological variables.

Chapter 3 gives an overview of the design challenges of an integrated measurement system. The chapter tries to build the floor for the measurement circuit specifications.

Chapter 4 begins by presenting the existing integrated system architectures and discusses their advantages and drawbacks. With the set of constraints derived from chapter 3, this chapter proposes a novel hybrid architecture that is suitable within the context of the exploration of biological variables.

Chapter 5 dives into the signal generation block of the architecture. In this chapter, the stimuli generation part is presented. The key metrics defining the quality of the generated signal are presented, then different signal Generation optimizations are proposed for two scenarios: a frequency sweep generation and a wideband composite signal generation. lastly, simple implementations of this generators are presented and discussed.

Finally, Chapter 6 deals with the current driver of the architecture, which is a critical block. The chapter begins by highlighting the key parameters defining its performances, then different current driver architectures are compared, and finally a novel architecture that presents high performances compared to the state of the art is proposed.

Chapter 2

Biological Tissue Composition assessment

2.1 Introduction

The analysis of biological tissue composition is of particular interest in the field of biologging. Ranging from the fast and easy to the most complex and precise ones, a large range of measurement techniques are used to better comprehend the physiological processes and their overall impact on the biological state of the studied subjects. Depending on the application, they provide different but insightful informations that could assist efficient decision making. Researchers have debated the ideal way to measure body composition for years, testing, comparing, and refining correlation formulas in order to determine the most appropriate approach (Lukaski, 1987; Wagner and Heyward, 1999; Nelson et al., 1996; Breitenstein and Shaw, 1998; Lee and Gallagher, 2008; Mehta et al., 2014). However, with the variation in the existing techniques comes fluctuation in terms of accuracy, design complexity, portability, width of the scope of measurable biomarkers,

The main objective of this thesis is to design an integrated measurement system able to analyze biological tissue composition. Therefore, the first steps of the present research were the analysis and comparison of existing techniques in the literature. As depicted in chapter 1, throughout this process the choice made had to be consistent with the case study within the POPSTAR project. As a result, a technique to analyze tissue composition matching the requirements of our research will be selected as the basis on top of which the integrated measurement system will be conceived.

The second section of this chapter provides a comparison of some of the largely used tissue composition assessment techniques. It acts as a justification for the choice of the technique that will be used for the design of the integrated measurement system. The third section of this chapter provides a theoretical background for the chosen technique. The main goal is not to be theoretically exhaustive, rather it is meant to bring a detailed understanding of the key principles that will be used for the design of the integrated measurement system in the next chapters.

2.2 Tissue composition analysis techniques

2.2.1 Introduction

In this part, we present the exploration of several techniques that can be found in the literature for the estimation of biological tissue composition.

Our approach consists in studying the following aspects for each technique: operating principle, advantages and the drawbacks taking into consideration our main constraints which are integration, measurement accuracy and power consumption. In addition, a particular consideration was given to the range of applications possible for each technique and its possible risks and limitations. A preliminary scan of the literature allowed us to quickly eliminate several techniques, mainly because they are difficult to integrate. In this category we found techniques such as Dual-energy X-ray absorptiometry (DEXA), Nuclear magnetic resonance (NMR) or Total Body Electrical Conductivity (TOBEC). These techniques need large-size equipments which make them ultimately unsuitable for live fish deployment and miniaturization. Other techniques such as biochemical analysis, anthropometric measurement based estimations, or hydrostatic densitometry have obviously been eliminated because they were not suitable for in-vivo measurements.

Finally, we have chosen to limit our comparative study to the exploration of the following techniques for biological tissue composition analysis:

- Micro-wave propagation
- Near Infrared Spectroscopy
- Ultrasonic waves
- Bioimpedance Spectroscopy

In the following subsections we provide for each of these techniques: the operating principle, advantages and drawbacks, followed by a comparative status and a conclusion.

2.2.2 Micro-wave propagation

Operating principle

(Kent, 1990) describes a portable device for measuring fat levels in fish. The principle is to put a transmission line in contact with the biological tissue. Since this biological tissue is largely composed of body water, it presents dielectric properties when an electromagnetic field is applied to it. In fact, the complex dielectric permittivity could be analyzed since the real part corresponds to the capacity of the tissue to absorb energy and the complex part corresponds to the dissipated energy. Thus, by putting a transmission line (a planar coaxial conductor) in which an electromagnetic wave is generated in contact with the fish tissue (see figure 2.1), the dielectric characteristics of the biological tissue will modify the parameters of the transmission.

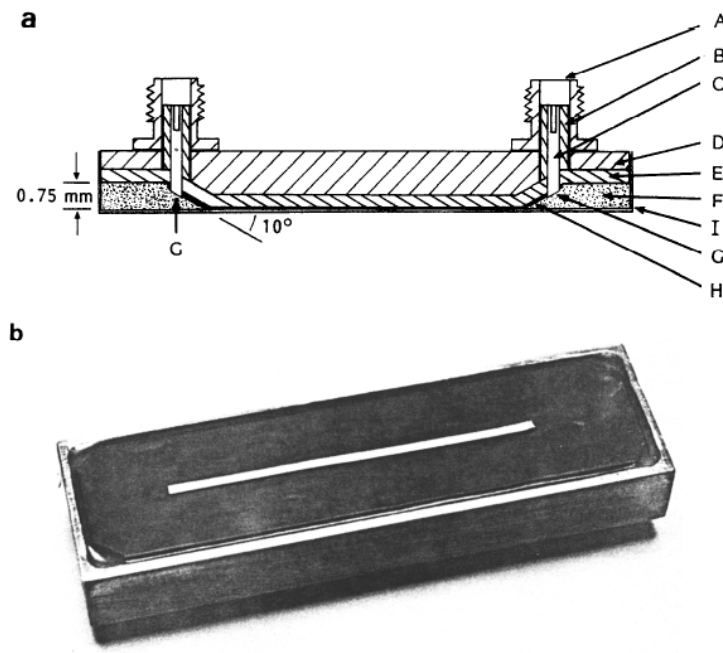


FIGURE 2.1: Design of the portable device propagating microwaves, reproduced from (Kent, 1990)

The transmission parameter that is measured is the signal energy attenuation, also called the insertion loss. This parameter can be correlated with the amount of water present in the tissue, which itself is correlated with the fat content by regression models already established for different fish species (see figure 2.2).

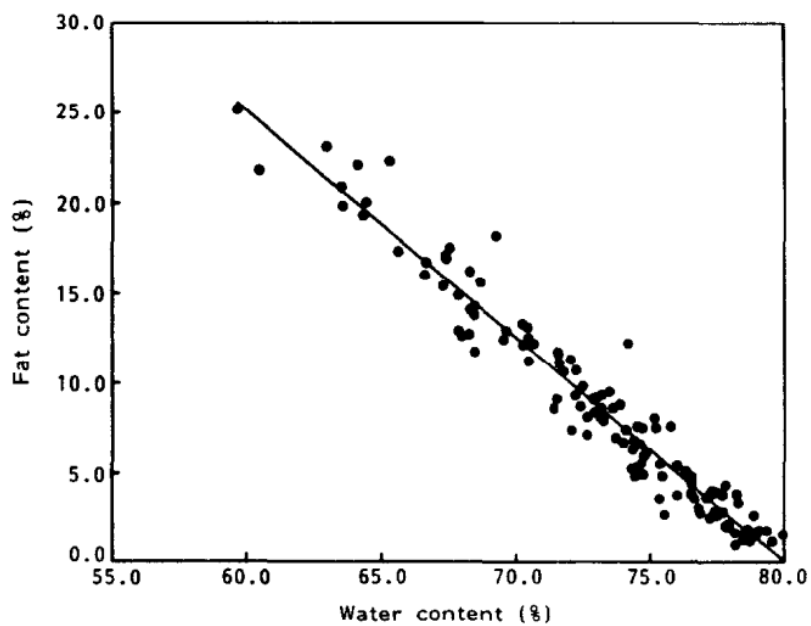


FIGURE 2.2: Correlation between total body water and the fat rate for Atlantic herring (Kent, 1990)

Advantages, drawbacks and limitations

This technique has the advantage of being simple, fast and non-invasive. One of the drawbacks of this technique is that only the amount of body water is measured which is then correlated with the fat content via regression models, this process may produce inaccuracies. Indeed, a great variability of the measurements results can be observed in (Clerjon, 2007). The correlation between the measurements made by this device and the measurements made with a conventional method such as biochemical analysis is not very strong (Douirin, 1998). This may be due to several parameters that can distort the measurement results of the device such as the density of cutaneous fat as well as subcutaneous fat, which decreases the propagation of the wave in the muscle.

Because of its strong variability, we chose to not select this technique for the context of our research.

2.2.3 Near Infrared Spectroscopy

Operating principle

Near-infrared spectroscopy exploits the principle of absorption and reflection of light by the biological tissue. Indeed, each type of tissue presents a different behavior when subjected to near-infrared radiation (Weijun, 2009). The fat tissue contains less chromophore (the part of the molecule responsible for color) and therefore absorbs less light. These cells have a size of several hundred microns while the near-infrared wavelengths range from 600 nm to 1300 nm, thus we have a stronger reflection. Muscle tissue, on the other hand, behaves in an opposite way, there is more absorption and less reflection. The figure 2.1 presents the results of a study (Song et al., 2009; Lin Ling, 2001) highlighting the optical parameters of the muscular tissues, notably the absorption coefficient noted u_a and the reflection coefficient noted u_s .

	Subject	$u_a(\text{mm}^{-1})$	$u_s(\text{mm}^{-1})$
Fat	1	0.003	1.200
	2	0.005	1.200
	3	0.004	1.200
Muscle	4	0.022	0.450
	5	0.026	0.450
	6	0.024	0.450
	7	0.026	0.500
	8	0.020	0.400
	9	0.022	0.450
	10	0.022	0.500

TABLE 2.1: Optical parameters of muscle and fat tissue, reproduced from (Song et al., 2009)

The emitter and receiver electronic circuitry is relatively simple to implement. Indeed, for the emission, one or several components emitting near-infrared light can be used, either Light Emitting Diodes (LED) or Lasers. For reception, photoelectric conversion circuits based on photo-voltaic cells (Weijun, 2009) can be used (See figure 2.3)

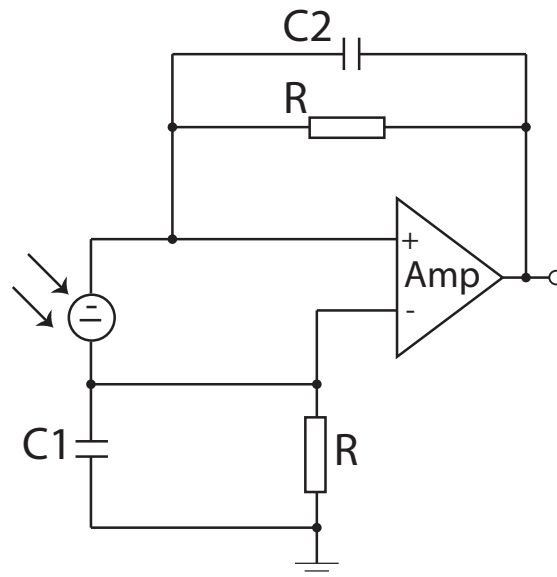


FIGURE 2.3: Photo-electric conversion circuit

Advantages, drawbacks and limitations

This technique has the advantage of being simple to implement, accurate and fast. The disadvantage of this method is the relatively large power consumption. Indeed, near-infrared LEDs and lasers commercially available generally have consumptions around 70 mA. In our case study, where measurement campaigns of several months are required, such power consumption can not be accepted. Moreover, near-infrared spectroscopy causes increases in the temperature of the tissue to which it is applied, up to 10° C (Bozkurt, 2004), this might induce discomfort that could change the behavior of the species under study. This risk is even more important in the case of frequent measurements. The increase in temperature is mainly caused by the overheating of the emitter components.

Because of these two main disadvantages, this technique was abandoned.

2.2.4 Ultrasound

Operating principle

Ultrasound operates in the frequency range between 20 kHz and 20 MHz. The operating principle of a measurement consists in propagating ultrasound waves through the biological tissue and then the reflected acoustic wave is analyzed. In fact, the reflected wave parameters will vary depending on the acoustic

impedance of the different components of the biological sample that the wave will pass through during its propagation. For humans, for example, we can find the following acoustic impedance values :

- Air : $0 \text{ g cm}^{-1} \text{ s}^{-1}$
- Fat : $0.138 \text{ g cm}^{-1} \text{ s}^{-1}$
- Muscle : $0.170 \text{ g cm}^{-1} \text{ s}^{-1}$
- Bones : $0.78 \text{ g cm}^{-1} \text{ s}^{-1}$

In order to measure tissue composition using ultrasound, a probe is needed as well as the electronic circuitry for emission and response signal processing.

Regarding the probe : it is generally composed of the following elements (*Basix principle of medical ultrasonic probes*) (See figure 2.4):

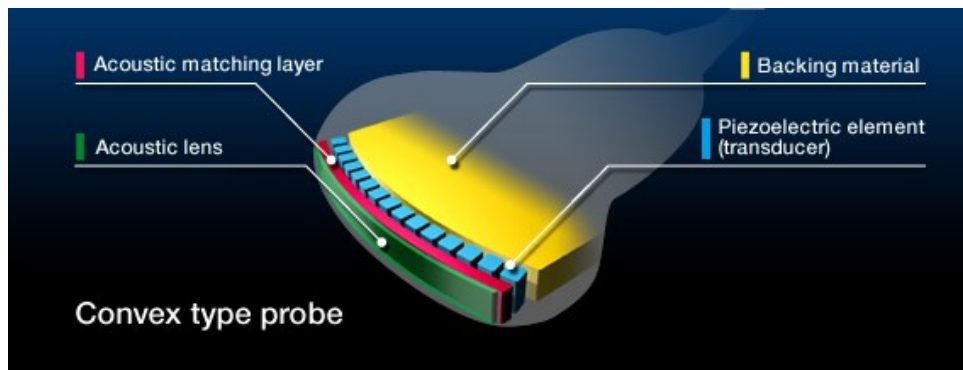


FIGURE 2.4: An ultrasound probe components, reproduced from (*Basix principle of medical ultrasonic probes*)

- The piezoelectric transducer: It contains piezoelectric crystals. This crystals are deforming (expansion and contraction) at the frequency of the electrical voltage that will be applied to them, thus generating an acoustic wave that propagates in the biological tissue. The higher the acoustic wave frequency is, the better the resolution, the lesser wave penetration depth we have. However, we observe the use of the 5 MHz frequency in most biomedical applications. Conversely, if a vibration is applied to the transducer, this element will generate an electrical voltage proportional to the applied vibration.
- The backing material: This element limits excessive vibrations of the transducer.
- The matching layer: This element is used to adapt the acoustic impedance of the biological tissue by reducing the mechanical friction.
- The acoustic lens: It is used in order to focus the ultrasound waves on the tissue region to be analyzed.

Regarding the ultrasound wave generation, level shifters (charge pumps or boost-converters) are used to create high voltages (typically around 40 V) required to deform the piezoelectric element.

In order to analyze the response signal, several techniques are used:

- A signal detection block with a timer, in order to measure the delay of the response signal.
- A peak detection block followed by an integrator in order to measure the energy of the response signal.
- High speed Analog-to-Digital Converters (ADC) may be used to analyze the response signal in the frequency domain.

These blocks may be used separately or combined depending on the constraints of the application.

Advantages, drawbacks and limitations

Biological tissue composition analysis using ultrasound has the advantage of being precise and fast, it also allows with a single measurement to collect information on fat, muscle and bone content of the analyzed tissue.

The main disadvantage of this technique is the use of level-shifters necessary to deform the piezoelectric element. These level-shifters require external components (inductances / capacitors), which is cumbersome in the case of an implanted device. The need to use high voltages is also problematic since it results in a significant power consumption, this can be reduced by exciting the tissue with shorter time frame waveforms (Johansson J, 2006), unfortunately this can only be done at the cost of the accuracy of the measurement.

2.2.5 Bioimpedance Spectroscopy

Operating Principle

Bioimpedance Spectroscopy consists in estimating the composition of a given biological tissue by measuring its complex electrical impedance over several frequencies. Using 2, 3 or 4 electrodes, a controlled current or voltage is used to stimulate the tissue to be analyzed. Conversely, a voltage or a current is then measured, thus making it possible to recover the electrical impedance (see figure 2.5).

Bioimpedance is a function of physiological processes, thus offering interesting opportunities for monitoring a large field of bio-markers. In the literature several studies demonstrating its wide range of applications can be found, from the estimation of body composition (Smith, Johnson, and Nagy, 2009), to cancerous tissue detection (Aberg et al., 2004), or blood characterization (Dai and Adler, 2009).

Each biomolecule has a different response for a given frequency. Schwan (Schwan, 1957) identified 3 frequency regions: dispersion α (Hz - KHz), dispersion β (KHz - MHz) and dispersion γ (MHz - GHz). Each dispersion is ruled by different physiological processes. To be able to make a rigorous electrical

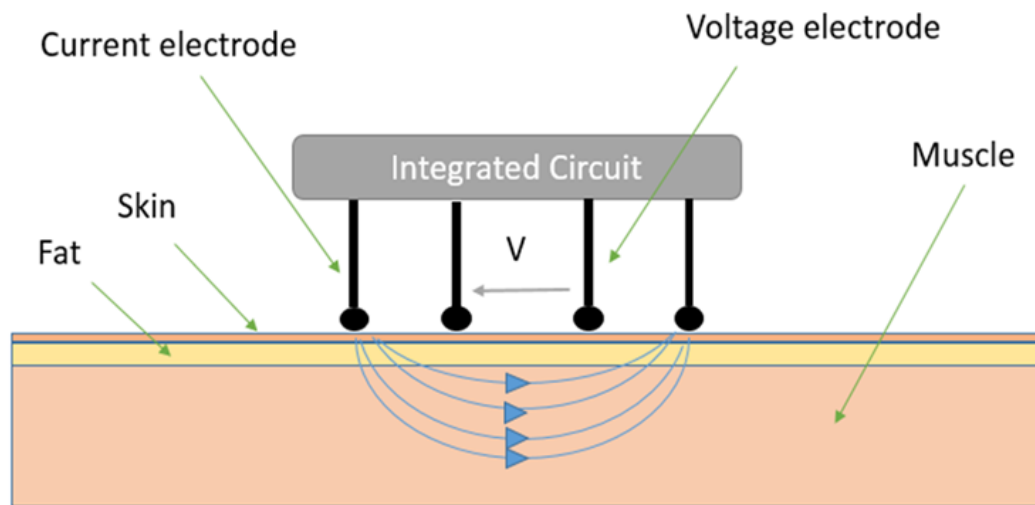


FIGURE 2.5: Bioimpedance analysis operating principle

characterization of the biological tissue, it is necessary to analyze its complex impedance over a wide frequency range.

Advantages, drawbacks and limitations

Bioimpedance spectroscopy is a relatively simple technique to implement. The ability to monitor multiple biological indicators with a single measurement is a great advantage. In addition, bioimpedance measurements have already been carried out on several fish species (Cox and Hartman, 2005; Duncan et al., 2007; Willis and Hobday, 2008) in the objective of assessing their tissue composition. This research studies have shown more or less good correlations between electrical parameter at 50 kHz and body composition parameters such as the fat content or water content.

It is also interesting to note that bioimpedance analysis is a widely used technique in biomedical/healthcare applications. Studies (Aberg et al., 2004; Dai and Adler, 2009) have shown that the technique has a great potential as a non-invasive characterization and monitoring tool of the human biological tissue properties.

The main disadvantage of bioimpedance spectroscopy is its sensitivity to several parameters such as temperature or muscle activity.

2.2.6 Comparative status

Table 2.2 shows a status of advantages and drawbacks of the techniques studied above

The microwave propagation and near infrared spectroscopy having been eliminated for the reasons detailed in the preceding subsections, the choice of the techniques to be used in the context of our application was restricted to ultrasound and bioimpedance spectroscopy.

Technique	Microwave propagation	NIR Spectroscopy	Ultrasound	Bioimpedance Spectroscopy
Advantages	Simple to implement, fast, non invasive	Simple, fast, accurate	Accurate, Measures fat/muscle/bone content, fast	Fast, low cost, low power consumption, wide range of biomarkers could be monitored, measurements already performed on several fish species
Drawbacks	Wide variability of measurements, Measures only water content	Relatively important power consumption, Risk of tissue damaging on the long term	Use of cumbersome external components, relatively important power consumption	Measurement sensitivity to temperature and muscle activity.

TABLE 2.2: Comparative status on the studied techniques

For its low complexity, its ability to achieve low power consumption and especially for the wide range of biological indicators it allows to monitor, we chose bioimpedance spectroscopy as the technique to be used for our application.

2.3 Bioimpedance spectroscopy : From electrical properties of tissue to its electrical impedance

2.3.1 Introduction

Bioelectrical methods deal with the interactions of endogenic or exogenic electricity and biological tissue. While Bioelectricity is about studying the ability of biological tissue to generate electricity, as it is the case for the heart for example (electrocardiography). Bioimpedance, on the other hand, deals with ability of the biological tissue to oppose (impede) an applied electric current flow. From this perspective, Bioimpedance describes the passive electrical properties of tissue (muscle, fat, blood or bones, ...), as changes in the bioimpedance can reflect changes in the biomaterial.

To be able to measure such a bioimpedance we can use electrodes, a controlled current or voltage is generated to stimulate the tissue to be analyzed and, conversely, a voltage or a current is then measured. When studying bioimpedance, it is important to decompose the study into circuit and biochemical issues. In fact, charge carriers flowing into wires are electrons while the charge carriers in biological tissue are ions. The electrodes interface is responsible for the conversion of the charge carriers from electrons to ions and from ions to electrons.

2.3.2 Cell electrical properties

The cell is the basic structural unit of living tissue. The understanding of its structure and components is essential to better comprehend the properties of biological tissue. Cells are of uneven size with various functions (muscle cells, nerve cells, bone cells, ...). Therefore, for an accurate analysis, the cell model must take into account the various nature of cell types. However, in order to showcase the basic principles of cell electrical modeling, we consider a simple case of a volume containing cells in interstitial fluids (see figure 2.6). We can observe that the cells are contained in an Extracellular Fluid (ECF). The intracellular space is composed of the cell nucleus, and the Intracellular Fluid (ICF) which contains components such as the cytoplasm and organelles. The cell membrane separates the intracellular space from the extracellular space.

The ICF, ECF and cell membrane account for cell and tissue electrical properties, which can be divided to conductance properties and dielectric properties (Grimnes and Martinsen, 2014).

The intracellular and extracellular fluids contain ions. Due to this free ions (mostly Na^+ and K^+), ECF and ICF are considered as electrolytes, which means that they have the ability to conduct electric current in the presence of an external electrical field. Therefore, the biological tissue can be considered as an ionic conductor.

The cell membrane is predominately constituted of polar lipids. These lipids are responsible of the capacitive nature of cells and by extent of biological tissue.

The cell membrane is a layer that separates ICF and ECF and forms two sharp boundaries against them. The cell membrane consists of phospholipids

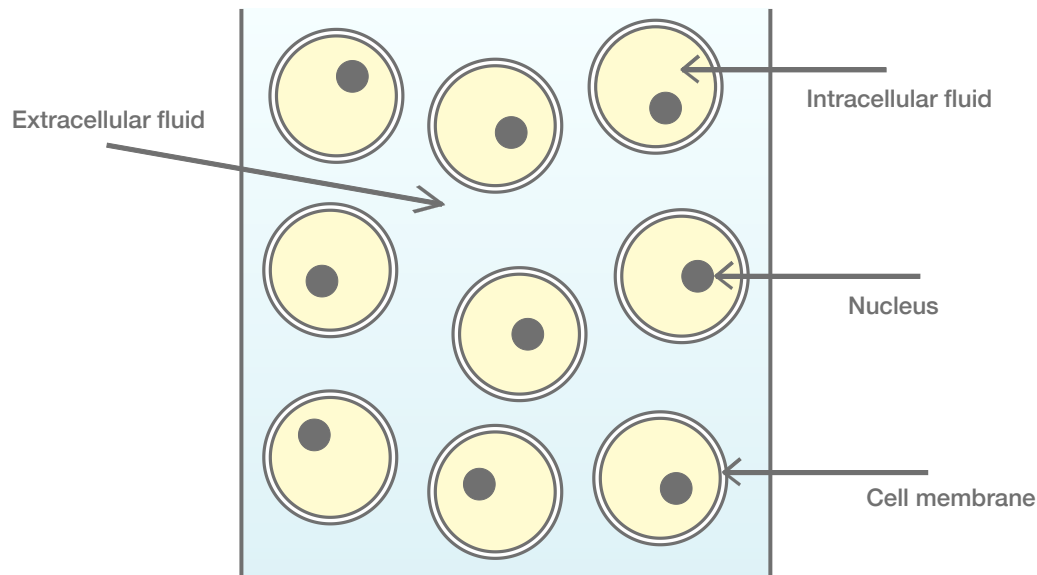


FIGURE 2.6: Cell components

that form a Bilayer Lipid Membrane (BLM). The structure of the phospholipid molecules consists of two hydrophobic fatty acid tails and a hydrophilic head. Each mono-layer has its hydrophobic part oriented inward and its hydrophilic part outward facing the intracellular or extracellular fluids (see figure 2.7), which makes the membrane a bad conductor for ions.

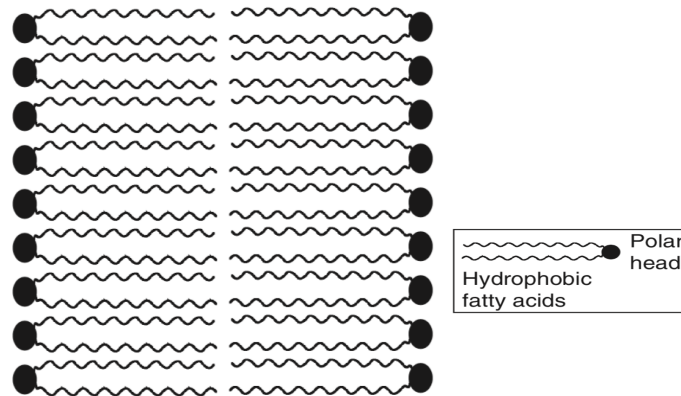


FIGURE 2.7: Bilayer lipid membrane

This structure forms a continuous double layer known as the lipid bilayer. The conductivity of the lipid bi-layer is very poor and is mainly considered as a dielectric.

2.3.3 Cell electrical model

The conductance and dielectric properties of biological tissue can be modeled as an equivalent electrical circuit. Obviously, the complexity of biological processes makes it difficult to accurately model the cell properties using simple electrical components. However, for illustrative purposes we will consider a simple electrical model which is the Fricke model (Fricke, 1924; Fricke and Morse, 1925).

The Fricke model is one of the earliest equivalent electrical models to be introduced in the literature. It is illustrated in figure 2.8. The extracellular and intracellular fluid are associated with resistive components, while the cell membrane is associated with capacitive and resistive components. The ionic currents can flow between the extracellular space of the cell and its intracellular space through existing ionic channels across the bilayer lipid membrane.

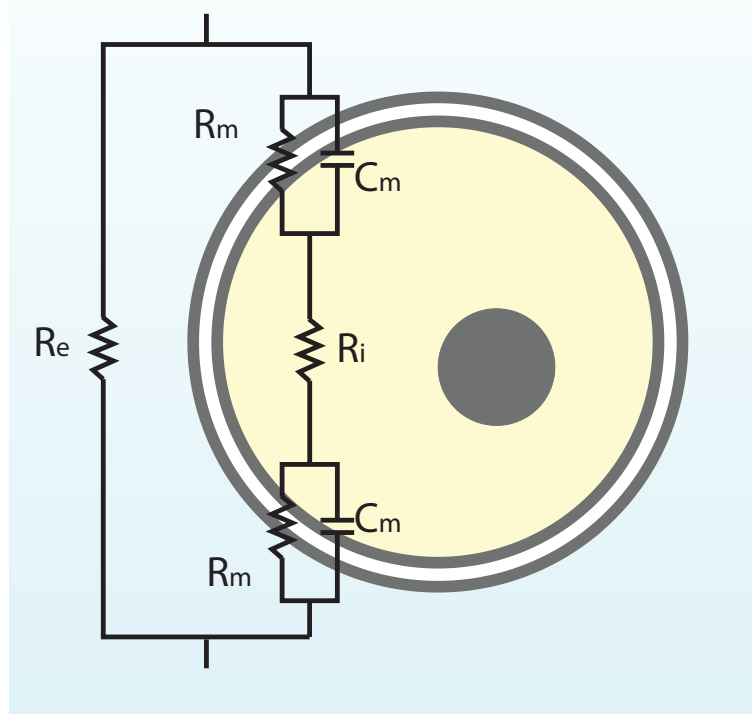


FIGURE 2.8: Fricke's Electrical Equivalent Model

The cell equivalent circuit is then represented by the ECF R_e resistor, the ICF R_i resistor, and the cell membrane is represented by a resistor R_m in parallel with a capacitor C_m . Since the conductivity of the cell membrane is poor, the cell electrical model could be simplified by representing the cell membrane only by the capacitor C_m .

The total impedance can be written as :

$$Z_{cell} = R_e // \left(R_i + \frac{1}{jC'_m \omega} \right) \quad (2.1)$$

With $C'_m = \frac{C_m}{2}$ and j the imaginary unit

$$Z_{cell} = R_e // \frac{1 + jR_i C'_m \omega}{jC'_m \omega} \quad (2.2)$$

$$Z_{cell} = \frac{R_e (1 + jR_i C'_m \omega)}{1 + jC'_m \omega (R_e + R_i)} \quad (2.3)$$

It is interesting to observe the frequency dependency introduced by the cell membrane capacitance. Indeed, at low frequencies the cell membrane acts as

an insulator blocking the current from penetrating into the intracellular space (see figure 2.9).

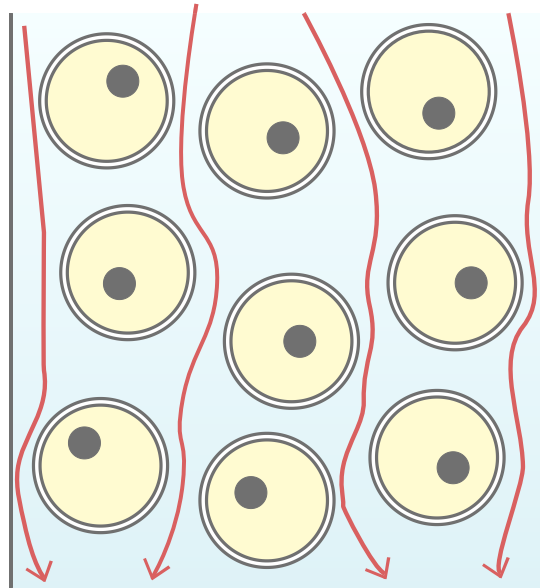


FIGURE 2.9: Low frequency current path

Therefore, at low frequencies the biological tissue impedance is equivalent to the resistance of the extracellular fluids. This can be easily checked by using equation 2.3 :

$$\omega \rightarrow 0 \implies Z_{cell} = R_e \quad (2.4)$$

On the other hand, at high frequencies, the impedance of the cell membrane decreases, and the current flows through the extracellular space as well as the intracellular space (see figure 2.10).

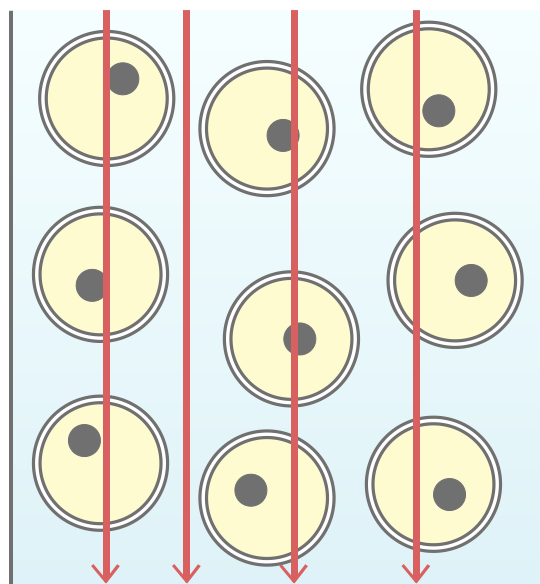


FIGURE 2.10: high frequency current path

Therefore, at high frequencies the biological tissue impedance is equivalent to the resistance of the extracellular fluids in parallel with the resistance of the intracellular fluids. Which also can be easily checked using equation 2.3.

2.3.4 Dispersion regions

The biological tissue is dispersive because its permittivity and conductivity are functions of frequency. This frequency dependency have been identified by Schwan in his study (Schwan, 1957). Indeed, he classified three major dispersions, that he named α , β , and γ dispersions (see figure 2.11). The α dispersion extends from few Hz to few KHz, the β dispersion from KHz to few MHz, while the γ dispersion has a broad range from hundreds of MHz to several GHz.

Each biomaterial has a different behavior when an electrical field is applied to it at a specific frequency. The three dispersions are ruled by different physiological processes. To be able to make a rigorous electrical characterization of the biological tissue, especially in an exploration context, it is necessary to analyze its complex impedance over a wide frequency range.

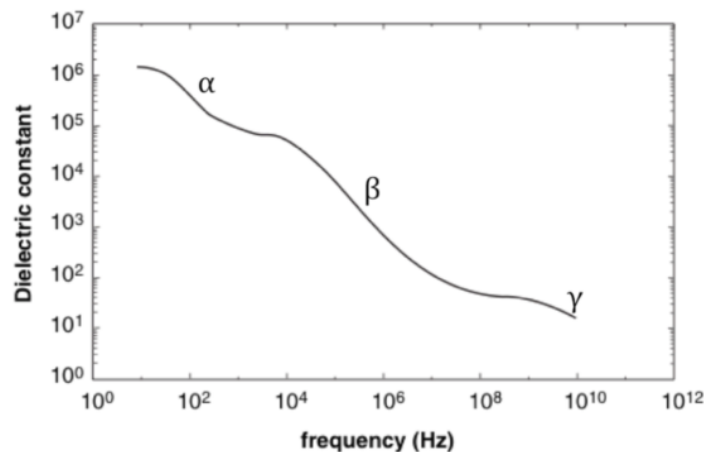


FIGURE 2.11: Dispersions of biological tissue (Schwan, 1957)

α dispersion

The α dispersion covers low frequencies from around 10 Hz to 10 kHz. Not all the contributing physiological mechanisms to this frequency region are clearly identified. Still, the best established contributing mechanisms are (Schwan, 1994) :

- The effect of frequency dependent on surface conductances and capacitances, largely caused by the response of the counter-ion atmosphere existing near the charged cell surface.
- The effect of the sarcoplasmic reticulum (which is a membrane-bound structure that regulates the calcium ion concentration in the cytoplasm of muscle cells).

- The frequency dependent conductivity of the channel proteins inside the cell membrane .

β dispersion

The β dispersion occurs in the range from around 10 kHz to 10 MHz. It is mainly caused by the cellular structure of biological tissues, with poorly conducting cell membranes separating the intracellular and extracellular space. Other mechanisms contribute to the β dispersion such as:

- Relaxation effects caused by proteins and to a lesser extend amino acid residues
- Maxwell-Wagner effects caused by organelles in the cytoplasm, such as the cell nucleus and mitochondria.

γ dispersion

The γ dispersion covers high frequencies from around 100 MHz to 100 GHz. This dispersion is mainly due to the high content of water in cell and tissue. This effect is not surprising since water molecules have a dielectric relaxation frequency near 20 GHz and biological tissues are mainly constituted of water. Aside from the water content of tissues, small contributors to this dispersion are amino acids and polar subgroups of proteins.

Later, a fourth dispersion has been identified by Schwan (Schwan, 1994) and named the δ dispersion. It is a weak relaxation at the limits of the β and γ dispersions, from approximately 100 MHz to approximately 2 GHz. It is mainly caused by proteins and amino acids.

Summary of dielectric dispersions

As presented previously, each biomaterial has a different behavior when an electrical field is applied to it at a specific frequency. Therefore, the three main dispersions are defined according to the physiological mechanisms ruling them.

To summarize, the α dispersion is mainly linked to the membrane surface structures. The β dispersion is mainly linked to the cellular structure of biological tissues with low frequency properties caused by cell membranes and high frequency properties caused by the organelles present in the intracellular space of the cell. Finally, the γ dispersion is mainly linked to water molecules present in the biological tissue.

In medical and healthcare applications in general, and in the context of tissue composition analysis in particular, the most interesting dispersions are the α and β ones, since they are associated with relevant parameters related to changes in tissue composition as well as differences between healthy and pathological tissues.

2.3.5 Single frequency vs spectroscopy analysis

The electrical bioimpedance of a given biological tissue can be measured at a single frequency, at a few frequency bins (multi-frequency bioimpedance analysis), or within a frequency range (bioimpedance spectroscopy).

Single frequency bioimpedance analysis is widely used. Indeed, a lot of studies in the literature (Cox and Hartman, 2005; Duncan et al., 2007; Willis and Hobday, 2008) analyze tissue at the frequency of 50 kHz. Several commercial systems also use this frequency, such as the Quantum body analyzer series from RLJ Systems.

However, because dielectric properties of the biological tissue vary with frequency following the main dispersions discussed in subsection 2.3.4, analyzing the tissue over a large frequency range opens up possibilities to retrieve a wide scope of insightful data, especially in an exploration context.

2.3.6 Biological vs. bioimpedance correlation approaches

The ultimate goal of most of the research on bioimpedance is to develop processes that can be used to predict a biological variable or state from electrical bioimpedance measurements of tissue.

Equivalent electrical model fitting methods

An extensively used process in bioimpedance analysis consists in building equivalent electrical models that try to describe the electrical properties of tissue such as the *Fricke* model or the *Cole* model, and then estimating the biological variable by fitting the measurement to the mathematical expression of the model parameter.

The *Fricke* model is a simple model describing the electrical properties of a cell with its ECF and ICF, but its validity is limited. Indeed, studies (Kanai, Sakamoto, and Haeno, 1983; Jaffrin et al., 1997) have demonstrated the validity of the *Fricke* model for blood containing one dominant cell species, the erythrocytes, but not tissues containing various types of cells. For the latter case, The *Cole* model is more suitable, since it generalizes the *Fricke* model to the case where different types of cells are present in parallel. This is achieved by adding a log-Gaussian distribution of time constants to equation 2.3, which gives us the following impedance equation :

$$Z_{cole} = R_{\infty} + (R_0 - R_{\infty}) \int_0^{\infty} \frac{f(\tau)d\tau}{1 + (j\omega\tau)} \quad (2.5)$$

Which then can be approximated to (S. Cole and H. Cole, 1941) :

$$Z_{cole} = R_{\infty} + \frac{R_0 - R_{\infty}}{1 + (j\omega\tau)^{\alpha}} \quad (2.6)$$

With R_0 being the resistance at low frequencies, R_{∞} the resistance at high frequencies, τ the relaxation time constant and α which takes a value between 0 and 1, allows to describe different spectral shapes. For instance when $\alpha = 1$ we recover the *Fricke* model. When using this method, the α constant is set to

the value giving the best fit to the experimental data. The resistances R_0 and R_∞ are retrieved by using curve fitting techniques.

The biggest advantage of processing experimental data through the electrical models method is that this approach reduces the measurements and prediction models to few parameters, which is convenient from a statistical point of view.

The biggest drawback of this method is due to the complexity of the biological tissue. Indeed, even fancy models such as the *Cole* model are not able to accurately model the complex biological processes (i.e the Constant Phase Element (CPE)), it is extremely difficult to mimic the electrical behavior of biological tissue with ordinary, physically realizable components. Customized models with multiple experimentations setups and advanced fitting techniques are then needed in order to discriminate the contribution of each biological process.

Statistical methods

Another technique, consists in applying statistical techniques (Grimnes and Martinsen, 2014; Tronstad and Pripp, 2014), such as descriptive statistics and/or inferential statistics to the measurement results in order to correlate the complex bioimpedance values to a biological variable or state. The choice of the statistical technique to be applied depends on the type of measurement data and the biological variable to investigate.

This process generally begins with a correlation hypothesis, which then defines the experimentations setup and the needed measurements, and finally the statistical method to be applied is chosen. For instance, let us look at the following hypothesis : The bioimpedance signature of cancerous tissue is different than the signature of healthy tissue. In order to investigate this hypothesis, we need to perform bioimpedance measurements on a number of tissue samples of each type. The statistical technique to be applied in this case would be for example a test for the comparison of the means of each group of tissues, such as the Student's t-test.

The statistical method has the advantage of being able to build predictive models without the need of mimicking the electrical behavior of biological tissue through complex electrical models.

The biggest drawback of the statistical method is the need of handling large amounts of data. Often in bioimpedance measurements, especially in an exploration context we aim to examine more than one variable per measurement. Moreover, we have limited knowledge beforehand on the biological variables or state we investigate. Thus, to maximize the chances of a significant finding, we may need to acquire several bioimpedance variables (Module, phase, ...) for several frequency points, which can lead rapidly to huge amounts of data that need to be handled. however, thanks to advances in computing power, information storage and data science, the statistical method seems to be the best compromise for the biological state exploration context.

2.4 Conclusion

This chapter deals with the biological tissue composition techniques. a comparison of several well-adopted techniques has been presented in the first part. From this comparison the bioimpedance spectroscopy is chosen to be used for this research work. A theoretical background for the concept of bioimpedance spectroscopy analysis has then been presented. From the dielectric properties of a single cell to the methods used for the correlation of biological variables with the bioimpedance measurement parameters, the chapter sought to bring a detailed understanding of the key principles of bioimpedance spectroscopy that will be used for the design of the integrated measurement system.

Chapter 3

Design challenges

3.1 Introduction

The main objective of this thesis is to design an integrated bioimpedance measurement system capable of assessing biological tissue composition. After defining the context of this research work in chapter 1, we compared, in chapter 2, several tissue composition techniques, and we chose Bioimpedance Spectroscopy (BIS) as the most suitable technique for our case studies. Then, we dived into its theory from a single cell electrical properties to the correlation methods that link bioimpedance measurements to the biological variables or states. The following step of this process consists in identifying the design challenges of a bioimpedance integrated measurement system.

In fact, designing an integrated measurement system capable of measuring a wide range of biomarkers for long periods of time is an outstanding challenge. Obviously, by tailoring the system to explore a large scope of physiological states, the design of such a system becomes rapidly ruled by strong constraints such as bandwidth, precision, measurement time and safety.

The first objective of this chapter is to clearly identify the design challenges of such an integrated measurement system. Once the design challenges are well-established, the second research objective is to narrow down as much as possible the integrated circuit specifications, this step is critical as it is the foundation of the integrated circuit design guidelines.

3.1.1 Methodology

Figure 3.1 depicts the research process that has been followed throughout this thesis. In order to identify the design challenges of the bioimpedance integrated measurement system, we based our methodology on three main steps:

- The first step consists of an in-depth literature review of the existing bioimpedance measurement systems as well as the bioimpedance theoretical concepts.
- Because design challenges are very application dependent, the second step consists in taking into account the constraints related to the measurement environment and configuration.
- Given that the majority of bioimpedance measurements on fishes that can be found in the literature use single frequency measurements (Cox and

Hartman, 2005; Duncan et al., 2007; Willis and Hobday, 2008) performed at 50 kHz, which gives poor information in comparison with bioimpedance spectroscopy measurements. Thus, the third step of this methodology consists of experiments. Several experiments have then been conducted on fish species such as bluefin tuna, sea bass, sardine or sea bass in order to assess the missing parameters.

The experiments have been performed using appliances such as a hand-held measurement system based on the AD5933 circuit that has been developed for in the field operations. For in-lab experiments, a high precision impedance analyzer have been used.

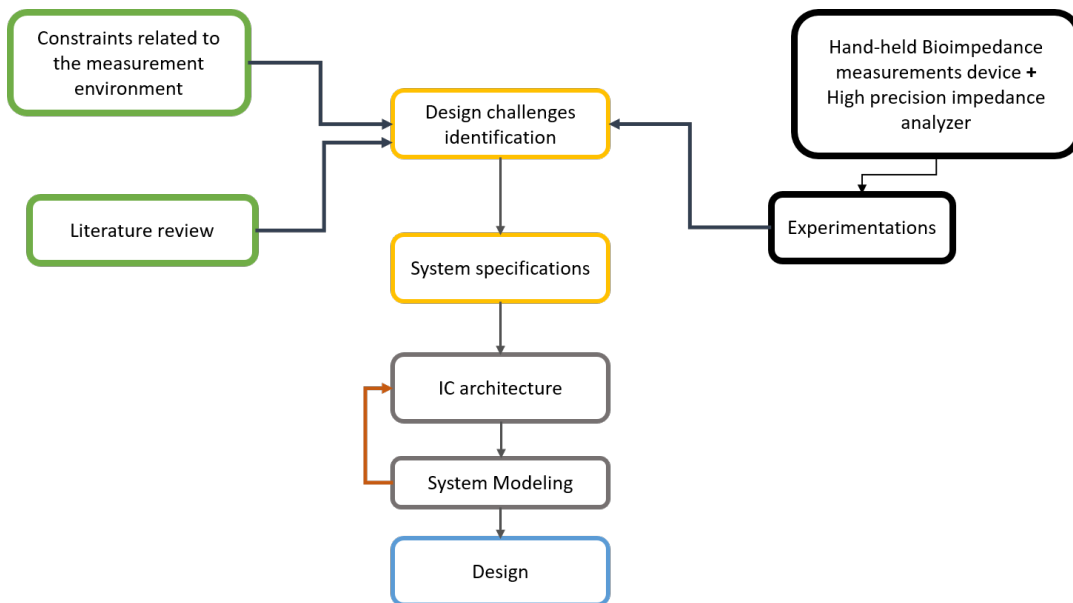


FIGURE 3.1: Methodology

3.1.2 Research questions

Based on the three enumerated steps of the followed methodology, we identified several technical and scientific questions that we will aim to answer in the next sections of this chapter in order to better comprehend the design challenges of a bioimpedance integrated measurement system. The research questions are the following :

- Is the fish biological tissue linear or does it have non-linear signatures? If they exist, does these non-linear signatures provide insightful information about the fish biological state?
- Analyzing the tissue over a large frequency range opens up possibilities to retrieve a wide scope of insightful data, especially in an exploration context (see section 2.3). Therefore, what is the frequency range we need to cover? What are the consequent circuit design limitations?

- What electrode configuration(s) do we need to use? Moreover, the electrode-tissue interface changes during the measurement campaign due to physiological processes. Can we leverage the electrode-tissue interface impedance to bring more insights on the fish physiological state?
- What is expected in terms of the impedance range for fish measurements?
- In terms of the biological tissue excitation and the response signal acquisition? What is the best combination for the measurement system: controlled current tissue excitation and voltage response signal acquisition or controlled voltage tissue excitation and current response signal acquisition?
- Generally, bioimpedance measurements are performed on steady subjects in controlled environments. This measurement process is performed in order to limit sources of error such as muscle activity or environment related errors (i.e. temperature changes). In our case study, fishes have permanent activity (24/7) and we cannot control the environment, which might be very harsh. From that perspective, what is the influence of these error sources on bioimpedance measurements? and how can we make the measurement as clean and reliable as possible to be suitable for analysis?

3.1.3 Chapter content

Before answering the enumerated research questions, the next section presents a brief overview of the tools that have been used for the experiments. Then section 3.3 details the frequency range choice, section 3.4 answers the measurement system combination question and section 3.5 discusses the electrodes configuration choice and the effect of the electrode-tissue interface on the circuit design. Next, section 3.6 provides measurement results that sets a range for the expected bioimpedance values and section 3.7 presents the fish tissue non-linearities investigation results. And finally, section 3.8 assesses the measurement configuration related errors using a series of experimentations. Hence, the impact on the accuracy of the integrated measurement system design is discussed.

3.2 Experimentation resources

As depicted before, one of the main components of our methodology is experiments. Because the majority of bioimpedance measurements data on fishes are single frequency measurements performed at 50 kHz on immobile subjects in controlled environments, this research work is exploring a novel approach that has not been done before, namely designing an *in vivo* integrated measurement system for the exploration of the fish biological state. Therefore, it is important that we perform preliminary experiments in the objective of narrowing down our system specifications and answering some of the research questions enumerated previously. To do so, a handheld measurement system based on the AD5933 circuit (*1 MSPS, 12-Bit Impedance Converter, Network Analyzer 2005*) and an

STM32 microcontroller have been developed for experiments in the field. For in-lab experiments, the *MFIA* impedance analyzer from Zurich instruments was used (*MFIA User Manual 2008*). Measurements have been performed on several fish species such as bluefin tuna, sea bass, sardine or sea bass. Moreover, several electrodes have been developed and used in these experiments.

3.2.1 Electrodes

In the context of the POPSTAR project, several generations of electrodes have been developed and used in the experiments. The first generation of electrodes is quite simple. Indeed, it consisted of four iron nails maintained with resin (see figure 3.2). While these electrodes were handy and simple to manufacture for the first experiments, the first generation of electrodes was rapidly abandoned as their design was not optimized for *in vivo* measurements, and their electrical impedance was not optimal.

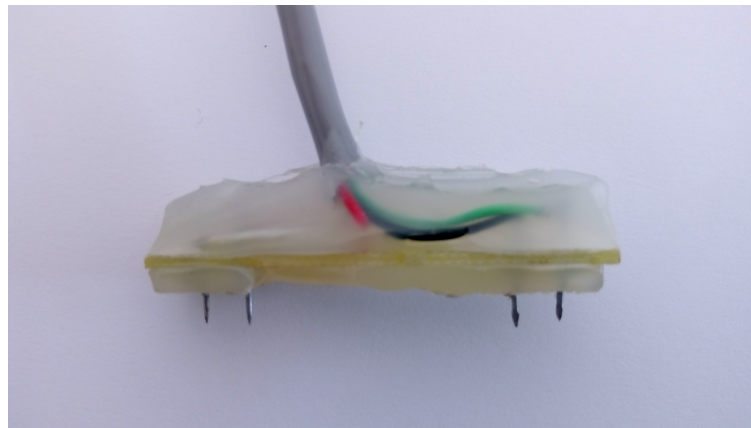


FIGURE 3.2: First generation of electrodes

The second generation of electrodes to be used in experiments is flexible (see figure 3.3), in order to maximize the tissue contact surface, and minimize the risk of pathological tissue processes such as inflammation or fibrosis. Electrodes were processed on Kapton flexible substrate, the contacts are made of Au-Pt (gold and platinum), the electrical pathways are protected by a bio-compatible SU-8 photo-resist layer. Their design is optimized in order to minimize the impedance of the current injecting contacts, maximize the current flow through. The electrodes thickness is 25 μm which thus makes them suitable for implanted monitoring measurement of bioimpedance.

3.2.2 The handheld AD5933 measurement system

A hand-held measurement system (see figure 3.4) based on the AD5933 circuit and an STM32 microcontroller have been developed for experiments in the field.

The AD5933 is a high precision impedance converter system solution that combines an on-board frequency generator with a 12-bit, 1 MSPS, analog-to-digital converter (ADC). The frequency generator allows an external complex impedance to be excited with a frequency sweeps. The response signal from the

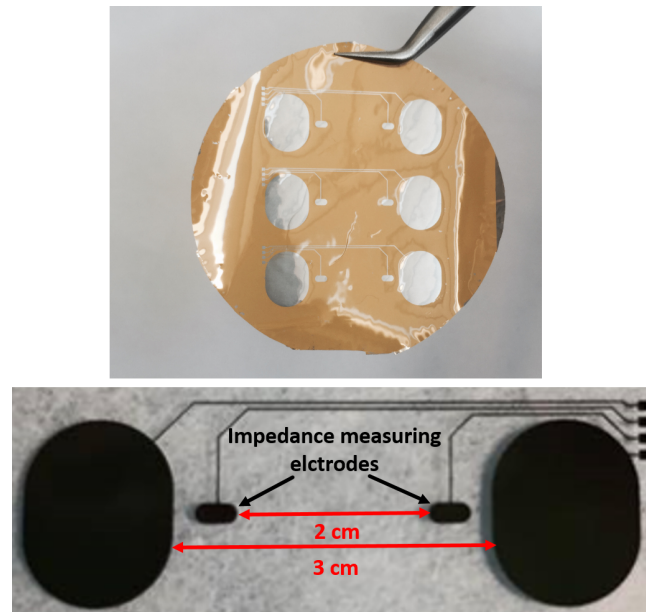


FIGURE 3.3: flexible Electrodes



FIGURE 3.4: AD5933 Hand-held bioimpedance measurement system

impedance is sampled by the on-board ADC and a 1024 points discrete Fourier transform (DFT) is processed by an on-board DSP engine. The DFT algorithm returns a real (R) and imaginary (I) data-word at each output frequency. Its functional diagram is presented in figure 3.5. The STM32 microcontroller communicates with the AD5933 circuit via I2C.

The Hand-held bioimpedance measurement is capable of exciting biological tissue at $100\ \mu\text{A}$ and $400\ \mu\text{A}$ with frequency sweeps ranging from 300 Hz to 100 kHz. While it permitted the development of the hand-held device for experiments in the field, the AD5933 can not be integrated in the measurement system that we are developing mainly due to its limited frequency range of operation and its high power consumption.

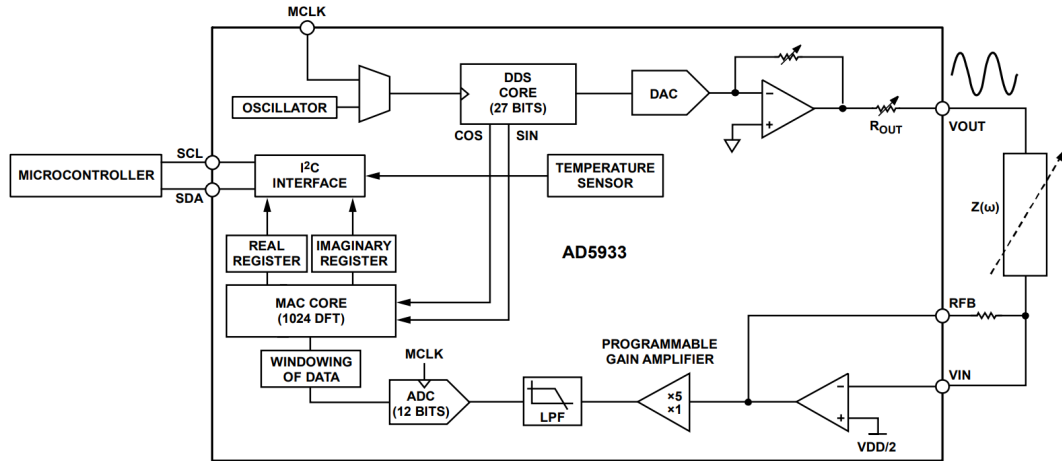


FIGURE 3.5: AD5933 system function blocks diagram



FIGURE 3.6: The MFIA impedance analyzer

3.2.3 The MFIA impedance analyzer

While the AD5933 bioimpedance measurement system is handy for experimentation field. Its accuracy is limited and its frequency range of operation covers only the frequency region : from 300 Hz to 100 kHz. In order to have more insights on the fish tissue impedance values we use an in-lab high-precision instrument, which is the MFIA from Zurich Instruments. It is a digital impedance analyzer and precision LCR meter that operates in the frequency range from DC to 5 MHz. The MFIA provides 0.05% basic accuracy and a measurement range spanning from 1 mΩ to 1 TΩ.

3.3 Frequency range

As presented in section 2.3.4, the biological tissue is dispersive because its permittivity and conductivity depend on frequency. This frequency dependency have been identified by *Schwan* in his study (Schwan, 1957). He then classified three major dispersions, that he named α , β , and γ dispersion (see figure 2.11). Each biomaterial has a different behavior when an electrical field is applied to

it at a certain frequency. The three dispersions are ruled by different physiological processes. In order to perform a rigorous electrical characterization of the biological tissue, especially in an exploration context, it is necessary to analyze the complex impedance over a wide frequency range.

However, in medical and healthcare applications in general, and in the context of tissue composition assessment in particular, the most interesting dispersions are the α and β ones, since they are associated with relevant parameters related to changes in tissue composition, as well as changes between healthy and pathological tissues. The reader may refer to section 2.3.4 in the second chapter which presents the main electrical dispersion regions of biological tissue and their respective contributing elements. In terms of circuit design constraints, covering a wide range of frequencies, from few Hz to several MHz, is challenging. The main factors constraining the design of a wideband measurement system are the following:

- At low frequencies, two main constraints can be observed:
 - The flicker noise becomes predominant.
 - The measurement duration tends to grow as the frequency diminishes. This mainly caused by the length of the excitation signal that is inversely proportional to the frequency point of interest, and also the significant time constants of the different filters of the architecture.
- At high frequencies two main constraints can be observed:
 - The parasitic capacitances degrade the circuit performances.
 - The conductivity of biological tissue decreases as frequency increases. Therefore, low impedance values are expected at high frequencies, which means that at the response analysis side high performances are needed in order to process these low values.

We are thus going to cover the α et β frequency ranges with the following specifications :

- The number of frequencies to be used is an important parameter. It should be high enough to cover accurately each dispersion, and small enough to have an acceptable measurement duration. From that perspective, we chose to distribute frequencies as powers of 2.
- We will limit the maximum range value to 8 MHz. Thus, we will be able to cover almost totality the β range while involving a reasonable circuit design effort.
- We will break down the analysis into three different bands: 8 Hz-256 Hz; 256 Hz-131 kHz; 131 kHz-8 MHz. The idea is to optimize the accuracy of the measurement on the nominal band (256 Hz-131 kHz) which is the range commonly used in the measurements of Bio-impedance (i.e the AD5933 circuit used in the hand-held Bioimpedance measurement system). On

this nominal band we will seek to accelerate the duration of the measurement to make the measurement less sensitive to external disturbances. The high and low frequency bands will make it possible to test the relevance of these frequency ranges in the POPSTAR project.

It is clear that these values remain fairly empirical because we have not defined the expected physiological signature yet. The objective being the exploration of different physiological variables. Therefore, the main goal is to cover a maximum range that remains achievable regarding circuit design constraints. As soon as significant physiological signatures are found and tested, the range may be redefined.

3.4 Current vs voltage stimulation

In any bio-impedance measurement system, the excitation subsystem is a critical component. Bio-impedance measurements can be performed by applying either a controlled current or a controlled voltage to the biological tissue and then measuring the bio-modulated voltages or current respectively.

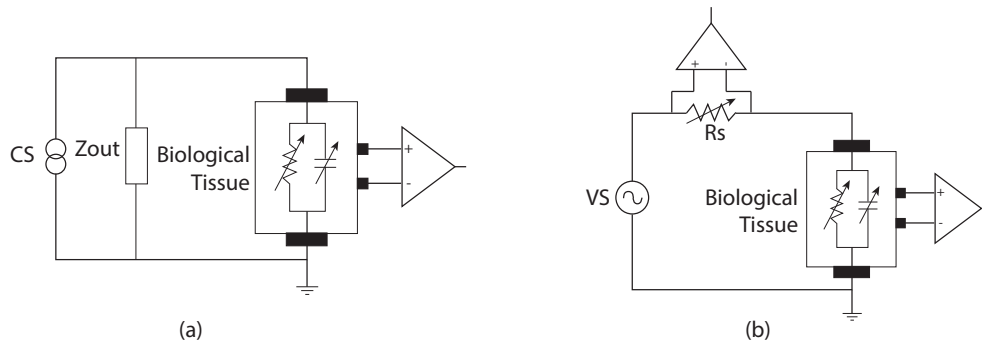


FIGURE 3.7: Structure of a : (a) current excitation system (b) voltage excitation system

3.4.1 Voltage excitation system

While current sources are the most used for bioimpedance spectroscopy measurement, studies using voltage excitation sources can be found in the literature (Yoo et al., 2010). Figure 3.7.b presents the voltage excitation structure. The voltage from the constant voltage source is divided by an internal current-sensing resistor and the biological tissue under test. The resulting voltages across current-sensing resistor and the biological tissue are measured simultaneously. A feedback loop is then used to adjust the value of the current-sensing resistor so that the magnitude of the voltage across the living tissue is maintained at a constant value. On the response analysis side a trans-impedance amplifier is generally used in order to output a voltage that is a function of the bio-modulated current. Obviously, the use of a feedback system to sense the current and adapt the voltage makes the design more complex. Moreover, an

error of the feedback control system could lead to high magnitude currents that could damage the biological tissue.

3.4.2 Current excitation system

Figure 3.7.a presents the current excitation structure. The current excitation source is the most used excitation source in bioimpedance measurement systems. This excitation source should deliver and absorb current independently of the voltage. This is achieved by having a high output resistance compared to the biological tissue one. Unfortunately, the drawback of current sources is that at high frequencies parasitic capacitances shunts the output resistance decreasing its value, thus decreasing its accuracy.

Various studies comparing voltage and current excitation sources can be found in the literature (Yoo et al., 2010; Mohamadou et al., 2012; Qureshi, Chatwin, and Wang, 2013), with results leaning in favor of current sources. This results are not surprising as current generation simplifies the generation circuitry of the architecture. Over and above all, it ensures a higher level of safety. Indeed, since the injected current is not dependent on the value of the measured impedance, there is no risk of over-stimulating the biological tissue, which can cause either a discomfort that may change the behavior of the species of interest, or in the worst case damage the biological tissue. We therefore chose this type of excitation for the integrated circuit bioimpedance measurement system.

Regarding the excitation current magnitude, it should be small enough to avoid any tissue damage or any discomfort that may lead to a possible change in the behavior of the fish. It also should be high enough to ease the response analysis. The conducted experiments on several fish species using the handheld bioimpedance measurement system have shown that a current magnitude of 400 μA provokes involuntary muscle contractions. As the current magnitude limit for each specie is unknown, it has been decided that for the integrated measurement system the current magnitude should be tunable ranging from 10 μA to 300 μA .

Various current source architectures can be used. In the literature we observe the use of Howland circuits for discrete electronics measurement systems (Bertemes-Filho et al., 2012; Tucker et al., 2012), and OTA based circuits for the integrated measurement systems (Hong, Lee, and Ha, 2015; Constantinou et al., 2014; Constantinou, Bayford, and Demosthenous, 2015)

3.5 Electrode configuration

In order to perform an impedance measurement, only two electrodes are sufficient in theory. The drawback of using a 2-electrode configuration (illustrated in figure 3.8) is that the electrode-tissue interface Z_{e-i} is in series with the tissue under test impedance Z_{tissue} . The electrode-tissue interface impedance may vary over time with the possible appearance of pathological processes such as

fibrosis or necrosis. It also depends on the quality of the physical contact between the electrodes and the tissue surface which can also vary with the physical activity of fish during measurement.

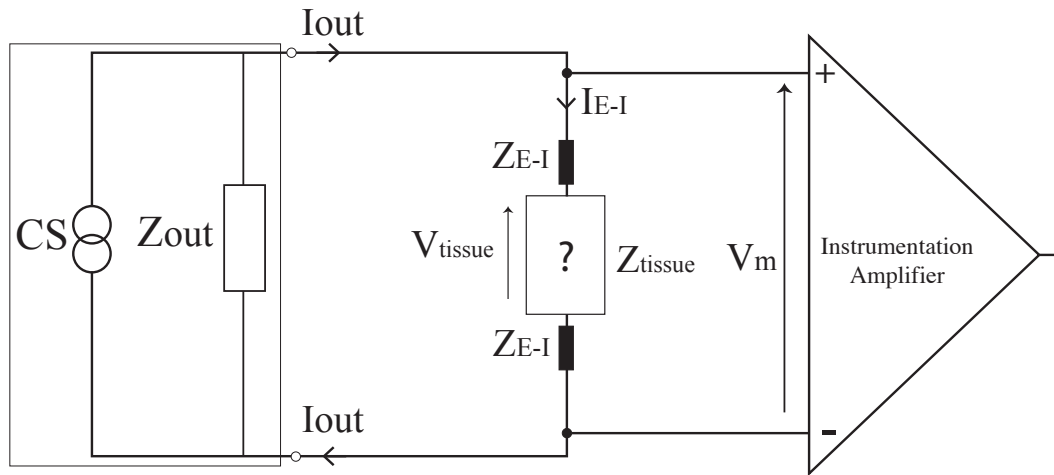


FIGURE 3.8: 2-electrode configuration

In applications where we want to get rid of the electrode-tissue interface impedance, a 4-electrode configuration (see figure 3.9) could be used. In this configuration, two electrodes are used for the current signal generation and the other two electrodes are used for the voltage measurement. As operational amplifiers (Op-Amp) are generally used as the first element of response analysis chain, the electrode-tissue interface Z_{e-i} is eliminated since no current flows in the input terminals of the Op-Amp, the measurement only "sees" the tissue impedance Z_{tissue} .

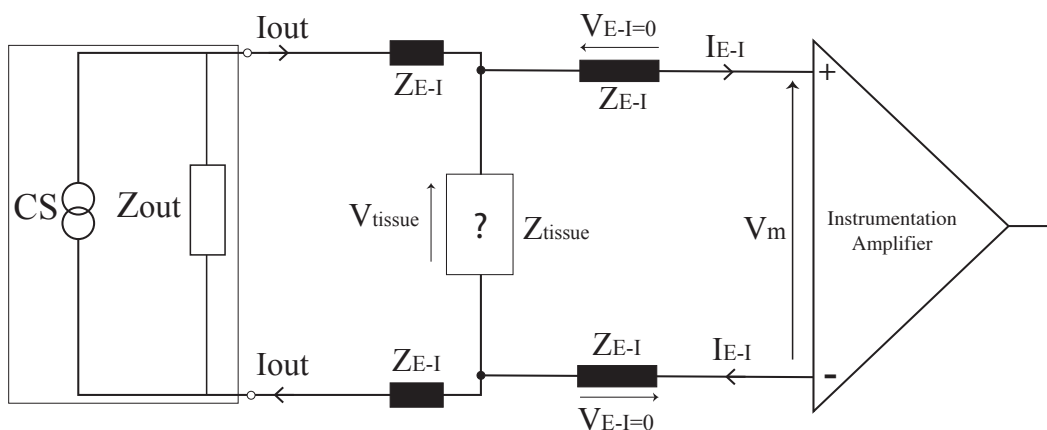


FIGURE 3.9: 4-electrodes configuration

It is interesting to note that another approach is possible. In an exploration context, the electrode-tissue interface impedance may be interesting to monitor, as the evolution of this impedance is a translation of the physiological

processes happening in the interface. From that perspective we decided to use both the 4-electrode and the 2-electrode configurations, by subtracting the measured impedances of the two configurations, we can isolate the electrode-tissue interface impedance in post-processing. This approach does not imply a significant design effort, since simple switches could be used in order to alternate measurements.

3.6 Electrode-tissue impedance range

The tissue expected bioimpedance values are of a great importance, since it allows to narrow down the specifications of the integrated measurement system.

In literature, *Willis et al* have conducted bioimpedance measurements on 360 Southern Bluefin Tunas using the Quantum II bioelectrical body composition analyzer from RJL Systems (Willis and Hobday, 2008). The authors used the separation between electrodes and an impedance parameter (reactance) as inputs in order to calculate a composition index. The separation between electrodes was retrieved from the length to caudal fork, multiplying the latter by a constant factor of 0.4. From the measurement results at 50 kHz frequency, they computed the bioimpedance module and found it ranging from 96.8 to 128 Ohms. Using the MFIA impedance analyzer and the flexible electrodes presented in section 3.2, we conducted bioimpedance measurements on bluefin tuna from DC to 5 MHz. The MFIA uses a voltage excitation signal, which has been set to 100 mV. The 4-electrode measurements are presented in figure 3.10 and the 2-electrode measurements are presented in figure 3.11

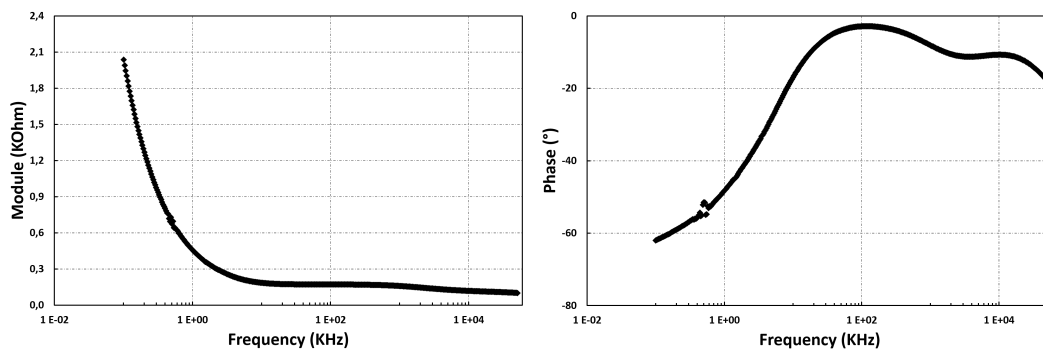


FIGURE 3.10: 4-electrode measurements on bluefin tuna using the MFIA impedance analyzer

We observe that in low frequencies the fish tissue bioimpedance module is around hundreds Ohms up to $2\text{ k}\Omega$ at the lowest frequency, and decreasing to few Ohms at high frequencies.

The total impedance (fish tissue, electrodes and interface) module is retrieved with the 2 electrodes configurations. We can observe that at low frequencies it is approximately five times superior compared with the impedance of the fish tissue.

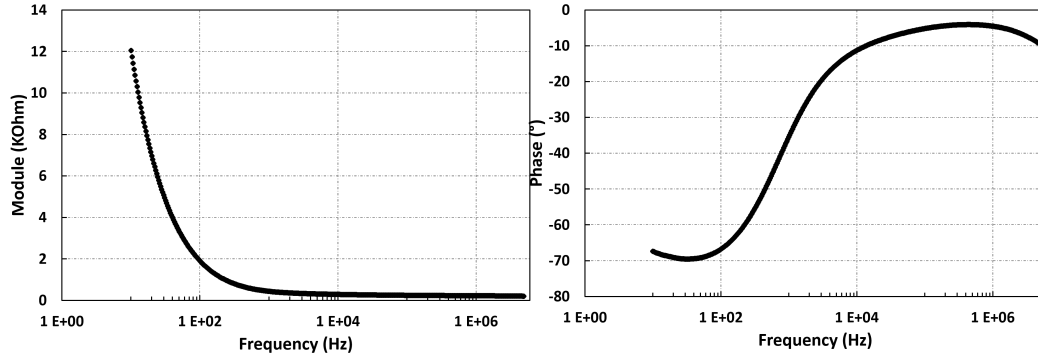


FIGURE 3.11: 2-electrode measurements on bluefin tuna using the MFIA impedance analyzer

Other experiments were conducted on sardines, sea breams and sea bass using the MFIA impedance analyzer and the hand-held bioimpedance measurement system presented results close to the ones of the bluefin. This confirms the expected bioimpedance value ranges.

3.7 Non-linearity investigation

3.7.1 Motivation

Implicitly, when we talk about impedance, we consider that the system is linear. However, in the literature, some studies interested in the phenomenon of non-linearity of the biological tissue and linked it to specific biological components. For instance, the study referenced in Yamamoto, 1981 concludes that the layer of keratin present in the skin is a source of non-linearities.

Based on this observation, we investigated if there was a useful non-linear signature in the bluefin tuna tissue. From the standing point of our research this seems to be an interesting lead, as this can open possibilities in terms of correlations with potential physiological parameters.

3.7.2 Experiments

In order to conduct our investigation of non linearity signatures, we set an experimentation where we send a single frequency signal to two different systems (see figure 3.12) :

- A linear system : which is a simple resistor.
- Bluefin tuna's biological tissue.

The linear system acts as a reference, if the biological tissue is non linear, we expect to see in the frequency spectrum of its response harmonics that are not present in the single frequency excitation signal. We chose stimulation frequencies of: 500 Hz, 2 kHz and 10 kHz, to see if the phenomenon of non-linearities is majorly present in the impedance spectrum.

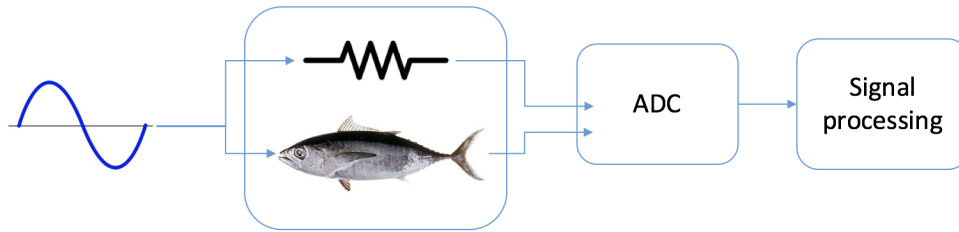


FIGURE 3.12: Experimentation setup

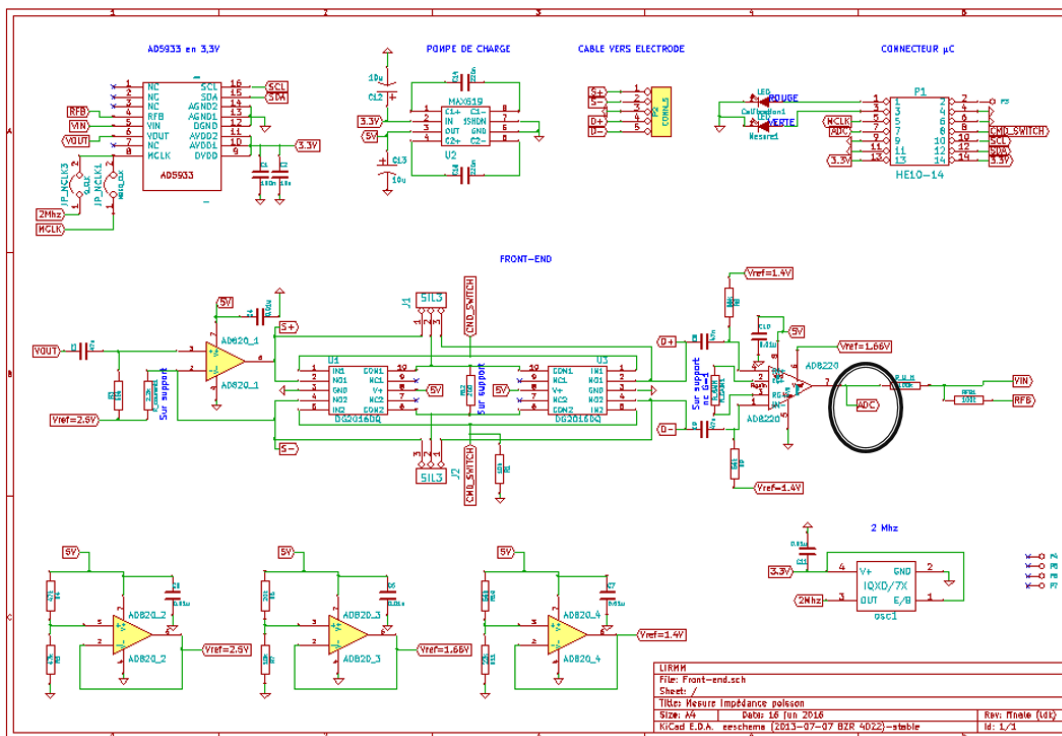


FIGURE 3.13: modified portable BIA device schematic

The portable BIA system has been modified in order to be able to estimate the nonlinear contributions of tissues to the measured impedance. To do so, an ADC has therefore been added to the front-end receiver chain (see figure 3.13) in order to digitize the response signals of the biological tissue.

After digitization, a signal processing algorithm is applied to the response signals post-processing in order to evaluate as precisely as possible their spectral content (see figure 3.14). After extracting the acquisition data from the measurement file, we apply a moving average filter in order to get rid of the DC component without losing a significant number of samples. We then compute a whole number of periods and apply a hamming window to the data. Finally, we apply a Fast Fourier Transform (FFT) in order to analyze the data in the frequency domain.

The sampling frequency of the ADC as well as the length of the acquisition were chosen in such a way as to have the smallest possible (FFT) frequency

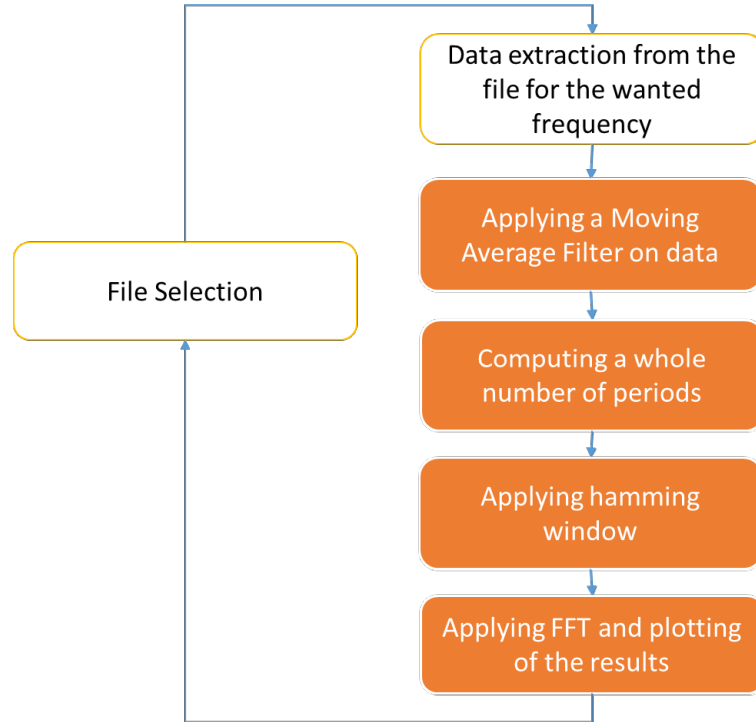


FIGURE 3.14: Data processing algorithm

resolution, given the system constraints. In fact the FFT frequency resolution is defined as:

$$Resolution = \frac{f_s}{N} \quad (3.1)$$

With f_s being the sampling frequency of the ADC and N the number of samples. The ADC sampling frequency has been set to 3.79 MHz and the length of acquisition to 50000 points, which gives us a frequency resolution of:

$$Resolution = \frac{3.79 \text{ MHz}}{50000} \approx 76 \text{ Hz/bin} \quad (3.2)$$

3.7.3 Results and conclusion

We conducted several experiments on living and dead bluefin tunas. Figure 3.15 represents the frequency spectrum of responses of a calibration signal and 3 acquisitions on bluefin tuna for the input signal at 10 kHz. We can observe that the acquisition response signals do not contain harmonics other than those present in the excitation signal. The same thing is observed for the frequencies of 500 Hz and 2 kHz.

It has been suggested by Yamamoto in his study (Yamamoto, 1981) that the non-linearity of the biological tissue is strongly dependent on the excitation current density. The excitation current density is defined as the current magnitude divided by the contact surface. The higher the current density, the more likely it is to observe the non-linear properties of the tissue. However, in our research context, the current magnitude should be small enough to avoid any tissue damage or any discomfort that may lead to a possible change in the

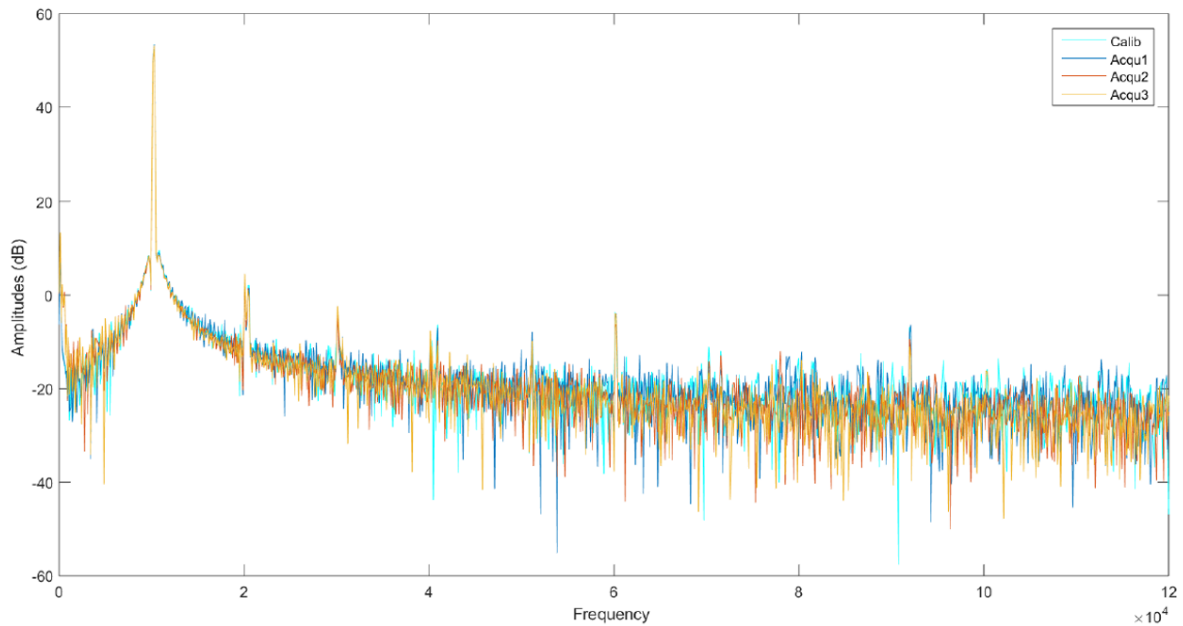


FIGURE 3.15: Frequency content of the response signals at 10KHz

behavior of the fish. The impact in terms of non-linearity not being obvious for the chosen current magnitudes. We have decided to abandon the study of non-linear properties. In the following parts of this work, we only focus on the study biological tissues linear properties.

3.8 Measurement environment related errors

Motivation

Generally, bioimpedance measurements are performed on immobile subjects in controlled environments. This measurement process is performed in order to limit sources of errors such as muscle activity or errors due to the surrounding environment (temperature changes, humidity,...).

Unfortunately, in our research context, measurements on immobile subjects in controlled environments are not possible. Indeed, The most outstanding innovation of the POPSTAR project is the *in situ* recording of data related to key biological processes of wild populations of fish in their natural environment. Therefore, bioimpedance measurements will be performed all along the trajectory of fish in high seas. Moreover, swimming is an indispensable activity in fish life (McKenzie, 2011), especially for bluefin tunas as the flow of water and O_2 is ensured by swimming and not the movements of their opercule like for most fish species. Whether it is for nourishment seeking, predator evading, or simply to engage in social movements, fish swim continuously.

Swimming requires the use of several muscle groups. Obviously, muscle contractions during swimming activities create a type of "bioelectrical" signals

which may interfere with the bio-modulated voltages representing passive electrical properties of tissue, thus leading to measurement errors.

Experimentation setup

From that perspective a series of experiments have been conducted on the gilt-head breams (*Sparus aurata*) (HACHIM, 2017), which is a fish of the bream family that can be found in the Mediterranean sea. The main goal of these experiments is to identify the influence of the swimming activity on the bioimpedance measurements.

To do this, 9 male gilt-head breams of approximately 27 cm long and approximately 400 g that come from the IFREMER Palavas-les Flots fish farming station were the subjects of the experiment.

After anesthetizing the subjects of the experiment, surgery has been performed in order to implant electrodes for bioimpedance spectroscopy, Electromyography (EMG) and Electrocardiography (ECG). For BIS, wired silver electrodes of 0.6 mm diameter have been implanted .

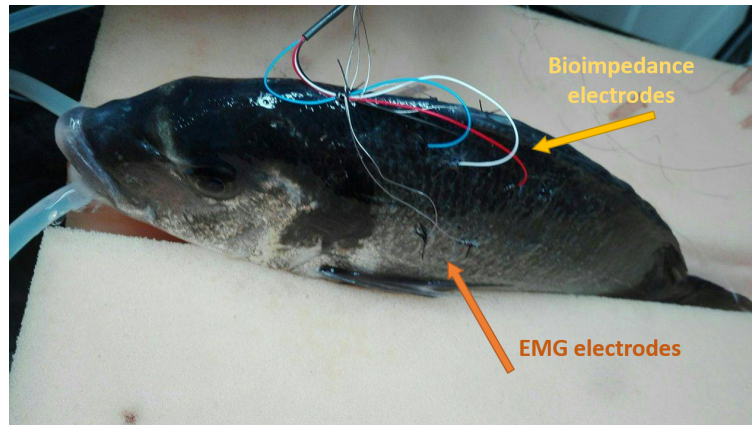


FIGURE 3.16: BIS and EMG electrodes implanted on the gilt-head bream

Figure 3.16 shows the implanted EMG and BIS electrodes. After surgery, the subjects have then been transferred into a swim-tunnel. The swim-tunnel is designed to create a uniform (non turbulent) water flow, where the velocity of the current can be controlled. The fish swims spontaneously against the current, by a reflex known as rheotaxis. By adjusting the speed of the water current, different swimming activity levels can be induced.

After a recovery period of 24 hours. The fish have been subjected to a swimming speed corresponding to 1 body length (BL) per second during 20 minutes. The swimming speed has then been gradually increased by 0.5 BL/s each 20 minutes. Fish fatigue is noted when the subject rests his caudal fin on the gate at the back of the swim tunnel. When that happens, the velocity of the current is immediately set to a swimming speed of 1 BL/s.

During the experimental setup, bioimpedance spectroscopy has been performed using the AD5933 based hand-held device for a frequency range from 300 Hz to 100 kHz, with a current excitation signal of 100 μ A. Each frequency sweep took 15 s to be completed.

Results and discussion

Figure 3.17 presents the impedance module and figure 3.18 the impedance phase of a gilt-head bream tissue during different swimming speeds (BL/s). The first 6 plots (5-10) represents measurements for low swimming speeds (from 1 BL/s to 2 BL/s), the plots from 11 to 14 measurements for a swimming speed of 2.5 BL/s, the plot 15 represents a measurement at a swimming speed of 3.5 BL/s. Then the swimming speed was decreased to 1 BL/s in the plots 16 and 18. The plot 19 corresponds to the measurement of the fish dead outside of water.

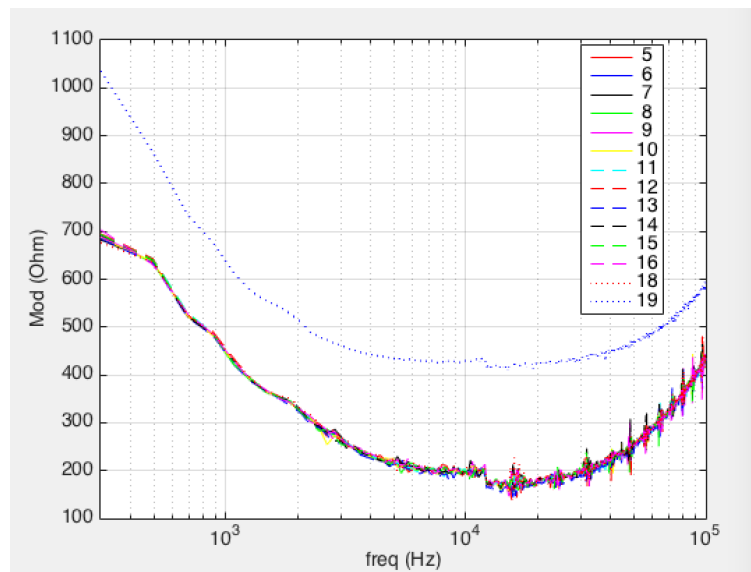


FIGURE 3.17: Bioimpedance module of a gilt-head bream during different swimming speeds

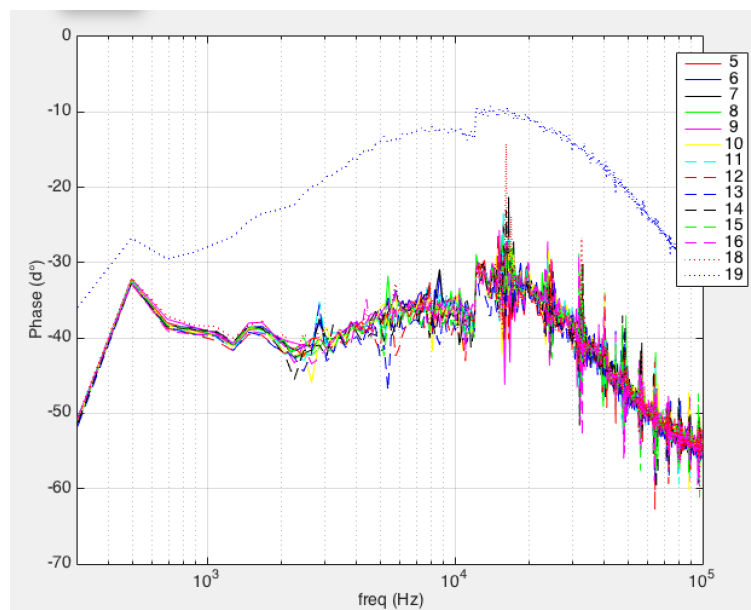


FIGURE 3.18: Bioimpedance phase of sea bream during different swimming speeds

Following these measurement results, several observations could be made. Firstly, we observe relatively small differences in the impedance module and phase between different swimming speeds plots. In view of the results, a clear tendency between swimming speed and impedance module and phase can not be concluded.

Secondly, we can observe a clear decrease of the impedance module and phase between measurement in the swim-tunnel and the 19 measurement outside water. This is mainly due to highly conductive properties of water. Indeed, some of the field lines spread in water outside of biological tissue. The measured voltage sees small impedances in parallel which diminishes the overall impedance.

Finally, and on more global scale we observe when comparing the plots of the dead motionless fish and the plots of fish swimming, that the global shape of the bioimpedance modules and phase remain identical. However, we can clearly see that there are less peaks on the dead fish plot compared to those corresponding to fish swimming. While this measurement result shows clearly that swimming activity interferes with the bioimpedance measurement, the nature of this interference remains unconfirmed. A possible explanation of this interference can be the mechanical modulation of the cell constant and the tissue composition.

The integrated bioimpedance measurement system must be able to measure accurately the fish bioimpedance signature. Knowing that the frequency sweep took 15 seconds for the hand-held measurement system, a solution to this matter consists in shortening as much as possible the measurement duration in order to get rid of the swimming activity related interferences.

Moreover, it has been demonstrated that fish swim with two types of muscles (McKenzie, 2011), one used for punctual activities such as chasing or escaping predators and one for continuous slow to moderate swimming. An EMG recording block embedded in the measurement system could additionally provide us with insightful data about key events related to the fish behavior.

3.9 Summary of system specifications

Taking into consideration the research questions that has been discussed previously, this section presents a summary of the retrieved system specifications:

- The measurement system must cover the frequency region ranging from 8 Hz to 8 MHz. The analysis will be divided into three different bands in order to optimize separately the design of each one of them:
 - the low frequency band 8 Hz-256 Hz
 - the nominal band 256 Hz-131 kHz
 - the high frequency band 131 kHz-8 MHz.
- As for the measurement combination, a current excitation signal and a voltage response analysis system must be used. The stimulation current has to be tunable ranging from 10 μ A to 300 μ A.

-
- Regarding the electrodes configuration, it has been decided to use both the 4-electrode and the 2-electrode configurations, which will enable us to retrieve not only the fish tissue impedance but also isolate the electrode-tissue interface impedance in post-processing.
 - In terms of the expected bioimpedance values. the experimentations using the MFIA impedance analyzer and the hand-held system show:
 - Fish tissue impedances ranging from several hundreds of Ω at low frequencies, decreasing to tens of Ω at the MHz region.
 - Total impedance (tissue electrode interface) values ranging from tens of $k\Omega$ at low frequencies to tens of Ω at the MHz region.
 - The fish tissue does not show any non-linear signatures, at least at the densities of current we are using. Theoretically, by increasing the current density non-linear signatures may appear, however this goes against the safety requirements that we have defined. Therefore, we simply limit our study to linear characteristics of the fish biological tissue.
 - The conducted experiments have shown that fish swimming activity may interfere with bioimpedance measurements, introducing measurement errors. In order for the integrated measurement system to be accurate, fast bioimpedance measurement must be performed. Moreover, in order to explore muscle activity related fish behavior, we need an EMG recording block embedded in the measurement system.

Chapter 4

Architecture definition

4.1 Introduction

The main objective of this thesis is to design an integrated bioimpedance measurement system capable of measuring a wide range of biomarkers for long periods of time (typically, from 6 months to 1 year measurement campaigns). Obviously, by tailoring the system to explore a large scope of physiological variables, the constraints ruling the design of such system become challenging.

In the previous chapter, several design challenges have been presented and discussed, a preliminary set of specifications has been summarized in section 3.9. Taking into consideration the design challenges enumerated previously, the main goal of this chapter is to define the most suitable architecture for the case studies of this research work.

4.1.1 Methodology and research questions

Following the research methodology detailed in chapter 1, the study presented in this chapter aims to be as much general as possible for exploration of biological tissue electrical properties. Thus, the defined architecture could serve for a wide scope of bioimpedance applications ranging from body composition assessment (Smith, Johnson, and Nagy, 2009) to blood characterization (Dai and Adler, 2009) or cancerous tissue detection (Aberg et al., 2004). This chapter aims to answer the following research question: taking into account the challenges ruling the design of bioimpedance spectroscopy integrated measurement systems, what is the most suitable integrated circuit architecture? After demonstrating that the constraints ruling the design of the architecture type could be categorized in two main measurement techniques depending on the frequency band of excitation, a state of the art of bioimpedance spectroscopy architectures is then presented. After comparing their advantages and drawbacks, a novel integrated circuit hybrid architecture suitable for exploratory bioimpedance applications is proposed.

Finally, a design process status of the first generation chip in-board critical blocks of the integrated circuit hybrid architecture is presented in the last section.

4.2 Specifications impact on the architecture

Taking into consideration the design challenges that has been discussed previously in chapter 3, the architecture of the bioimpedance integrated system should respect the following specifications:

- The α and β dispersions must be covered, which means that the architecture components should be able to operate at frequencies ranging from 8 Hz to 8 MHz.
- The architecture measurement combination is as follows : a controlled current signal is used to stimulate the biological tissue and the bio-modulated voltage is recorded for analysis.
- The stimulation current amplitude should be tunable ranging from 10 μ A to 300 μ A.
- The architecture must be able to switch between the 4-electrode and the 2-electrode configurations.
- The load impedance values range from tens of Ω at the highest frequencies to several hundred of Ω at the lowest frequencies for the 4-electrode configuration and from tens of Ω at the highest frequencies to several $k\Omega$ at the lowest frequencies for the 2-electrode configuration. The architecture components, especially the current driver and the instrumentation amplifier should be optimized for those values.
- The conducted experiments have shown that fish swimming activity may interfere with bioimpedance measurements, introducing measurement errors. In order for the integrated measurement system to be accurate, fast bioimpedance measurement must be performed. Ideally, a muscular activity recording block might be embedded in the measurement system as it could provide insightful data about the fish activity.
- As experiments have demonstrated that the fish tissue does not have any non-linear signatures (at the current magnitudes used in the experiments), simultaneous frequency excitation techniques can be used in order to shorten the measurement time frame.

4.3 Design constraints

4.3.1 Constraints

The main constraints ruling the design of integrated bioimpedance spectroscopy measurement systems are : measurement duration, precision, design complexity, and bandwidth.

In the context of the POPSTAR project, the integrated measurement system we are seeking to develop aims to be low cost in order to be deployed in large quantities, which means that design complexity should be kept minimal. The measurement campaigns have time horizons ranging from several months to a

year, the system power consumption is to be considered. Hence, clock speeds have to be maintained as low as possible.

As depicted previously, the α and β dispersions should be covered. Thus, the architecture blocks must operate in the frequency region ranging from 8 Hz to 8 MHz.

In our research context, bioimpedance measurements will be performed *in-vivo*, which means that different sources of errors such as muscle activity or temperature changes may have a significant interference on the bioimpedance signature if the measurement duration is too long. Therefore, fast bioimpedance spectroscopy should be performed not only to respect the system invariance criterion, but also to immune the measurements from interference related to the measurement configuration. In this context ruled by biological constraints, it is difficult to precisely define a minimal measurement duration. However, as a rule of thumb, in the following study we will target measurement durations below the second.

As a precision metric, the Signal to Noise Ratio (SNR) is to be considered. In our research context, the impedance expected values are relatively low. Obviously, the SNR cannot be improved by increasing the amplitude of the excitation signal, since it is limited by safety requirements (cf. chapter 3). Thus, care must be taken in order to maximize SNR over the frequency range of interest, whether it is by reshaping the noise level and/or by ensuring that the useful frequency component magnitude is maximal regarding the safety constraints.

In order to perform bioimpedance spectroscopy two measurement techniques can be found in the literature. The first measurement technique consists in measuring impedance one frequency at a time until the targeted frequency range is entirely covered. This is referred to as frequency sweep. This approach has the advantage of providing a high SNR, since the energy of the signal is concentrated on a single frequency bin at each iteration. However, since all the measurement chain is processed in series for each frequency component, this approach can lead to long measurement durations.

The second measurement technique consists in exciting the tissue using a composite signal containing all the frequency components of interest. It has the advantage of shortening the measurement duration as the whole bioimpedance spectroscopy is performed simultaneously. However, since the energy of the excitation signal is divided over all the frequency components of the band of interest, the SNR of each frequency component is decreased regarding the frequency sweep approach. Therefore These two approaches provide different trade-offs between measurement time and precision.

Before defining any architecture block, one can notice that an integrated circuit covering the α and β dispersions will face different design constraints depending upon whether it is operating at the lower limit or the upper limit of the frequency range of interest. Therefore, the analysis of the constraints can be divided into three different bands in order to optimize separately the design of each one of them :

- The low frequency band 8 Hz-256 Hz
- The nominal band 256 Hz-131 kHz

- The high frequency band 131 kHz-8 MHz.

The low frequency band

At the low frequency band, the main constraint is the measurement duration. This is essentially due to two factors. The first one has to do with long signal periods. Also, measurement time frames are longer if the entire measurement chain is processed for each frequency. Therefore, the use of a wideband simultaneous excitation is of great help. However, it is interesting to note that even with the use of wideband simultaneous excitation, the measurement duration is still significant. Indeed, the measurement duration is defined by the period of the lowest frequency components. In our case study, the low frequency band measurement duration will be constrained by the 8 Hz frequency which has a period of 125 ms.

The second factor is linked to filters. As their use in the architecture is mandatory, at this frequency band their establishment time is critical. Indeed, since we are dealing with low frequencies, the cut-off frequency of the filters has to be kept low, which enlarges their time constants, and by extension prolongs the measurement duration.

On the other hand, at this frequency band, the architecture has the advantage of requiring a low sampling clock frequency. Furthermore, the bioimpedance values are the highest at low frequencies, which does not constraint the SNR of the measurement.

The nominal frequency band

The nominal frequency band is the most used frequency band, whether it is in the literature or in commercially available circuits such as the AD5933 from *Analog Devices* or the AFE4300 from *Texas Instruments*.

At this frequency band, wideband simultaneous excitation could provide short measurement duration as the entire frequency band components are processed once. Compared to the operation of the same approach at the low frequency band, it is interesting to note that the measurement duration can be drastically reduced due to the relatively small periods.

The cut-off frequency of the architecture filters could be placed at higher frequencies, which will make the establishment times smaller than that of the same block at the low frequency band. However, the measurement duration is still significant.

On the other hand, at this frequency band, the architecture has still the advantage of requiring a relatively low generation clock frequency. The constraints on the SNR of the measurement are still not critical.

The high frequency band

At the high frequency band the main constraint is the measurement accuracy. This is mainly due to the fact that at high frequencies the bioimpedance magnitudes are the lowest. In this case, Series excitation could provide a high SNR,

since the energy of the signal is concentrated on a single frequency bin at each iteration.

It is interesting to note that due to relatively small periods and shorter establishment times for the architecture filters, the wideband stimulation technique does not provide a significant enhancement in terms of shortening the measurement duration.

Discussion

Figure 4.1 presents a visual summary of the previously detailed constraints of each BIS measurement approach depending on the frequency band.

BIS Approach	Frequency bands		
	8 Hz – 256 Hz	256 Hz – 131 kHz	131 kHz – 8 MHz
Series excitation	--	-	++
Simultaneous excitation	+	++	--



FIGURE 4.1: Constraints summary for each BIS measurement approach

We can observe that the constraints ruling the design of an integrated bioimpedance measurement system operating at the α and β dispersions will vary depending upon the frequency band of interest and the BIS measurement approach.

In order to break the trade-off between short measurement durations and precision, we have decided to use the wideband simultaneous excitation approach for the low and the nominal frequency bands, and the frequency sweep excitation for the high frequency band.

4.4 State of the art of BIS architectures

Building an integrated system for bioimpedance spectroscopy is very dependent on the application and ruled by several constraints. In fact, Designing an integrated measurement system capable of measuring a wide range of biomarkers for long periods of time is an outstanding challenge. Naturally, by tailoring the system to explore a large scope of physiological states, the design of such system becomes rapidly ruled by strong constraints such as bandwidth, precision, measurement time and safety.

In the literature, many bioimpedance analysis research studies use single frequency (mainly the 50 kHz frequency) bioimpedance architectures (Cox and

Hartman, 2005; Duncan et al., 2007; Willis and Hobday, 2008). However, we demonstrated previously that the complex impedance must be analyzed over a large range of frequencies, in our case the α and β frequency regions, to be able to extract pertinent physiological tissue properties.

From this perspective, we are only interested in BioImpedance Spectroscopy (BIS) architectures. As depicted previously, we can differentiate two types of BIS architectures. Architectures exciting the tissue at each frequency point in series (frequency sweep), and architectures exciting the tissue using a composite signal made of all the frequency components of interest. These architectures provide different trade-offs between measurement time and precision. In the next subsections we will dive into the characteristics of each architecture type.

4.4.1 Frequency sweep excitation architectures

In bioimpedance spectroscopy applications where high precision is needed, frequency sweep architectures (Rodriguez et al., 2016; Chen et al., 2017; *1 MSPS, 12-Bit Impedance Converter, Network Analyzer* 2005) are used in order to have a maximal SNR, since the energy of the signal is concentrated over a single frequency point each time.

On the signal generation side, different techniques can be used in order to generate the excitation wave. An analog sine wave generator for bioimpedance measurements has been presented in (Yufera et al., 2005), it uses a ramp integrator followed by a band-pass filter to generate the sinusoidal output. However, using this circuit over a wide frequency range is not an easy task. In fact, multiple channels are needed, which multiplies the complexity of the generation circuit or each of its blocks needs to be designed for a wide band operation which also increases the complexity of the circuit and the design effort.

One of the most used sine wave generation technique is Direct Digital synthesis (DDS) (*1 MSPS, 12-Bit Impedance Converter, Network Analyzer* 2005; *AFE4300 Low-Cost, Integrated Analog Front-End for Weight-Scale and Body Composition Measurement* 2017). DDS generates a discrete-time signal at a given frequency (usually a sine wave, but it can also generate triangular or square wave signals) in digital form, then digital to analog conversion (DAC) is performed to get the analog output. The output frequency depends on the generation clock frequency, and the binary tuning word which is hard-coded into the frequency register. The tuning word is fed to a phase accumulator which then outputs a code corresponding to a phase. A phase to amplitude converter (a look-up table) outputs the digital value to the DAC which converts the digital value to an analog voltage.

Because the DDS is digitally programmable, it offers the advantage of generating easily different waveforms as well as the ability to tune frequency without modifying the circuit components as it is the case for analog sine wave synthesis. However, its performances are also depending on the DAC precision. Also, the need of a DAC increases design complexity and the design effort.

Another interesting technique consists in combining digital signals to generate an analog sine-wave (Barragan et al., 2015; Rodriguez et al., 2016; Malloug et al., 2016). This technique consists of a first digital block generating square-wave signals with various characteristics (amplitude and/or relative phase).

Then, these signals are provided to another block that performs a clever summing, aiming at cancelling some harmonics on the output signal. As square-wave signals have harmonics which amplitudes decrease. The basic principle of harmonic cancelling is to concentrate the energy of the signal on the fundamental frequency bin while cancelling the harmonics. This technique is preferred for on-chip sine wave generation because it requires minimal resources while providing high performances.

On the response analysis side, the two widely used blocks are the lock-in amplifier (Yufera et al., 2005; Yang et al., 2009; Rodriguez et al., 2016) and the Discrete Fourier Transform (DFT) (*1 MSPS, 12-Bit Impedance Converter, Network Analyzer 2005*; *AFE4300 Low-Cost, Integrated Analog Front-End for Weight-Scale and Body Composition Measurement 2017*; Xu et al., 2015). Since the frequency sweep measurement approach is intended to be performed in the high frequency band, the DFT is not optimal as it requires the use of high speed Analog to Digital Converters (ADC).

On the other hand the lock-in amplifier technique is well suited for measurement in this frequency region. In fact, as lock-in amplifiers use phase-sensitive detection in order to extract the component of interest of the signal and reject the noise signal, the measurement of small AC signals is optimal.

Moreover, the architecture of the lock-in amplifier can be entirely digital using square signals as the reference frequencies and simple switches for the operation of multiplication which reduces drastically the complexity of this architecture block. Nevertheless, care must be taken to ensure that the harmonics of the square signals do not affect the quality of the measured signal. After the mixing operation, the frequency component of interest is translated into the baseband, which means that simple low-rate ADC's can be used to perform the digital conversion.

4.4.2 Wideband simultaneous excitation architectures

The longer the measurement duration, the higher the risk of disturbance by various sources of errors such as muscle activity (see section 3.8) to the measurement. More generally, in bioimpedance spectroscopy applications where the properties of the tissue under test are rapidly changing over time, fast bioimpedance spectroscopy should be performed in order to ensure accurate measurements. In exploratory contexts, where large frequency ranges need to be covered, this task becomes difficult. A solution is to use wideband simultaneous excitation signals in order to cover the chosen frequency range in a short time frame. However, the energy of the signal is spread among its frequency points. Thus, wideband architectures provide short measurement time but their precision decreases with the number of frequency components contained in the excitation signal.

Multi-frequency excitation signals can be aperiodic such as white noise or periodic such as multi-sine, maximum length sequences, or binary multi-frequency signals. In the literature, multi-frequency excitation signals are mostly generated using lab-tools or discrete circuits (Sanchez et al., 2012). Some studies present the design of integrated analog front-end circuitry while the signal processing of generation and response analysis are performed off-chip (Sun et al.,

2007; Xu et al., 2015). Very few studies deal with integrated multi-frequency signal generation.

Kassanos presented a CMOS multi-sine signal generator for bioimpedance measurements in his study (Kassanos and Triantis, 2014). Its basic block consists of a voltage controlled oscillator (VCO) that outputs a triangular wave, then triangle-to-sine Wave conversion is performed using a nonlinear wave shaping circuit. A dedicated block is used for each frequency, then current summing is used in order to generate the simultaneous excitation signal. For wideband simultaneous excitations, the presented solution will require the use of multiple copies of the oscillator which leads to a large surface area and high power consumption.

An attractive solution consists in synthesizing the multi-frequency excitation signals in pre-processing, implementing the result in a memory and using a DAC to get the analog simultaneous excitation stimulus. In order to lower the design complexity, binary signals could be used. The DAC design will then be simple to implement as it only outputs two analog levels. A low pass filter could be used afterwards to cancel the high frequency quantization noise.

In the response analysis side, the two widely used techniques are DFT and multi-channel lock-in amplifier. A multi-channel lock-in amplifier integrated circuit has been proposed for bioimpedance measurements in (Kassanos et al., 2014). It uses multiple versions in parallel of a lock-in amplifier each at a reference frequency corresponding to a frequency component of the multi-sine excitation signal. However, when dealing with wideband excitation as it is the case in our research context, the number of frequency components is significant. Therefore, the use of significant number of versions of a circuit block in parallel is impossible since it would lead to large surface areas, especially when we are dealing with low frequencies that require the use of filters with low corner frequencies that need large capacitances and resistances. An ADC followed by a DFT is a more optimal solution since we are dealing with low frequencies.

4.5 Proposed hybrid architecture

4.5.1 Wideband simultaneous excitation

Based on the previously enumerated constraints and the literature review of the different architecture blocks, we defined the Wideband simultaneous excitation architecture as follows (see figure 4.2):

In the signal generation side, we chose to use a memory register where the multi-frequency signal is hard-coded. This register is thus sampled by a clock. The result is fed to a Digital-to-Analog Converter (DAC) that transforms the binary signal to pre-defined voltage levels. a Low Pass Filter (LPF) is used in order to get rid of the high frequency quantization noise. A current driver is then used to convert the composite signal voltage to an excitation current.

In the response analysis side, an Instrumentation Amplifier (IA) is used to amplify the bio-modulated signal, an Analog-to-Digital Converter (ADC) converts the amplified signal to the digital domain, then a Discrete Fourier

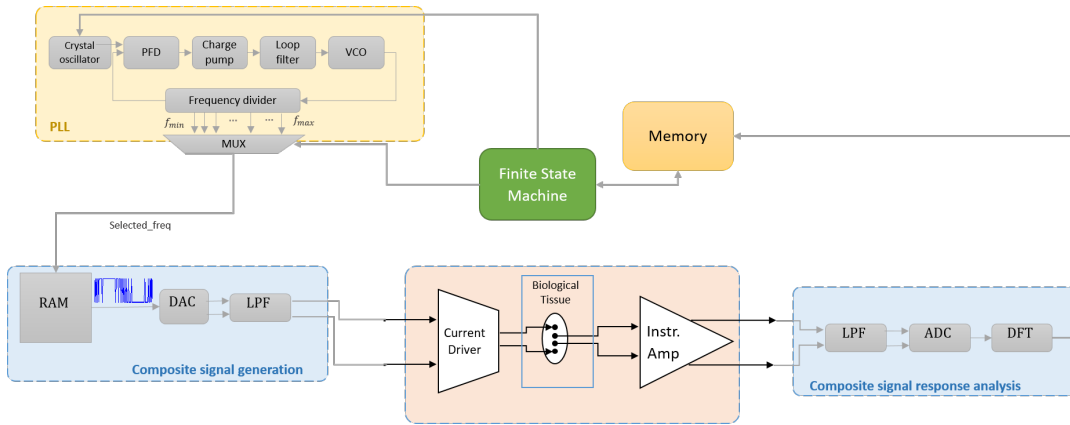


FIGURE 4.2: Wideband simultaneous excitation bioimpedance spectroscopy architecture

Transform is computed in order to determine the phase and amplitude of the frequency components of interest.

4.5.2 Frequency sweep excitation

Based on the previously enumerated constraints and the literature review of the different architecture blocks, we defined the frequency sweep architecture as follows (see figure 4.3 :

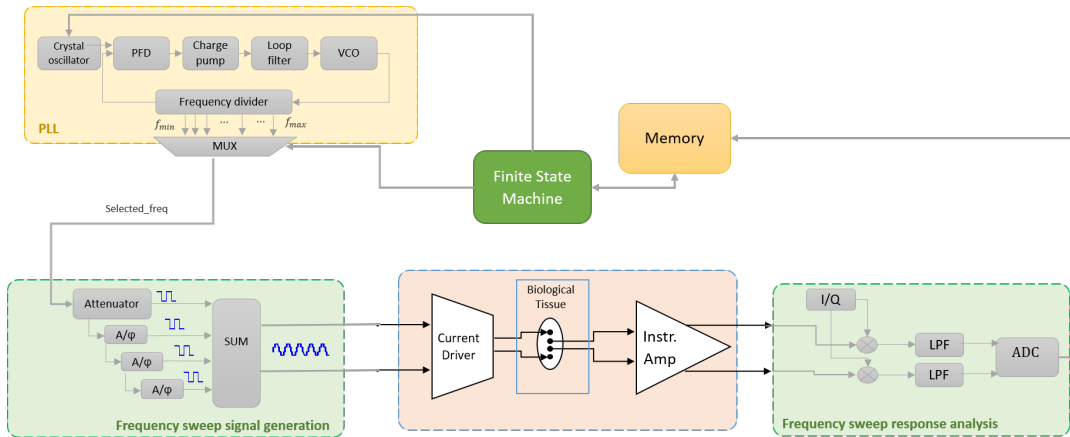


FIGURE 4.3: Frequency sweep bioimpedance spectroscopy architecture

In the signal generation side, a Phase locked Loop (PLL) is generally used as a frequency multiplier to get the higher frequency. On the negative feedback path, successive divisions are then performed to get the frequency components of interest. The digital signal is then scaled and delayed multiple times and the sum of the results is used to construct a sine wave of the targeted frequency. The scale coefficients and the phase shifts are computed so that the constructed signal has the lowest total harmonic distortion possible. A current driver is then used to convert the constructed sine wave voltage to an excitation current.

In the response analysis side, an IA is used to amplify the bio-modulated signal, then a lock-in amplifier followed by a simple low rate ADC is used to

feed the memory with bit words representing the real and the imaginary parts of the impedance.

4.5.3 Hybrid architecture

As previously presented in section 4.3. The constraints ruling the design of an integrated bioimpedance measurement system operating at the α and β dispersions will vary depending upon the frequency band of interest and the BIS measurement approach.

In order to break the trade-off between short measurement durations and precision, we have decided to use the wideband simultaneous excitation approach for the low and the nominal frequency bands, and the frequency sweep excitation for the high frequency band. From this perspective, we defined a hybrid architecture.

Figure 4.4 shows the proposed architecture, it is a combination of the frequency sweep and the simultaneous frequency excitation architectures described in subsections 4.5.1 and 4.5.2, hence the name "Hybrid architecture".

The Hybrid architecture uses a finite state machine in order to alternate between the multi-frequency generation and analysis for the low (8 Hz-256 Hz) and nominal 256 Hz-131 kHz frequency bands, then it switches to the frequency sweep architecture for the high frequency region (131 kHz to 8 MHz using the different multiplexers and demultiplexers).

For the multi-frequency part of the architecture, the size of the RAM is determined by the length of the generation bitstream and is defined by the following equation :

$$L_{bitstream} = \frac{F_s}{F_{min}} \quad (4.1)$$

with F_s being the sampling frequency and F_{min} the minimum frequency of the frequency band of interest.

It is interesting to note that by keeping the same ratio between the minimum frequency of the band of interest and the scanning frequency of the data register, and since frequencies are distributed as powers of 2 we can use the same bitstream for the low band and the nominal band. This is a significant advantage, since we only need to hard code the bitstream values in the data registers once and by just changing the sampling frequency it shall serve for both low and nominal frequency bands. The sampled data coming from the register are then fed to a DAC that converts the digital signal to pre-defined voltage levels. A LPF is then used to filter the quantization noise.

The architecture of the lock-in amplifier response analysis block is largely digital. The multipliers are simple switches controlled by the digital signals used for stimulus generation. This quasi-digital nature allows the architecture to be much more robust to the IC manufacturing variability and noise. On the other hand, this architecture only requires a reduced silicon surface and is easily configurable.

An EMG Signal acquisition chain is added to the architectures in order to record the muscular activity of the fish. It consists of an EMG amplifier, an anti-aliasing filter and an ADC. As the context of this work is exploratory and

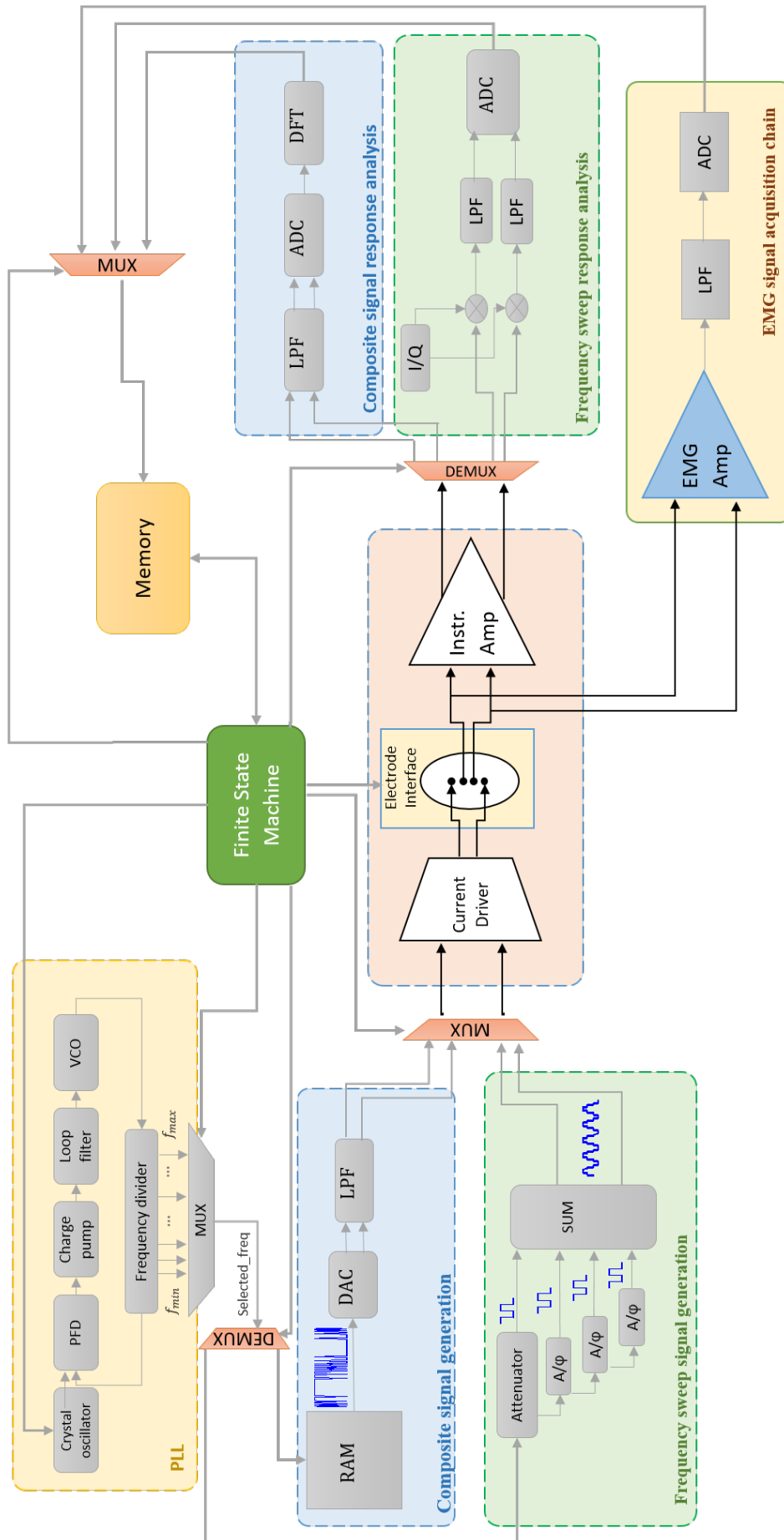


FIGURE 4.4: Hybrid bioimpedance spectroscopy architecture

muscular activity signatures could be related to key events in fish life such as chasing or escaping predators. The recorded data will be used in post-processing in order to study muscle activity related fish behavior and provide insightful data about fish short term and long term activity.

In order to monitor the evolution of the electrode-tissue interface impedance, which can translate the evolution of physiological processes happening in the interface. An electrode stimulation interface is used to switch between the 4-electrodes and 2-electrodes configurations. In post-processing the subtraction of the resulting impedances will permit the retrieving of the interface impedance.

The current driver and the instrumentation amplifier are common blocks to the two architectures. Thus, their design process is critical since they should be able to cover both the α and β frequency ranges. The instrumentation amplifier design and optimization are out of the scope of this research work as it only details the stimulation generation blocks of the architecture. From this perspective, chapter 5 presents a study of the stimuli generation blocks, the current driver design and optimization is detailed in the last chapter.

4.6 Design status of the integrated bioimpedance measurement system

Based on the results and conclusions presented previously in this chapter. The next step consisted in designing the first chip prototype implementing the bioimpedance integrated measurement architecture.

Aside from the architecture blocks enumerated in section 4.5, other blocks are needed in order to ensure several chip macro-functions. Globally, the chip should inboard the following blocks:

- The current driver that converts the constructed sine wave voltage to an excitation current.
- The instrumentation amplifier that amplifies the bio-modulated voltage
- The composite signal generation block
- The sine wave construction block
- The lock-in amplifier response analysis block
- The ADC-DFT response analysis block
- The finite state machine that will handle the different control signals of the architecture
- The Memory that will store the measurement data
- The EMG amplifier for the acquisition of muscular activity
- The measurement and stimulation interfaces that will enable the switching between the 4-electrodes and 2-electrodes configurations

- A power management block that will provide the reference currents and voltages
- A Phase Locked Loop which acts as a clock management block

The number of blocks to be implemented is significant regarding time considerations and human resources available to assist in the design process. Therefore, it has been decided to fragment the design process into incremental versions.

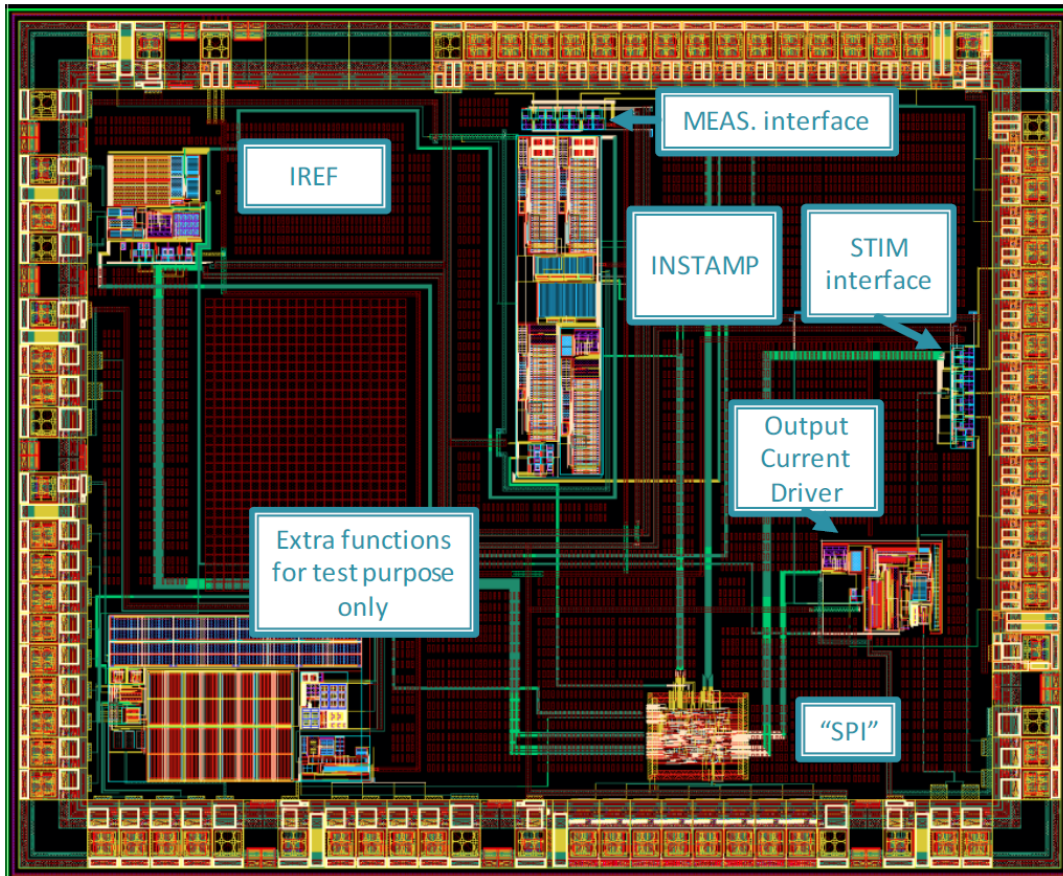


FIGURE 4.5: Layout of the first generation integrated circuit measurement system

The critical blocks are the ones that are near the interface with the biological tissue. Indeed, these blocks are under strong constraints that are not totally predictable. Moreover, the digital blocks are theoretically more robust to external interferences and don't need to be characterized in lab in order to validate their functionalities. indeed, digital blocks functionalities can be validated entirely by simulation using design automation tools. On the other hand the analog blocks design is pre-validated by simulations, but still needs silicium measurements for an entire validation. From this perspective, it has been decided that for the first version of the integrated measurement system, the following blocks are prioritized:

- The current driver that converts the constructed sine wave voltage to an excitation current

- The instrumentation amplifier that amplifies the bio-modulated voltage
- The measurement and stimulation interfaces that will enable the switching between the 4-electrodes and 2-electrodes configurations
- The power management block that will provide the reference currents and voltages
- A minimal digital communication interface which consists in digital registers for the control of the analog blocks parameters

The chip containing the previously enumerated blocks has been successfully designed in a 0.18 μm (Austria MicroSystems) AMS CMOS process operating at 1.8 V power supply. The circuit design, simulations and layout were developed with Cadence suite using the toolkit provided by the foundry. Figure 4.5 shows the layout of the chip.

The chip was designed by a team composed of 5 designers. Each designer worked on one of the previously enumerated blocks. After the design and simulation phase, each block was validated collectively during a design review session. In this chip design approach, I was in charge of the design and optimization of the current driver of the architecture.

The instrumentation amplifier, The power management block and the minimal digital communication interface design details are not presented in this work. The design of the current driver is presented in chapter 6.

4.7 Conclusion

A hybrid architecture providing fast measurements while maximizing precision has been presented in this chapter. It has been defined for the POPSTAR project as a special research context, and for biological tissue electrical properties exploration over a wide frequency range as general research context. The proposed architecture has critical blocks that need to be optimized for the system overall bandwidth (from 8 Hz to 8 MHz). Indeed, The current driver and the instrumentation amplifier are common blocks to the frequency sweep and the simultaneous frequency excitation sub-functions. Thus, their design process is critical since they should be able to cover both the α and β frequency ranges. The instrumentation amplifier design and optimization are out of the scope of this research work as it details the stimulation generation blocks of the architecture. From this perspective, chapter 5 presents a study of the stimuli generation blocks, while the current driver design and optimization is detailed in the last chapter.

This chapter also presents a status of the design process of the proposed architecture blocks. Due to time considerations and human resources constraints, it has been decided that the first version of the chip which has been designed and sent to fabrication contains as a matter of priority the critical blocks of the architecture as well some macro-functions blocks.

Chapter 5

Stimuli generation

5.1 Introduction

This thesis aims to design an integrated bioimpedance measurement system. It is dedicated for the measurement of a wide range of biomarkers for long periods of time. Therefore, strong constraints such as power consumption, design complexity, bandwidth of operation and accuracy rule the design of the system.

After presenting the design challenges of such measurement systems in chapter 3, an hybrid integrated circuit architecture suitable for the research context of this thesis has been defined in chapter 4. The signal generation blocks (see figure 5.1) are critical and their performances affect the whole architecture performances. In this context, this chapter deals with the design and optimization of the signal generation part of the architecture. More specifically, the chapter presents the stimuli optimization process for the frequency sweep and the composite signal generations.

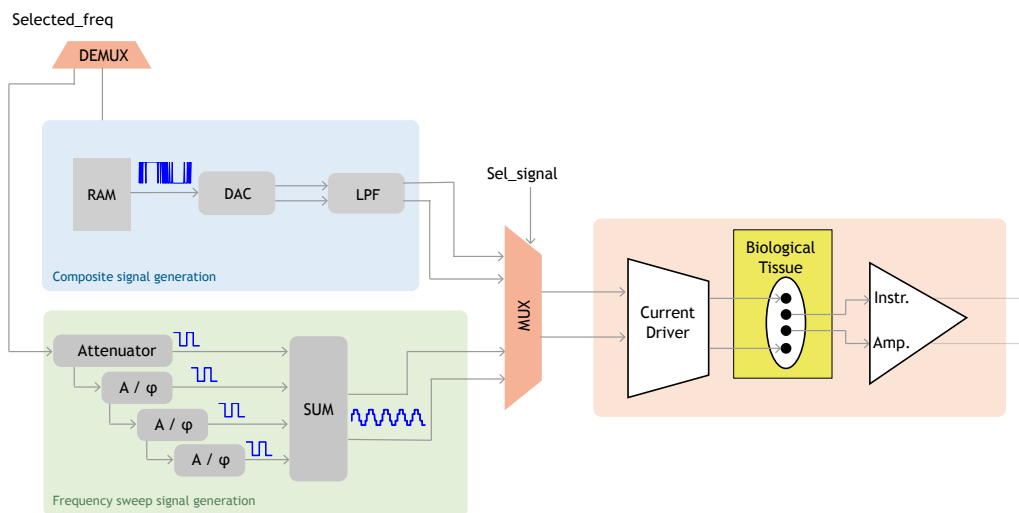


FIGURE 5.1: Excitation signal generation block

5.2 Sine-wave construction

5.2.1 Introduction

This section presents the stimuli optimization process for the frequency sweep part of the integrated bioimpedance measurement architecture (see figure 5.2).

The design of integrated sine-wave signal generator is a widely studied research topic. Such structures have several applications from impedance spectroscopy in general to bioimpedance spectroscopy in particular (Rairigh et al., 2009) They are also widely used in Built-In-Self Test (BIST) applications (Barragan et al., 2015). The main objective of designing an integrated sine-wave signal generator is to overcome the need for off-chip generation to drive the signal to the internal node. The constraints to design such an integrated generator are the required silicon area, the accuracy of the generated sine-wave signal and the robustness of the solution. As depicted in chapter 4, in order to minimize the generator size and its sensitivity to manufacturing process variations, it is relevant to use digital resources to generate the sine-wave signal.

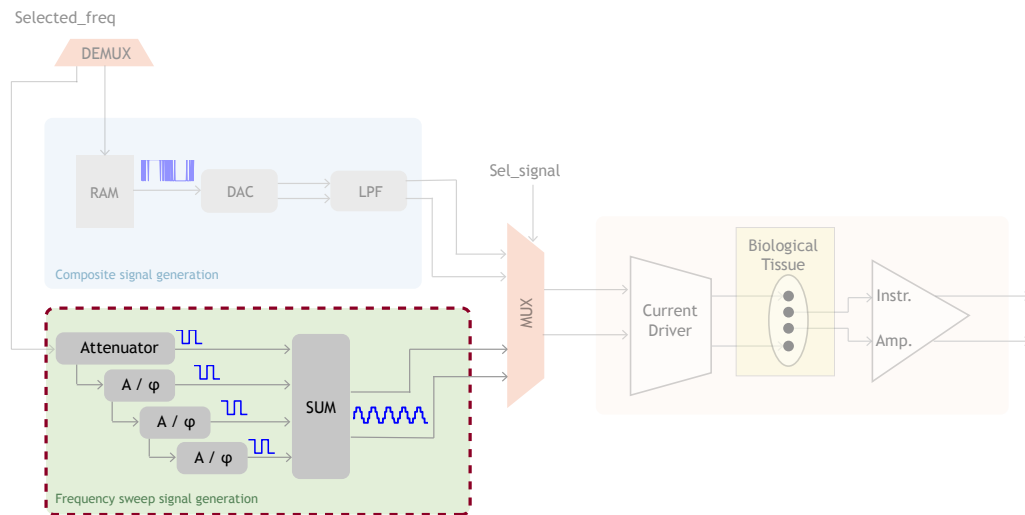


FIGURE 5.2: Sine wave construction block

An attractive solution consists in combining digital signals to generate the analog sine-wave (Barragan et al., 2015; Rairigh et al., 2009; Elsayed and Sanchez-Sinencio, 2010; Vasan et al., 2013; Aluthwala et al., 2014; Shi and Sanchez-Sinencio, 2015; Malloug et al., 2016). This solution, illustrated in Figure 5.2, consists of a first digital block generating square-wave signals with various characteristics (amplitude and/or relative phase). Then, these signals are provided to another block that performs a clever summing, aiming at cancelling some harmonics on the output signal. The basic principle of harmonic cancelling is to sum square-wave signals with different characteristics in order to concentrate the energy of the signal on the fundamental frequency bin while cancelling low-order harmonics. Generally, a low-pass filter is used to remove residual high-frequency harmonics. However, it has been demonstrated (Rodriguez et al., 2016) that for high frequency generated signals the impact of

residual high-frequency harmonics is negligible. In our case study, the sine-wave generation will be used for the high frequency band (from 131 kHz to 8 MHz), which means that the uncanceled harmonics of each frequency component are far away from its useful frequency band. Moreover, the biological tissue has a low pass behavior, which means that as far as the lower harmonics are canceled, we can neglect the residual high-frequency harmonics.

In order to implement such a solution, the number of required signals, amplitudes, frequencies and relative phase-shifts have to be defined. The architectures described in the literature are strongly application-driven solutions. As a consequence, there is no theoretical analysis of the optimized values of the required square-wave signal parameters.

Taking into account the constraints imposed by our research context, the sine-wave generation must be the most efficient trade-off between the three following constraints:

- **Quality** of the generated signal: We will mainly focus on performances in terms of linearity of the generated sine-wave. To that purpose, our key metrics will be the Total Harmonic Distortion (THD) ratio and the Spurious Free Dynamic Range (SFDR).
- **Hardware implementation:** The hardware implementation of the solution has strong impacts on accuracy. The hardware implementation complexity is also to consider. For instance, it is easier to generate a phase-shift as a fraction of the sine-wave period rather than an arbitrary phase-shift. Same thing for amplitudes: it is easier to generate signals with identical amplitudes rather than signals with arbitrary amplitudes.
- **Robustness** of the solution: The performances of the chosen approach must have a low sensitivity to parameters variations such as amplitude errors or jitter.

In order to define the digital sine wave generator parameters, several research questions dealing with our objective and constraints need to be answered:

- Is it efficient to strongly constrain the phase-shift of the square-wave signals and precisely adjust their amplitude?
- Is it more efficient to keep one amplitude for any square-wave signal and adjust precisely their relative phase-shift?
- Is adjusting precisely their phase-shift and amplitude the ultimate solution?

In the following subsections, these different approaches will be discussed and an analytical study of square-wave parameters for efficient sine-wave generation will be presented. After choosing the most efficient sine-wave generation technique, we will then discuss the implementation issues facing the integrated circuit designer.

To do so, we begin by defining the parameters of the square-wave signals to be tuned in order to perform the harmonic cancellation. We then provide the analytical study of harmonic cancellation for two different approaches. Finally, a study of the robustness of the best solution is provided in the last subsection.

5.2.2 Basic principle and constraints of harmonic cancellation techniques

Square-wave signal parameters

In order to change the distortion of a generated sine-wave signal, several square-wave signal parameters can be tuned. For each square-wave signal m , these parameters are the amplitude A_m , the phase φ_m and the duty cycle r_m . In order to optimize the harmonic cancellation with M square-wave signals $3 \times M$ parameters have to be defined. However, it can be demonstrated that it is possible to reduce the number of parameters to be considered.

Symmetry of generated square-wave signals

As illustrated in figure 5.3, using M square-wave signals to generate the sine-wave signal, if M is an even number, $M/2$ signals have symmetrical phase shift compared to the other $M/2$ signals. In case of odd number of square-wave signals, one of the signals is in-phase with the targeted sine-wave signal. Thus, $p = (M - 1)/2$ signals have symmetrical phase shift compared with the other p signals.

Therefore, we define the square-wave signal names m going from $-p$ to p . Since the signals are symmetrical $A_m = A_{-m}$ and $\varphi_m = -\varphi_{-m}$.

The duty cycle can be set aside. Indeed, if we consider two square-wave signals with a symmetrical phase shift φ_m , they are two signals with a duty cycle of $r_m = \frac{\pi - 2\varphi_m}{2p}$. As a consequence any duty cycle can be generated with symmetrical signals.

5.2.3 Fixed phase-shifts and adjustable amplitudes of square-waves

A possible solution for harmonic cancellation is to set the phase-shifts φ_m as ratios of the sine-wave period (keeping in mind implementation constraints) and arbitrarily adjust the amplitudes A_m of each square signal to sum. Such a solution has been described in (Malloug et al., 2016). Values of phase-shifts φ_m and amplitudes A_m of each square-wave to sum are expressed in Equation 5.1.

$$\begin{cases} \varphi_m = 2\pi \frac{m}{N} \\ A_m = \cos(2\pi \frac{m}{N}) \end{cases} \quad (5.1)$$

with $N = 4(p + 1)$ and $m = \llbracket -p, p \rrbracket$

We can analytically show that this solution cancels the first harmonics. Equation 5.2 gives the Fourier series decomposition of the sum of the M square-wave signals.

$$y(t) = \sum_{m=-p}^p \sum_{k=-\infty}^{\infty} C_{k,m} e^{ik\omega t} \quad (5.2)$$

The Fourier coefficients given by equation 5.3 are the sum of the Fourier coefficients of the square-wave signals.

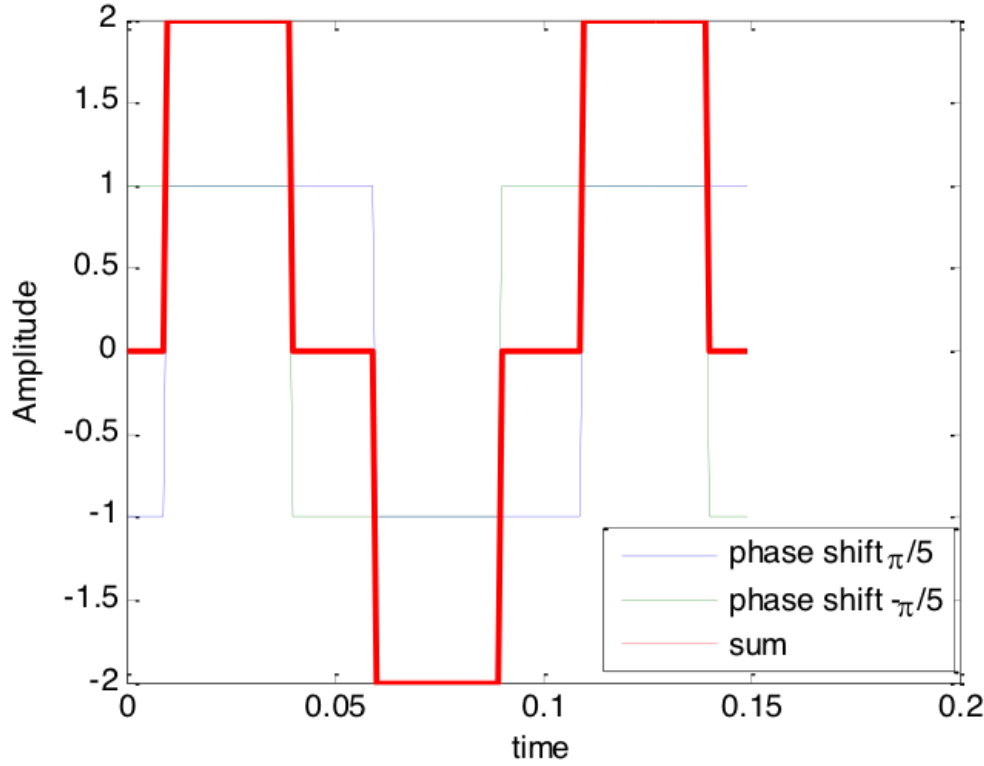


FIGURE 5.3: Symmetry of sine-wave signal generated by summing square-wave signals

$$C_k(y) = \sum_{m=-p}^p \frac{\cos(2\pi \frac{m}{N})}{k\pi} (1 - e^{ik\pi}) e^{-ikm2\frac{2\pi}{N}} \quad (5.3)$$

We can develop equation 5.3 as :

$$\begin{aligned} C_k(y) &= \frac{2}{k\pi} \sum_{m=-p}^p \frac{e^{2\pi \frac{m}{N}} + e^{-2\pi \frac{m}{N}}}{2} e^{-ikm2\frac{2\pi}{N}} \\ &= \frac{1}{k\pi} \sum_{m=-p}^p e^{2\pi \frac{m}{N}(k-1)} + e^{-2\pi \frac{m}{N}(k+1)} \quad (\text{for odd } k) \end{aligned} \quad (5.4)$$

Considering that the sum of the roots of unity is zero. We can observe that $\sum_{m=-p}^p e^{-2\pi \frac{m}{N}(k+1)}$ cancels when k is not equal to $N - 1$ (where, as defined previously, $N = 4(p + 1)$). This implies that $C_k(y)$ is equal to zero except for $k = \{1; 4(p + 1) - 1; 4(p + 1) + 1; 8(p + 1) - 1; 8(p + 1) + 1; \dots\}$.

Thanks to this approach, harmonics below $4(p + 1) - 1$ are cancelled. Thus, M signals can cancel harmonics with order below $2M + 1$ for odd M .

Figures 5.4 and 5.5 provide respectively the temporal and spectral representation of a sine-wave signal for five square-wave signals $M = 5$.

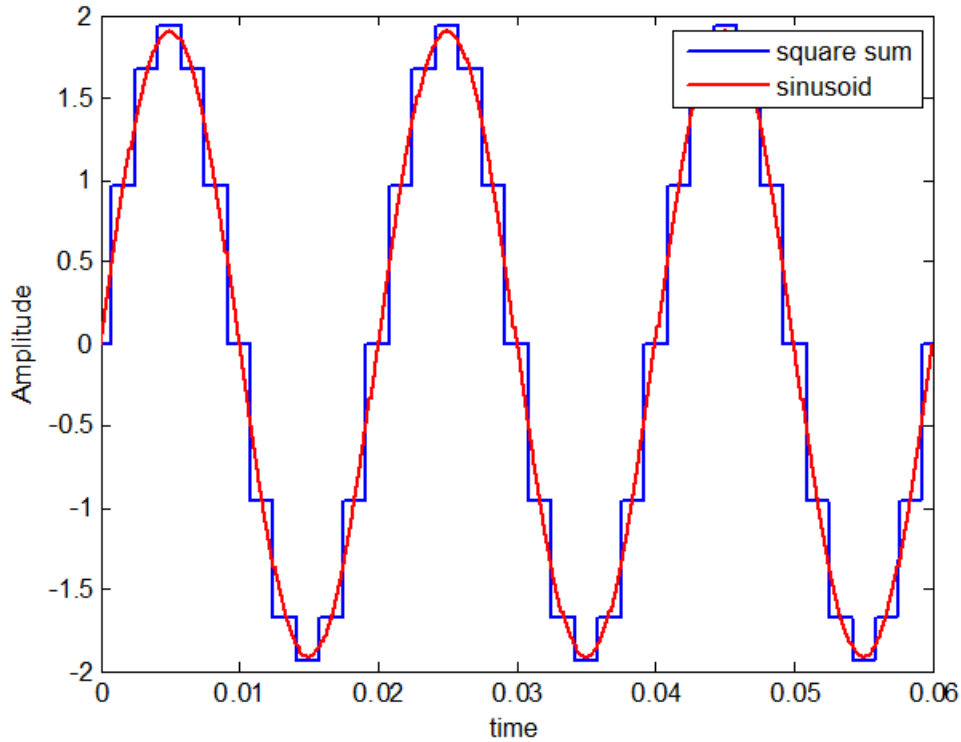


FIGURE 5.4: Sine-wave signal generated using square-wave signals with various amplitudes for five signals ($M = 5$)

5.2.4 Fixed amplitudes and adjustable phase-shifts of square-waves

Another approach consists in setting the amplitudes to the same value and adjusting the phase-shifts to cancel the harmonics.

$$\begin{cases} \varphi_m \text{ adjustable} \\ A_m = 1 \end{cases} \quad (5.5)$$

Two approaches can be used:

- A minimization technique, with a search over the phase shifts values for minimal THD.
- An analytic study with a theoretical approach.

Minimization technique

Let us consider the Fourier coefficients of the generated signal:

$$C_k(y) = \sum_{m=-p}^p \frac{-i}{k\pi} e^{-ik\varphi_m}, \text{ for odd } k \quad (5.6)$$

To define the values of the φ_m phase-shifts, we propose to minimize the THD ratio provided by Equation 5.7

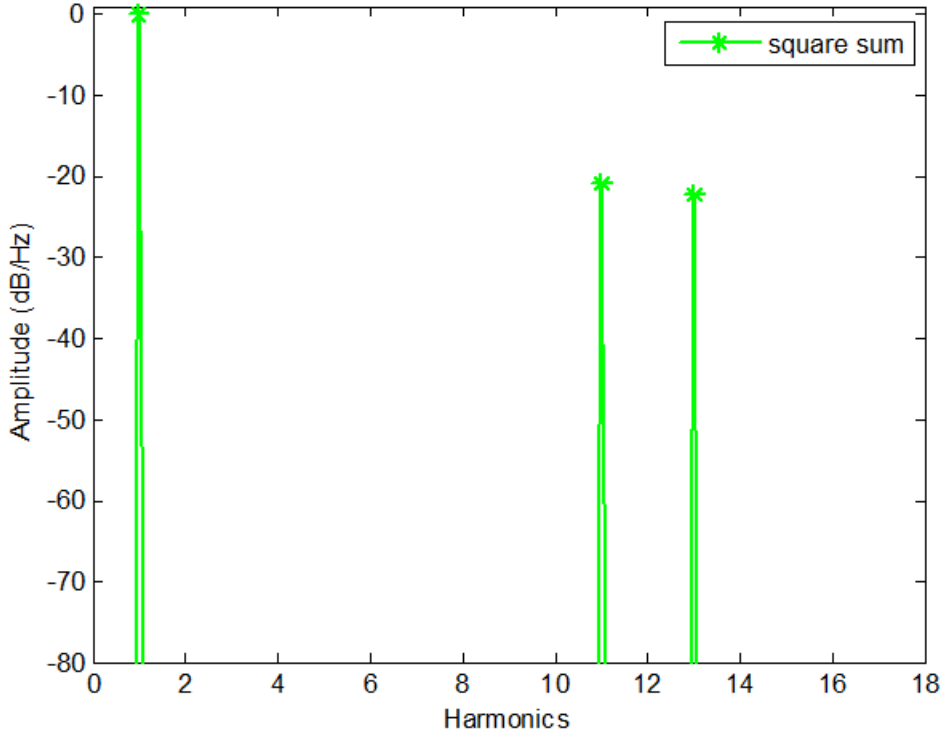


FIGURE 5.5: Spectrum of sine-wave signal generated using square-wave signals with various amplitudes for five signals ($M = 5$)

$$THD_{N_{har}} = \frac{\sqrt{\sum_{m=2}^{N_{har}} |C_k|^2}}{|C_1|} \quad (5.7)$$

N_{har} is the number of harmonics to be cancelled. For the first integer values of N_{har} we run a search for a minimum algorithm on $THD_{N_{har}}$ with equation 5.7 in matlab. We observe that it is possible to cancel $THD_{N_{har}}$ when N_{har} is below $M + 3$ and the number of signals M is even.

Figures 5.6 and 5.7 provide respectively the temporal and spectral representation of a sine-wave signal generated for six square-wave signals $M = 6$

The approach proposed in the subsection 5.2.3 can already be considered more efficient because it cancels more harmonics and requires less square-wave signals. In addition, it seems that the requested accuracy of the phase-shift is very constraining. Let's consider the equation 5.8 that provides the Fourier series coefficient affected by a phase-shift error.

$$C_k(y) = \sum_{m=-p}^p \frac{-i}{k\pi} e^{-ik(\varphi_m + 2\pi D_\varphi)}, \text{ for } k \text{ odd} \quad (5.8)$$

Figure 5.8 presents the harmonic distortion ratio variation for a random phase-shift deviation D_φ normally distributed from 10^{-4} to 10^{-2} of a period.

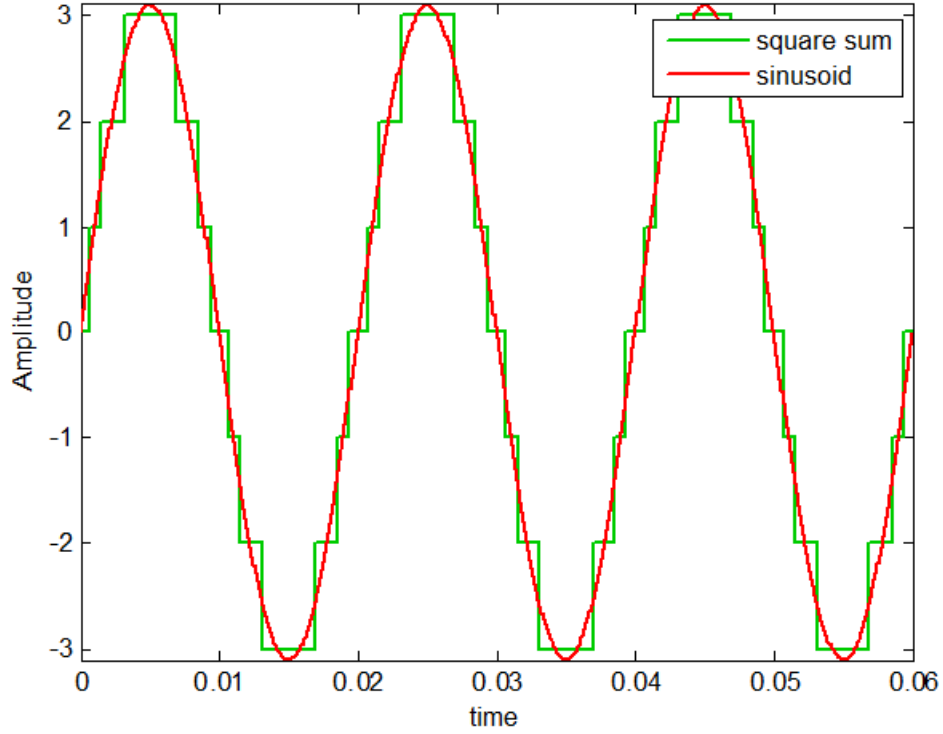


FIGURE 5.6: Sine-wave signal generated using square-wave signals with various phase shifts for six signals $M = 6$ with $[\varphi_1; \varphi_2; \varphi_3] = [0.2037; 0.4701; 0.9784]rad$

As presented by Figure 5.8, we observe by simulation that harmonic distortions affected by a phase-shift error of 10^{-3} of a period, have an amplitude of $-50dB$.

To give an example, as illustrated by figure 5.8, in order to reach a harmonic cancellation of the order of $-50dB$ when generating a sine-wave of frequency 10MHz, a digital frequency higher than 10GHz is necessary. Such a high clock frequency strongly constraints the design of the generator.

Analytical approach

Malloug and al. (Malloug et al., 2017) has analytically developed some solutions that cancel the harmonics by summing square signals with unitary amplitudes. The values of phase shifts are therefore analytically known and represent a reasonable fraction of the period of the main signal to generate. The analytical solutions, written as vectors, are:

$$\begin{cases} \varphi_p = \left[\varphi_{p-1} + \frac{\pi}{2(2p+1)} & \varphi_{p-1} - \frac{\pi}{2(2p+1)} \right] \\ A = \left[1 & 1 & \dots & 1 \right] \end{cases} \quad (5.9)$$

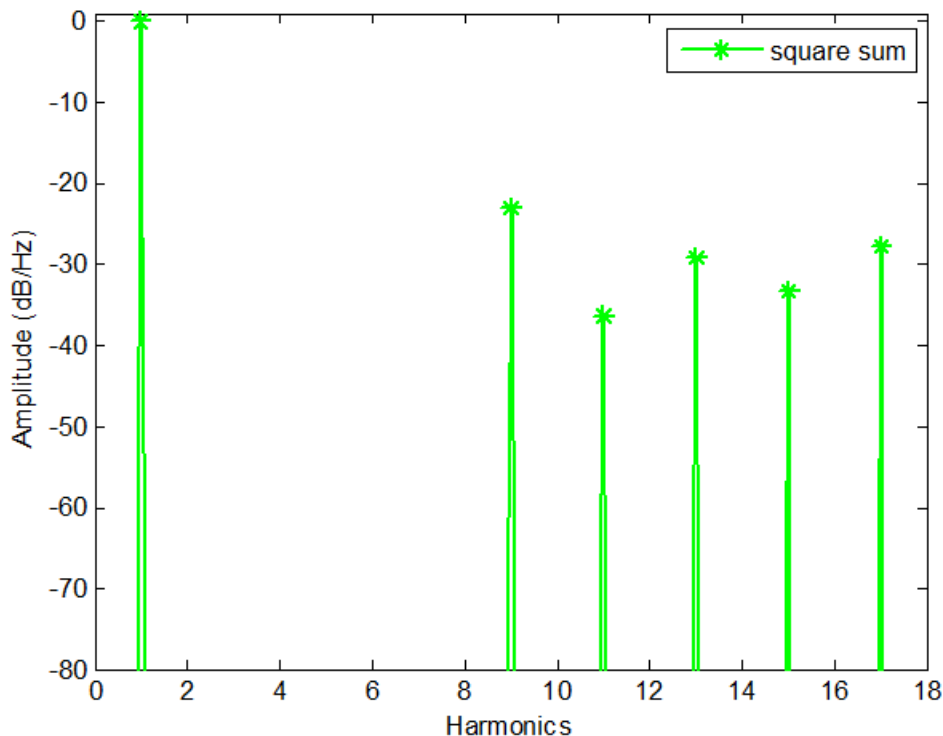


FIGURE 5.7: Spectrum of sine-wave signal generated using square-wave signals with various phase shifts for six signals $M = 6$

With φ_p being the phase-shift values and p being the number of odd harmonics cancelled. For example to cancel harmonic 3 and 5:

$$\begin{cases} \varphi_2 = \begin{bmatrix} \pi/6 + \pi/10 & -\pi/6 + \pi/10 & \pi/6 - \pi/10 & -\pi/6 - \pi/10 \end{bmatrix} \\ A = \begin{bmatrix} 1 & 1 & 1 & 1 \end{bmatrix} \end{cases} \quad (5.10)$$

This method permits to have phase shifts that represent an integer division of the period of the signal generated. This permits a much simpler implementation as it is very difficult to generate arbitrary phase shifts like it is requested in subsection 5.2.4. However the number of square signals that have to be summed grows exponentially with the number of harmonics to cancel.

5.2.5 Adjustable amplitudes and adjustable phase-shifts of square-waves

Releasing the constraints on amplitudes and phase shifts doesn't seem to enable the cancellation of more harmonics. Without an analytical theory it is impossible to conclude with certainty on this fact. However, we have sought to minimize the next harmonic with the minimization of $THD_{N_{har}}$ method in simulation and have not found any improvement. Moreover, an intuitive analysis of the number of parameters and the number of harmonics to cancel leads us

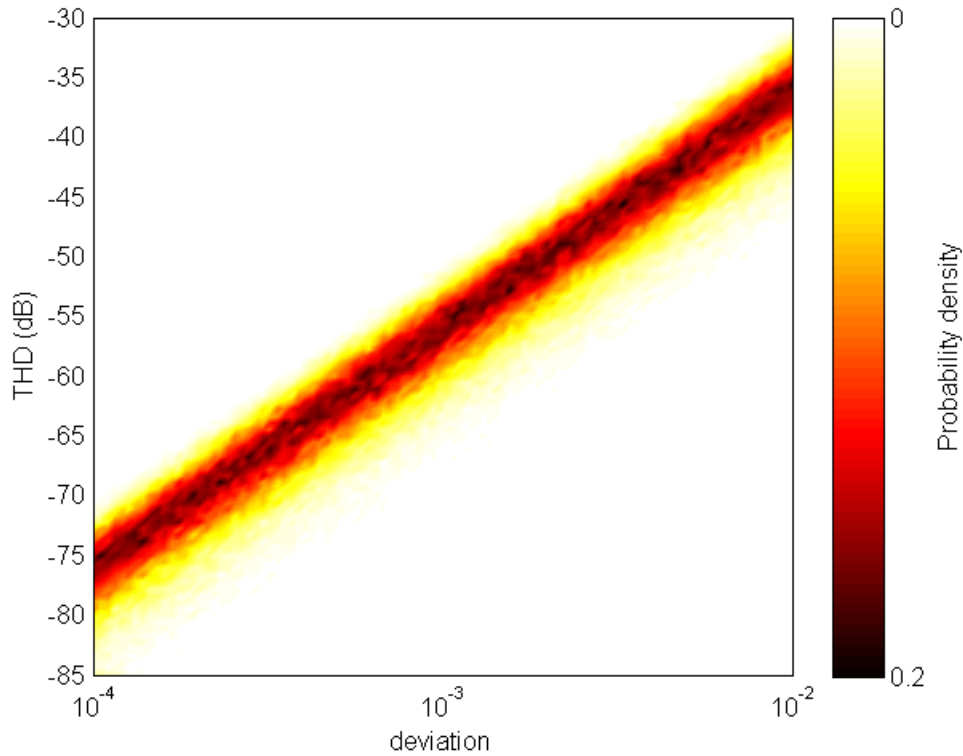


FIGURE 5.8: THD ratio variations due to varying phase-shift error Monte-Carlo results for a sine-wave signal generated using square-wave signals with various phase shifts for six signals $M = 6$

to think there is no improvement possible. Indeed, taking five signals $M = 5$ as an example, since amplitudes and phase shifts are relative to other square waves added, the parameters that we can adjust are the amplitude ratio and the phase shift of 4 signals, adding up to 8 parameters. The parameters are symmetric two by two, leading to only 4 adjustable parameters. The adjustable amplitudes method already permits to cancel the first 4 odd harmonics : 3, 5, 7 and 9. This does not provide any more degrees of freedom for parameters to cancel another harmonic. The default phase shifts used in the adjustable amplitude method are already optimum.

Therefore, we conclude that in fact combining the adjustable phase shifts and the adjustable amplitude method does not provide any improvement in the number of harmonics canceled.

5.2.6 Conclusion on harmonic cancellation techniques

As mentioned in subsection 5.2.2 one of the important parameters is M , the number of square-wave signals to generate. M can then be linked to the number of harmonics to cancel. The number of square-wave generators to design is thus linked to the accuracy specifications of the architecture.

Figure 5.9 shows the performances of the various solutions to cancel harmonics. Each one has pros and cons.

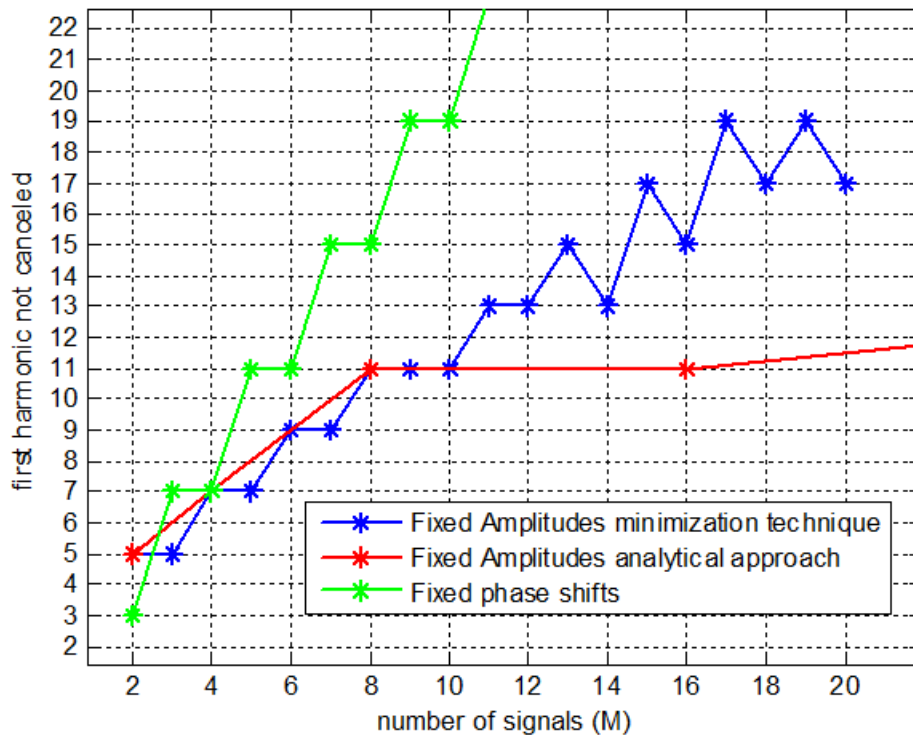


FIGURE 5.9: Comparison of harmonic cancellation techniques

The fixed amplitudes with minimization technique has the benefit of having equal amplitudes of square-wave signals but the requested accuracy of the phase-shift is very constraining.

Fixing amplitudes and determining analytically the phase shifts as described in (Malloug et al., 2017) offers a reasonable division of the main period. This allows a suitable implementation of the clock generation. Theoretically, this technique only cancels harmonics in a logarithmic way with the number of signals but still stays as efficient as the minimization technique for 8 or less signals.

Among these techniques, the technique using real coefficients as ratios of amplitudes for the summed square-wave allows to cancel the most harmonics. Moreover, the phase shifts generated are the largest and thus the easiest to implement. However, since the ratios are irrational numbers this technique is hard to implement for matching purposes.

5.2.7 Hardware implementation

The generation of square-wave forms with ratio amplitudes can be implemented through resistor voltage divider or current mirrors. We seek to benefit from the technique that cancels the most harmonics (i.e. Fixed phase shifts described in section 5.2.3) without matching issues.

In order to facilitate the matching of the components (resistors or transistors) in the implementation, it is required that the ratios between the amplitudes of the signals to be added are integer fractions. As illustrated in Figure 5.14,

introducing approximated ratios leads to harmonic distortions. Figure 5.10 has been computed in the particular case as an example of:

$$\begin{cases} \varphi_m = \frac{\pi}{6}, \frac{\pi}{3} \\ A_m = \frac{1}{2}, \frac{\sqrt{3}}{2} \end{cases} \quad (5.11)$$

$$\text{approximated to } \begin{cases} \varphi_m = \frac{\pi}{6}, \frac{\pi}{3} \\ A_m = \frac{1}{2}, \text{round}\left(\frac{\sqrt{3}}{2}d\right)\frac{1}{d} \end{cases} \quad (5.12)$$

We thus seek the integer fraction that introduces the lowest error. We observe in Figure 5.10 that it is not necessarily the integer fraction with the largest denominator that introduces the lowest distortion.

A better approach to approximate a real number with a rational number is through continued fractions of the form described in Equation 5.13. Indeed, if we take the continued fraction expansion of an irrational number α and cut it off after n^{th} iterations, this resulting rational number is known as the n^{th} convergent of α . From The Law of Best Approximates, a theorem by Lagrange (Theorem 5.9 in (Burger, 2000)), these convergents are precisely the best approximates of an irrational number. These values are reported as red dots in Figure 5.10.

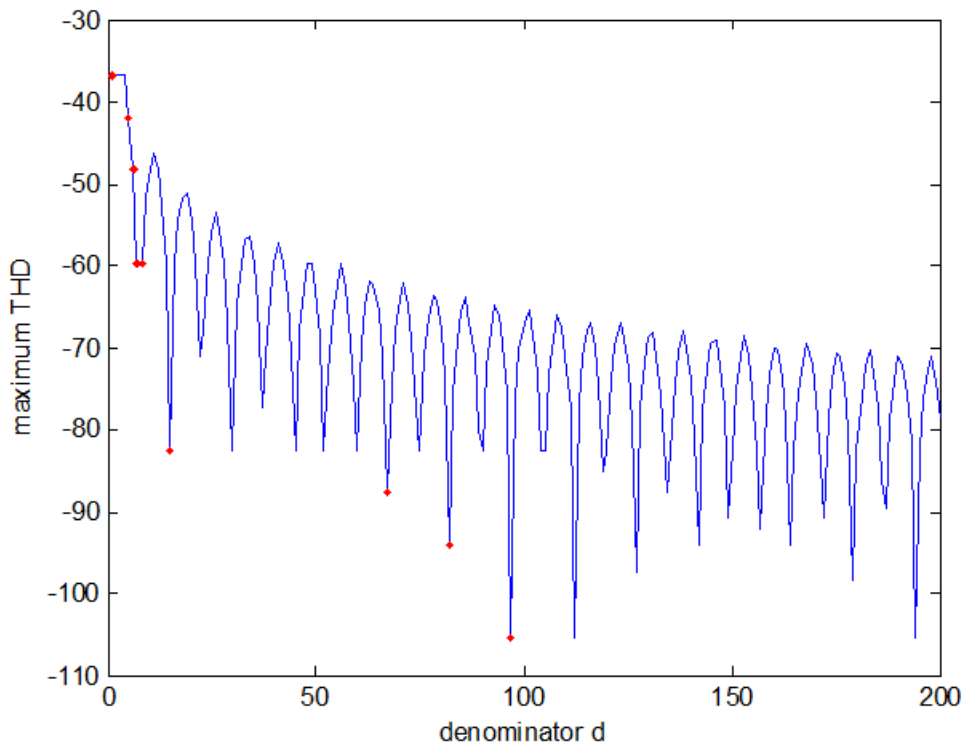


FIGURE 5.10: THD of a sine-wave generated using square-wave signals with approximated amplitudes with fraction with denominator d

$$a = a_0 + \frac{1}{a_1 + \frac{1}{a_2 + \frac{1}{a_3 + \ddots}}} \quad (5.13)$$

We can compute analytically the harmonic distortions generated with the signal composed of square-waves of amplitudes with the approximation up to n iterations on the continued fractions.

$$A_{mn} = a_{m0} + \frac{1}{a_{m1} + \frac{1}{a_{m2} + \dots + \frac{1}{a_{mn}}}} \quad (5.14)$$

The more iterations we proceed on the continued fraction, the more precise it becomes as illustrated in figure 5.11 .

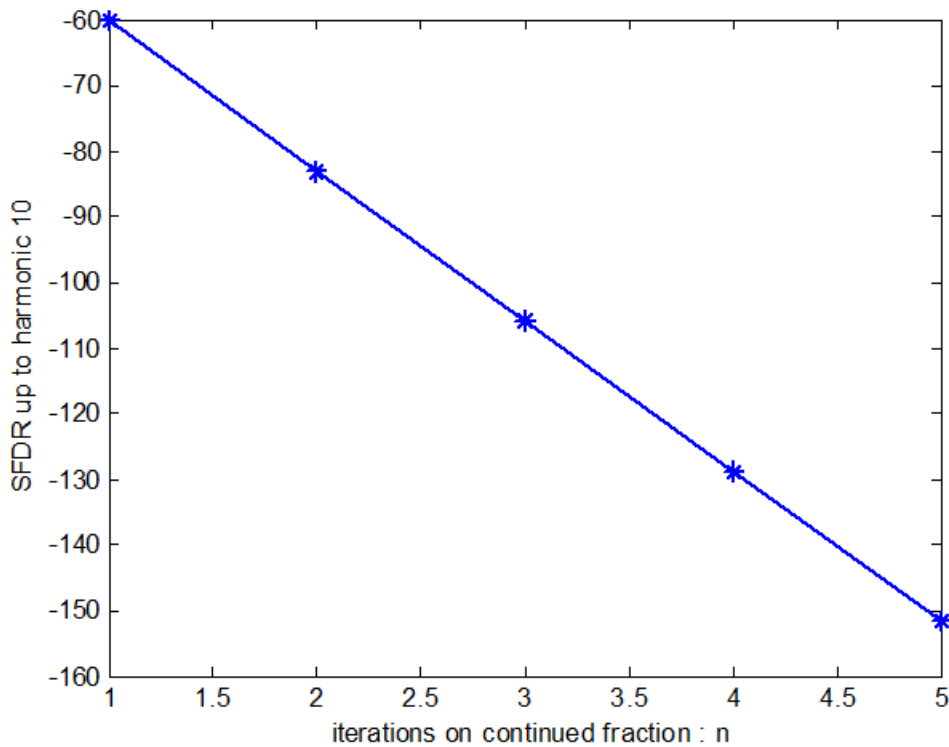


FIGURE 5.11: SFDR of a sine-wave generated using square-wave signals with approximated amplitudes with iteration on continued fraction

Figure 5.12 presents the THD and figure 5.13 the SFDR, for $N_{Har} = 11$ in equation 5.7, depending on the number of signals used and the number of iterations on the continued fraction. We can see that, although the SFDR is linear with the number of iterations on continued fraction (as shown in Figure 5.11),

for any given number of signals it varies from one number of square signals to another.

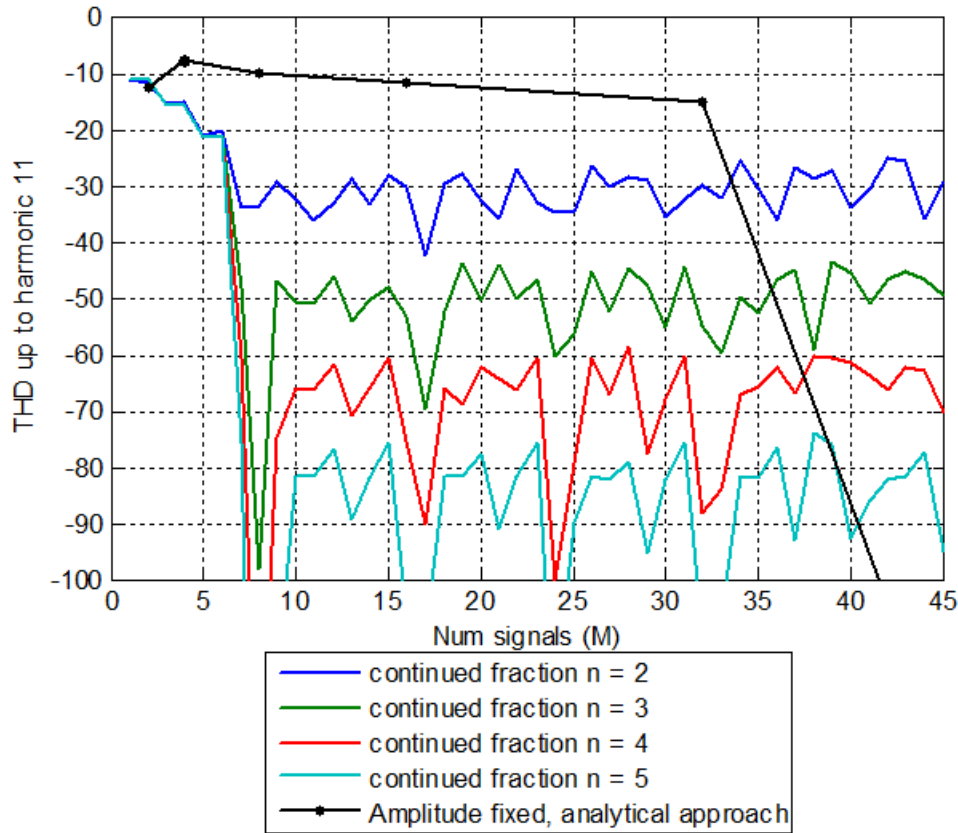


FIGURE 5.12: THD up to harmonic 11 of a sine-wave generated using square-wave signals with approximated amplitudes with n iterations on continued fractions

However, the number of iterations on continued fraction does not necessarily represent the complexity of the current mirror, or resistance bridge, that has to be implemented. Indeed, the number of components needed would rather be proportional to the sum of the denominator and the numerator. It is thus up to the integrated circuit designer to consider a solution with less square signals to sum but lots of components or a solution with more signals to sum but with a smaller number of components for each one and a faster generation clock. Regarding the constraints imposed by our research context, the first implementation approach is to be considered, as the number of square signals to sum and the slower generation clock reduce the design complexity and the power consumption.

5.2.8 Robustness study

Even if robustness is implicitly high because of the digital-based approach of the proposed methods, the impact of errors on the linearity for the generation were

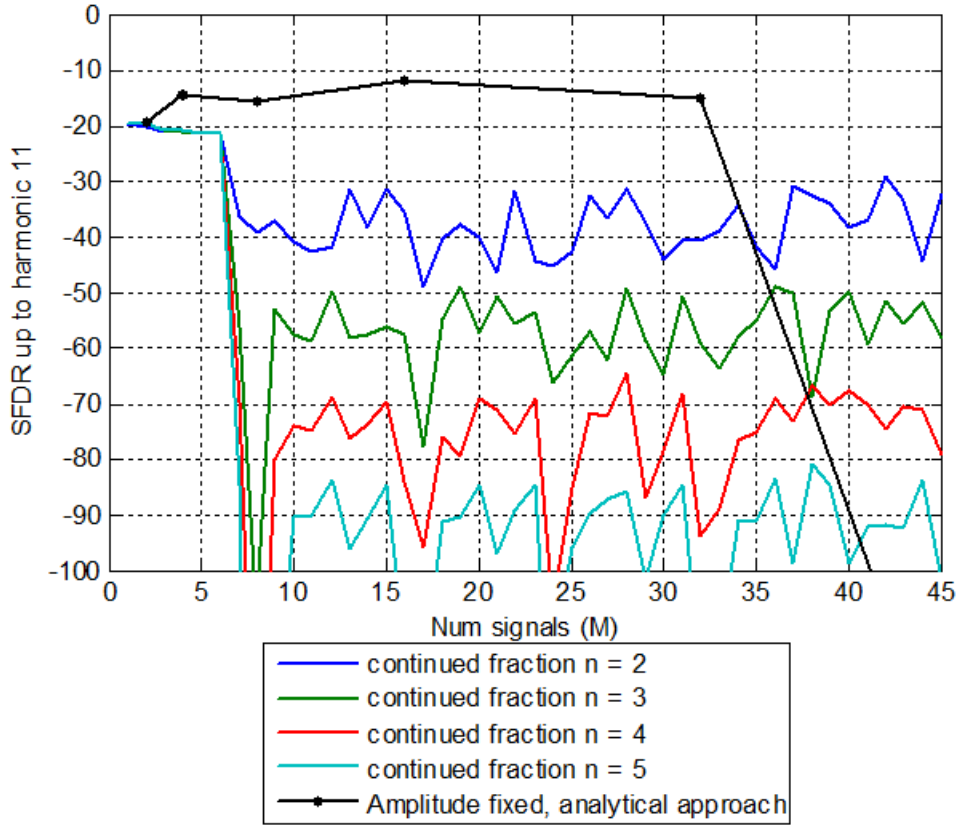


FIGURE 5.13: SFDR of a sine-wave generated using square-wave signals with approximated amplitudes with n iterations on continued fractions

studied using adjustable amplitudes of square-wave signals. For this purpose, an example was used with amplitudes defined as follows :

$$\begin{cases} \varphi_m = \frac{\pi}{6}, \frac{\pi}{3} \\ A_m = \frac{1}{2}, \frac{\sqrt{3}}{2} \end{cases} \quad (5.15)$$

$$\text{approximated to } \begin{cases} \varphi_m = \frac{\pi}{6}, \frac{\pi}{3} \\ A_m = \frac{1}{2}, \frac{13}{15} \end{cases} \quad (5.16)$$

In order to approximate $\frac{\sqrt{3}}{2}$, we use the algorithm presented in the previous section, with continued fraction expansion up to the 3rd iteration, as it is a good compromise between precision and design complexity. Possible variations are phase-shift error, jitter and gain error on amplitude. Jitter is a random value normally distributed added to the time variable in the simulation.

Figure 5.14 presents the spectrum of the sine-wave generated with $p = 2$, this is five square signals summed up : $M = 5$. This sine-wave signal is affected by jitter and/or gain error of the amplitude of the square-wave signals. We observe that the error on the amplitude of the square-wave induces an amplitude

increase of the harmonics initially cancelled. The jitter induces an increase of the noise level. The study in (Shi and Sanchez-Sinencio, 2017) presents a sinusoidal signal synthesizer architecture based on a fixed phase shifts with a similar approach. A robustness study has also been conducted by sweeping the amplitude and phase errors using transistor level monte-carlo simulation data. It is interesting to note that transistor-level simulation results for the third harmonic (HD3) are similar to the harmonic distortion results of our analytic model.

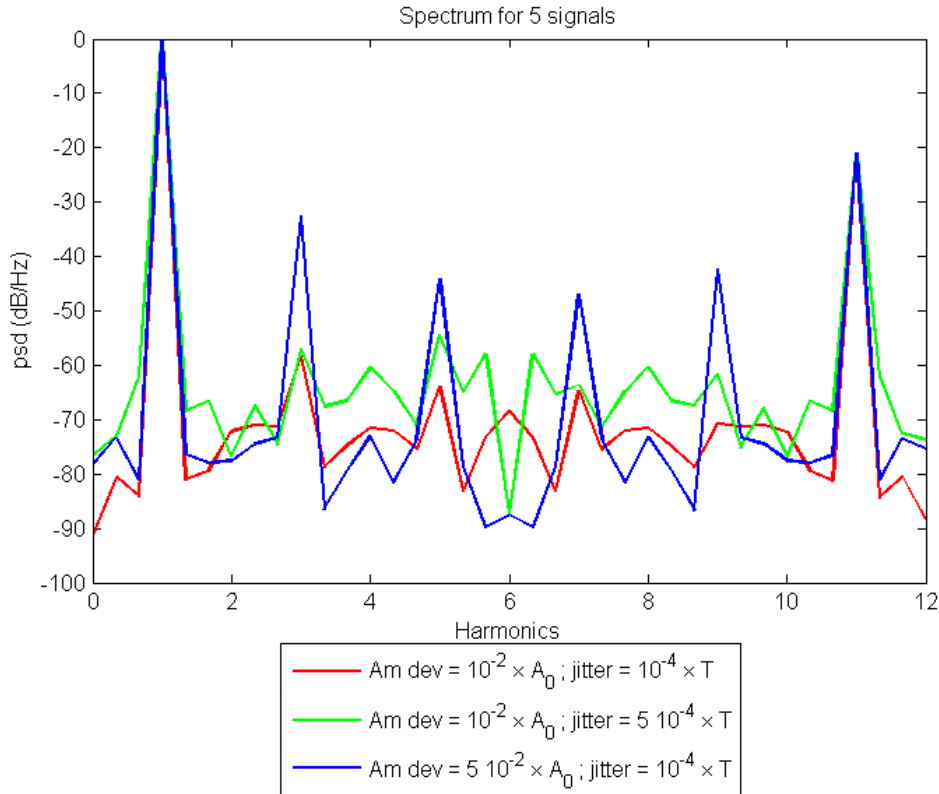


FIGURE 5.14: Spectrum of a sine-wave signal affected by amplitude error and/or jitter on the square-wave signals for sine-wave signal generated using square-wave signals with various amplitudes five signals $M = 5$

Figure 5.15 presents the computation of the harmonic distortion for various values of jitter. The jitter has also an impact that is significant on the harmonic distortion ratio. When the jitter is large, the noise floor created dominates the distortions introduced by the amplitude deviations.

According to the presented analytic study and simulation results we propose some features for an efficient implementation. Using five sine-wave signals, we can cancel harmonics below the eleven order. For a 10 MHz generated sine-wave, in order to have harmonic distortions at a maximum of -50 dB, jitter should be below 0.1 ns and the amplitude error should be limited to 1%. This approach can be used in any other combination of frequency, amplitudes and precision needed.

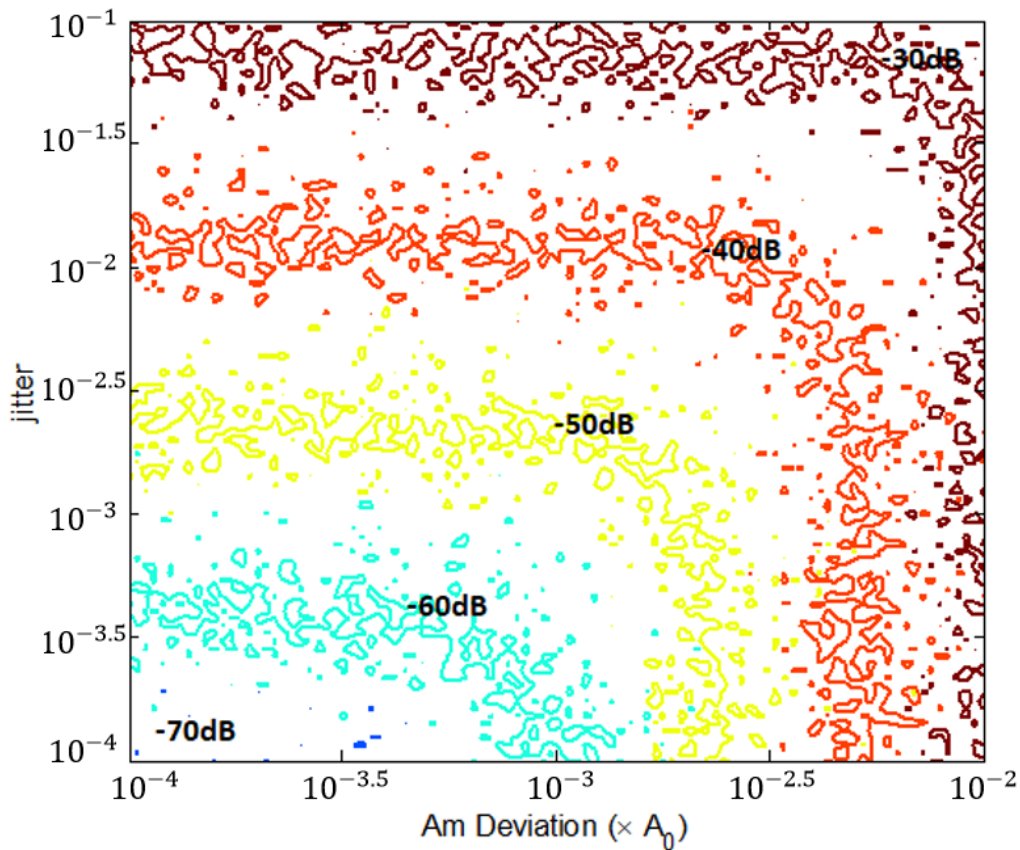


FIGURE 5.15: Total Harmonic distortion ratio of a sine-wave generated using square-wave signals with various amplitudes deviations and affected by various level of jitter

5.2.9 Conclusion

The research work presented in this section deals with generating sine-wave signals by summing square-wave signals in order to cancel low-order harmonics. The effectiveness of the harmonic cancellation is related to the characteristics of the square-wave signals. Two approaches are generally implemented. The first approach consists in setting the phase shifts according to the implementation technique and setting various amplitude values of the square-wave signals. The second approach is the inverse. It consists in setting the different amplitudes at the same value and setting various phase shifts of the square-wave signals. We have analytically proven that for a given number of square-wave generators, the first approach allows to cancel a higher number of harmonics. In addition, considering targeted specifications, we have proven by simulation that the first approach is less constraining in terms of clock generation. We have also offered a solution to the matching issue due to the irrational nature of the ratios. Thanks to a continued fraction development of the ratios computed analytically, a satisfying sine-wave approximation can be generated.

5.3 Composite signal generation

5.3.1 Introduction

The longer the measurement duration, the higher the risk of integrating different sources of errors such as swimming activity related interferences (see section 3.8) or temperature changes into the measurement. More generally, in bioimpedance spectroscopy applications where the properties of the tissue under test are rapidly changing over time, fast bioimpedance spectroscopy should be performed in order to ensure accurate measurements. In an exploratory context where large frequency ranges need to be covered, especially since low frequencies are considered, this task becomes difficult. A solution is to use composite signals in order to cover the chosen frequency range in a short time frame. However the energy of the signal is spread among its frequency points. Thus, composite signal generators provide short measurement times but their precision decreases with the number of frequency components contained in the excitation signal.

This section deals with optimization of the composite stimuli generation block (see figure 5.16). As depicted in the previous chapter, the low complexity constraints of the measurement system imposed the use of binary excitation signals. Thus, the stimuli data will be hard-coded into a memory, then a 1-bit Digital to Analog Converter(DAC) will be used to transform the binary signal to pre-defined voltage levels. A Low Pass Filter (LPF) is then used in order to get rid of the high frequency quantization noise. And finally, a current driver is used to convert the multitone voltage to an excitation current.

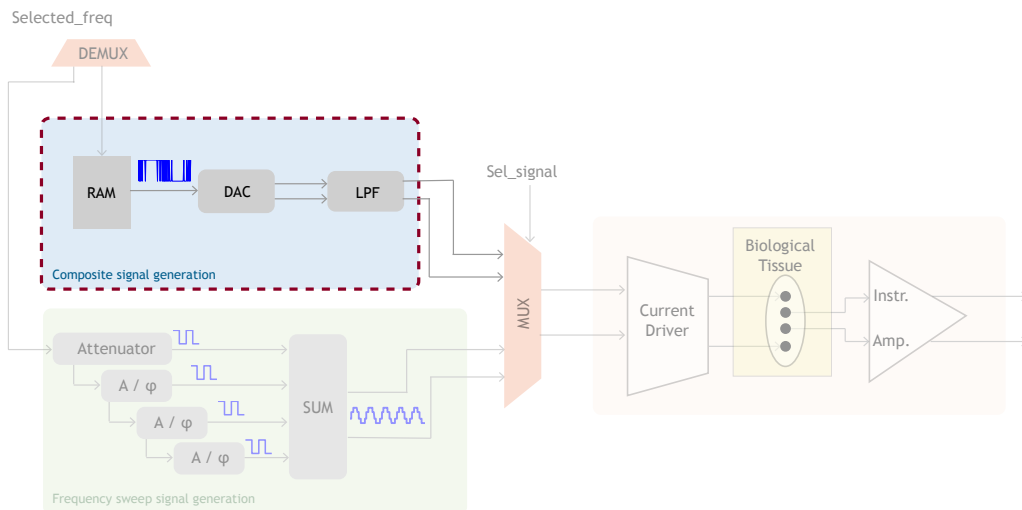


FIGURE 5.16: Multitone excitation signal generation block

The first multitone measurements of the impedance spectrum were presented in the early 1970s in a study (Creason and Smith, 1972) where the approach consisted in creating a signal composed of 15 ac waves for the characterization of the faradaic admittance of an electrochemical solution. One of the first pseudo random generators was presented in (Ichise, Nagayanagi, and Kojima, 1974).

The authors used a maximum length binary sequence (MLBS) generation based on a linear feedback shift register to characterize RC circuits.

More recently, the use of multitone excitation signals has not only emerged for impedance spectrum characterization of electrochemical systems in general (Gabrielli, Huet, and Keddari, 1992; Van Ingelgem et al., 2009; Jacek Ryl and Slepski, 2017) but also found its application in biological systems impedance characterization (Sun et al., 2007; Yang et al., 2009; Sanchez and Bragos, 2010; Land et al., 2011; Ojarand, Land, and Min, 2012; Xu et al., 2015; Ojarand, Rist, and Min, 2016).

However, choosing the most suitable excitation stimuli for a bioimpedance spectroscopy is not an easy task, especially in our research context where the measurement constraints imposed the use of a binary excitation signal and a low sampling frequency. In this particular case, care must be taken to ensure that the excitation signal quality is optimized. To do so, we will focus mainly on the signal to noise ratio (SNR) of the excitation signal as a key metric.

As our stimuli will be pre-synthesized on only 2 voltage levels and the sampling frequency is limited, the quantization noise will be the predominant source of noise, especially for the high frequency points of the band of interest.

The SNR of the global impedance measurement is dependent of the SNR of the injected current and the SNR of the bio-modulated voltage. Given that the bioimpedance spectra is decaying with frequency (see figure 5.17), the impedance magnitudes at the highest frequencies will be the lowest, and in order to ease the response analysis, we must ensure that the high frequency components of the injected signal are not drowned in quantization noise.

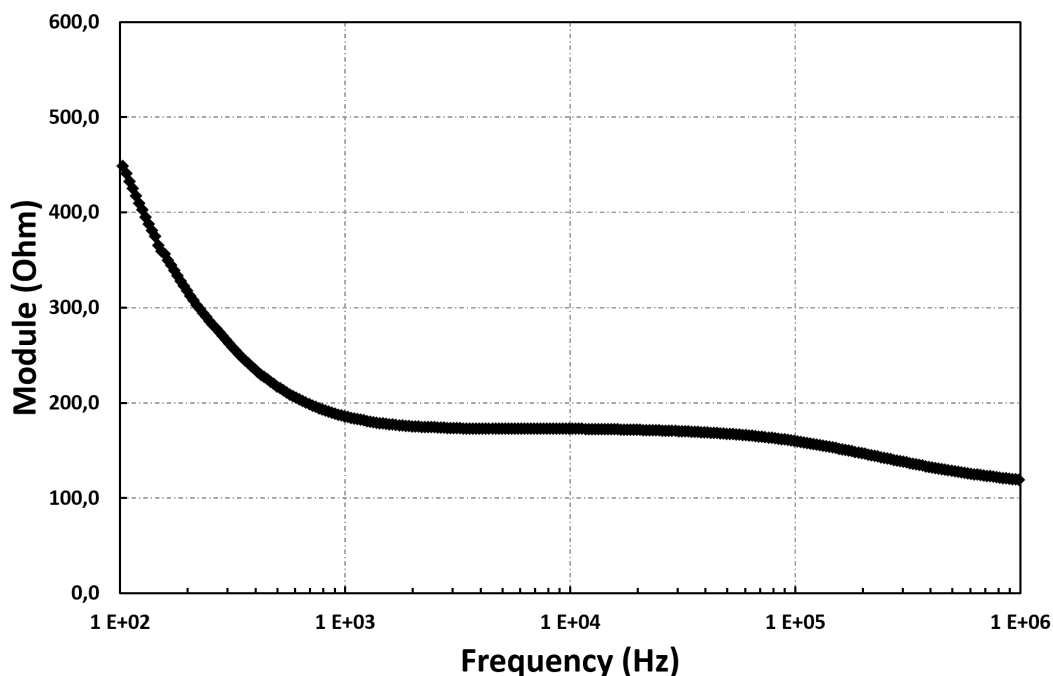


FIGURE 5.17: Bioimpedance magnitude of bluefin tuna using the MFIA impedance analyzer and the flexible electrodes (4-electrode measurements)

Furthermore, the amplitude of excitation is limited due to safety requirements. Knowing that the energy of the composite signal will be distributed among its frequency points, we must ensure as much as possible that the power level received by the load is maximal with respect to the excitation amplitude.

To this purpose, this section aims to find the most efficient excitation stimuli for exploratory applications of bioimpedance spectroscopy. To do so, the metrics defining the stimuli signal quality will first be introduced, then based on these metrics several multitone excitation signals will be compared and discussed. Finally, a novel multitone excitation optimized for bioimpedance spectroscopy measurements will be presented.

5.3.2 Signal quality metrics and comparison setup

For impedance measurements in general, several composite excitation signal types can be found in the literature. This excitation signals vary in terms of frequency and time characteristics. Therefore, in order to retrieve the best performing composite excitation technique, signal quality metrics need to be clearly defined for a fair comparison.

Signal to noise ratio (SNR) is an important metric, as it affects the accuracy of the bioimpedance measurements. The SNR is proportional to the power of the frequency components of the signal.

$$SNR_{dB} = 10 \log \frac{P_{signal}}{P_{noise}} \quad (5.17)$$

With P_{signal} being the power of the input signal and P_{noise} the power of noise. Noise can be caused by several sources such as the clock jitter, transistor noise, or quantization noise. In the following study we will assume that the quantization noise is the dominant noise source.

The Crest Factor (CF) is a widely used parameter in the comparison of composite excitation signals. It is defined by the following formula :

$$CF(x) = \frac{x_{peak}}{x_{rms}} \quad (5.18)$$

With x_{peak} being the peak value of the signal and x_{rms} being the root mean square value of the signal. The crest factor interpretation is quite simple, it is a measure of the DC equivalent level of the excitation signal for a peak injection value. Its lowest value is 1 and the closer the signal crest factor to 1, the more efficient is the excitation.

The CF and the SNR are closely related. In fact, if we consider a sine-wave signal digitized using an N_b bits analog to digital converter, it has been demonstrated (Sanchez et al., 2012) that the SNR and the CR are related by the following equation:

$$SNR_{dB} = 6.02.N_b + 1.76 - 20. \log \left(\frac{CF}{\sqrt{(2)}} \right) \quad (5.19)$$

Therefore, for a number of bits N_b the SNR is increased if the CF is low. It is interesting to note that if the input signal is a sine wave, which CF is $\sqrt{(2)}$,

the log term of the equation is canceled and we can retrieve the famous SNR formula of an Analog-to-Digital Converter.

In the next subsections we will be comparing several multitone stimuli generation techniques. For a fair comparison the simulation setup will be the same for each technique. The multitone signal will be composed of 8 frequencies distributed as powers of 2:

$$[1024 \ 2048 \ 4096 \ 8192 \ 16384 \ 32768 \ 65536 \ 131072] \text{ Hz} \quad (5.20)$$

The excitation time duration is set to 10 ms and the signal amplitude is set to 1. The sampling frequency is set to 4.194 MHz, which gives us an Over-Sampling Ratio (OSR) of 16.

As depicted in the previous chapter, the wideband simultaneous excitation architecture uses two filters, one at the generation side and one at the response analysis side. The filters order has been set to 2, as it is a good compromise between performances and design complexity. For illustrative purposes, the simulation of the filtered output will be done using a 4th order filter, which cut-off frequency will be set to $1.25 \cdot f_{max} = 164 \text{ kHz}$. The time domain signals have been multiplied by a Hanning window of the same length as the signals, before using a Fast Fourier Transform (FFT) to analyze their frequency content.

5.3.3 Multitone excitation techniques comparison

Square signal

The square-wave is the easiest composite excitation signal to generate. Its Fourier series decomposition can be written as:

$$x(t) = \frac{4}{\pi} \cdot (\sin(2\pi ft) + \frac{1}{3}\sin(2\pi 3ft) + \frac{1}{5}\sin(2\pi 5ft) + \dots) \quad (5.21)$$

Its frequency components are distributed as odd integer multiples of the fundamental frequency. However the amplitude of the frequency components decreases with the frequency (by a $1/f$ factor). The square-wave frequency content is presented in figure 5.18.

It can be demonstrated that 95% of the total energy of the signal is concentrated over the 4 first frequency bins. Obviously, this type of excitation is therefore inadequate for our research context as it can not provide enough energy for the higher frequencies of the range of interest.

Maximum Length Binary Sequence (MLBS)

The MLBS are pseudo-random periodic wideband binary excitation signals based on a sequence of length N. They can be easily implemented using digital resources. In fact, using a linear feedback shift register (LFSR) which is a shift register with exclusive or (XOR) feedback (see figure 5.19), the binary sequences can be generated to excite up to GHz frequencies using fast clocks. The length of the sequence (N_{MLBS}) is determine by the following equation, where n is the length of the used shift register.

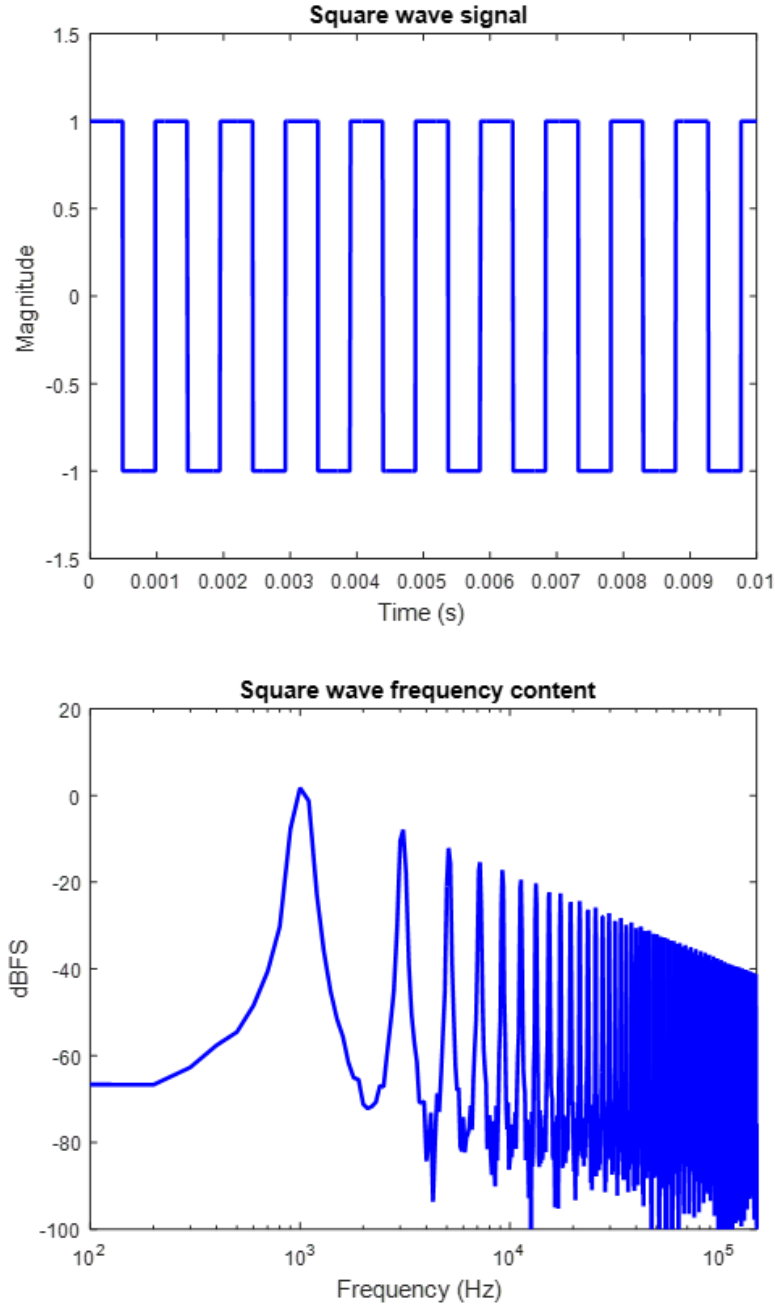


FIGURE 5.18: Square-wave signal in time and frequency domain

$$N_{MLBS} = 2^n - 1 \quad (5.22)$$

The frequency resolution of MLBS is a function of the clock frequency and length of the binary sequence:

$$f_{res} = \frac{f_{clk}}{N_{MLBS}} \quad (5.23)$$

The frequency spectrum of the MLBS signals follows a cardinal sine function, which means that its frequency components magnitudes decrease inversely with frequency. The biggest advantage of the MLBS excitation is its technical

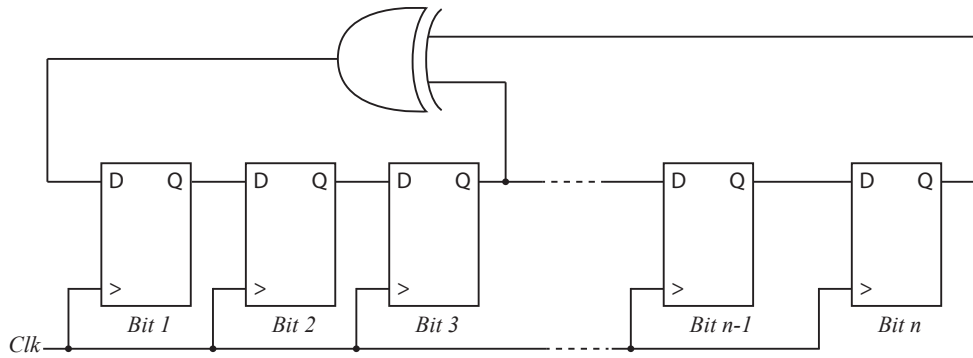


FIGURE 5.19: Linear feedback shift register based pseudo random generation

simplicity, and its robustness to noise due to the use of simple digital circuitry. However, because the energy is distributed densely over the whole frequency range, the signal energy is not all concentrated in the impedance frequency points of interest, and a relatively big part of it is wasted on exciting unwanted frequencies.

Binary Multitone Signals (BMS)

Binary Multitone signals are waveforms with only two discrete values $+A$ and $-A$. This signals are easy to implement and can be more effective than multisine signals (Land et al., 2011). This is mainly due to the fact that their crest factor is equal to 1, see equation 5.19 . For the same signal duration, the energy content of BMS is $\sqrt{2}$ higher than that of a multisine excitation signal.

Binary Multitone signals can be synthesized by summing the desired sine waves and then applying a sign function to the sum:

$$S_{BMS} = \text{sgn}\left(\sum_{k=1}^N A_k \cdot \sin(2\pi \cdot f_k \cdot t + \phi_k)\right) \quad (5.24)$$

The sign function could be implemented using level crossing at 0. The magnitudes A_k and phases ϕ_k of the frequency components and could be adjusted in order to reshape the frequency spectrum. In fact, when the properties of the system to be excited are unknown, it is convenient to keep the magnitudes and phases of equal values. When some of the properties of the system are known, it is interesting to reshape the frequency spectrum of the excitation signal in order to adapt it to the system.

Using Matlab, eight sinewaves corresponding to the frequency components of interests have been summed and the result normalized. In order to have a binary output signal, level crossing at 0 has been applied to the summed sinewaves. The power spectral density of the BMS is presented in figure 5.20. The power spectral density of the BMS signal after filtering is presented in figure 5.21.

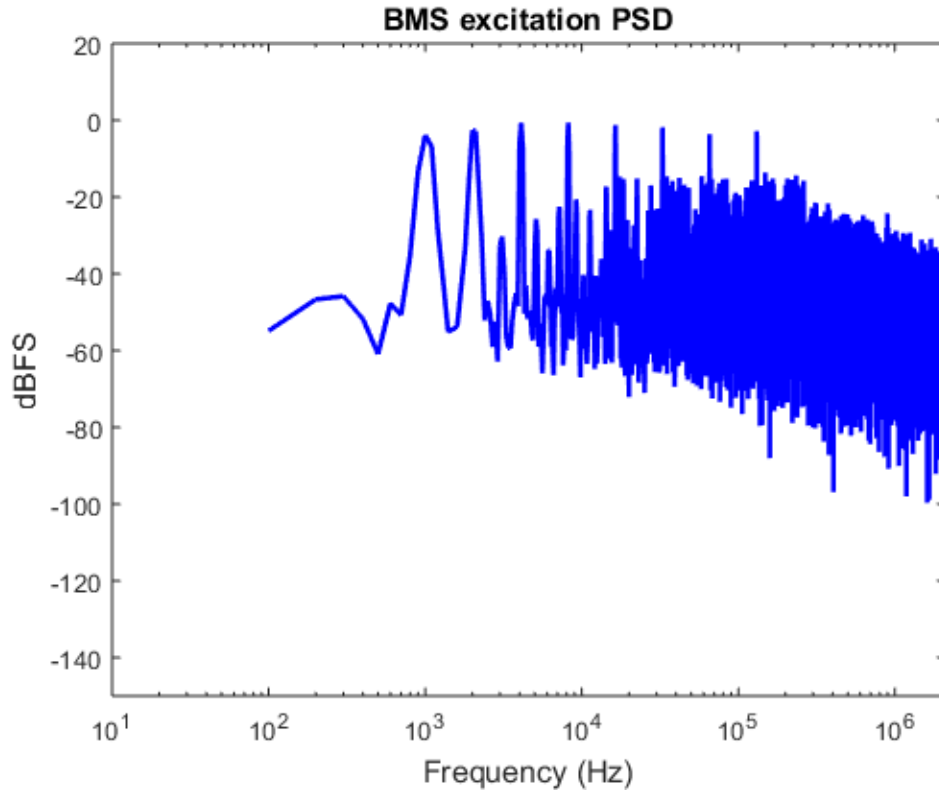


FIGURE 5.20: Frequency components of the BMS excitation technique

We can observe that the quantization noise is affecting the highest frequency components more than the lowest. This is problematic as the impedance spectrum of the biological fish tissue is decreasing towards high frequencies. In order to evaluate this phenomena we define a local SNR metric:

$$SNR_i(\text{dB}) = 10 \cdot \log\left(\frac{P_i}{N_i}\right) \quad (5.25)$$

with P_i the power of the frequency component of interest, and N_i the power of the local noise floor surrounding the frequency component of interest. We defined the noise floor N_i as the maximal power of the noise bins in the vicinity of the frequency point of interest. We defined the vicinity of the frequency point of interest as the frequency range $[0.8 \cdot f_i, 1.2 \cdot f_i]$.

Table 5.1 shows the local SNR's of the frequency components of interest.

In fact, the SNR of the global impedance measurement is dependent of the SNR of the injected current and the SNR of the bio-modulated voltage. Given that the impedance magnitudes at the highest frequencies will be low, and in order to ease the response analysis, the SNR of the high frequency components must be high to ensure that these components of the injected signal are not drown in quantization noise.

Frequency component (Hz)	Local SNR(dB)
1024	40.71
2048	30.71
4096	25.56
8192	20.36
16384	13.29
32768	12.9
65536	12.63
131072	10.41

TABLE 5.1: local SNR's for the binary multi-frequency excitation

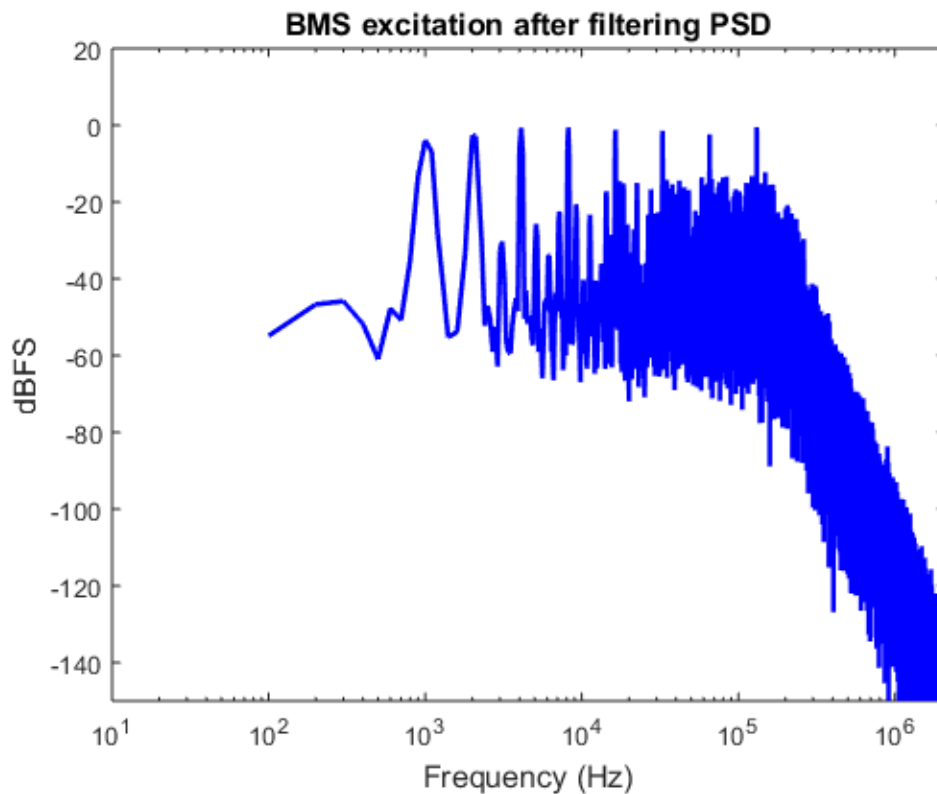


FIGURE 5.21: Frequency components of the BMS excitation technique after filtering

5.3.4 Proposed multitone excitation technique

Operating principle

The sigma-delta modulation is one of the most popular analog to digital conversion techniques. Thanks to its simplicity and its high performances, it is widely used especially in audio and mobile phone applications (Schreier, Pavan, and Temes, 2017).

Several sigma delta modulator topologies exist, this topologies differ depending on the use of analog or digital building blocks, but also on the structure of the modulator itself, whether it is using a feed-forward or feedback loop for instance.

However, since we are doing the binary signal synthesis in pre-processing, the constraints of building a physical design of a sigma delta modulator are out of the scope of this work.

The operating principle of a sigma-delta modulator is based on two main principles (Janssen and Roermund, 2011). It achieves a high SNR with the use of oversampling and noise shaping.

Oversampling consists in taking more samples than the required rate imposed by the Nyquist criterion. By doing this, the quantization noise is expanded over a large frequency range, making its power spectral density decreased, and thus the SNR increased. It can be demonstrated that the quantization noise decreases by 3 dB each time the oversampling rate is doubled. the OSR is defined as:

$$OSR = \frac{F_{sampling}}{2.BW} \quad (5.26)$$

Noise shaping enhances more the SNR. This operation consists in reshaping the frequency distribution of the quantization noise over the Nyquist band. In fact, the spectral density of the quantization noise is reduced in the signal band. As the quantization noise amount remains the same, the spectral density of the quantization noise is increased for the other frequencies of the Nyquist band.

In order to illustrate more in details the operation of a sigma delta modulator, a study will be carried out using the model presented in figure 5.22.

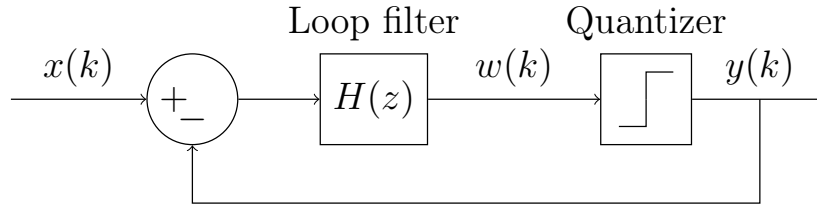


FIGURE 5.22: Functional diagram of a sigma delta modulator

In this model, $x(k)$ represents the oversampled input signal, $d(k)$ the difference between the input signal $x(k)$ and the feedback signal. The difference signal is then fed to the loop filter $H(z)$ and the resulting signal is fed to a quantizer that outputs the signal $y(k)$. The operation of the modulator can be written using the following equations:

$$\begin{aligned} y(k) &= w(k) + e(k) \\ y(k) &= H(z).(x(k) - y(k)) + e(k) \end{aligned} \quad (5.27)$$

$$y(k).(1 + H(z)) = H(z).x(k) + e(k)$$

$$y(k) = \frac{H(z)}{1 + H(z)}x(k) + \frac{1}{1 + H(z)}e(k) \quad (5.28)$$

With $e(k)$ being the quantization error. From the equation 5.28 we can observe that the output signal is composed of two parts: the result of a filtering operation of the input signal $x(k)$ and the result of a filtering operation of the introduced quantization error signal $e(k)$.

When $e(k) = 0$ we can retrieve the Signal Transfer Function (STF):

$$STF(z) = \frac{y(k)}{x(k)} = \frac{H(z)}{1 + H(z)} \quad (5.29)$$

When $x(k) = 0$ we can retrieve the Noise Transfer Function (NTF) :

$$NTF(z) = \frac{y(k)}{e(k)} = \frac{1}{1 + H(z)} \quad (5.30)$$

The objective is to have a high SNR for in-band frequencies and push the quantization noise to high frequencies. To do so, the loop filter $N(z)$ ideally must provide high gain for low frequencies and low gain for high frequencies which is the frequency operation of a low-pass filter.

In fact, with a low pass filter it can be observed that at low frequencies, the STF will tend to unity gain and the NTF to 0. On the other hand at high frequencies the STF will tend to 0 and the NTF to unity gain. which corresponds to the frequency operation that we target.

However several constraints related to the bioimpedance measurement in general and the research context in particular impose the design of a customized filter loop transfer function.

Synthesis of the binary sequence

As depicted previously, the bioimpedance magnitude spectrum is decreasing towards high frequencies (see section 3.6). Therefore, the SNR of the highest frequency components of interest should be high. It is true that the sigma delta modulation decreases the spectral density of quantization noise in the signal band. However, the efficiency of the noise shaping depends heavily on the oversampling ratio. In fact, the higher the OSR, the lower the spectral density of quantization noise inside the signal band.

In our research context, power consumption is a strong constraint, as the integrated measurement system is intended to be used for long measurement campaigns (from 6 months to 1 year), which means that the sampling frequency of the binary register is limited. More specifically, in our application case the OSR is set to 16. Therefore by using a classic loop filter in sigma delta modulation, the quantization noise spectral density increases within the signal band making the local SNR of the highest frequencies lower.

To illustrate this phenomena, we implemented a second order sigma delta modulator using the toolbox developed by Richard Schreier (Schreier, Pavan, and Temes, 2017). Figure 5.23 shows the power spectral density of the frequency components of the output binary signal. Table 5.2 shows the local SNR's of the frequency components of interest.

The simulation results confirm our assumption. We can observe that while the local SNR's of the lowest frequencies of the band are high, the local SNR's of the highest frequencies especially the last three are the lowest, which is not optimal for bioimpedance measurements. This is mainly due to the fact that the OSR is limited, which means that the quantization noise starts rising in the signal band.

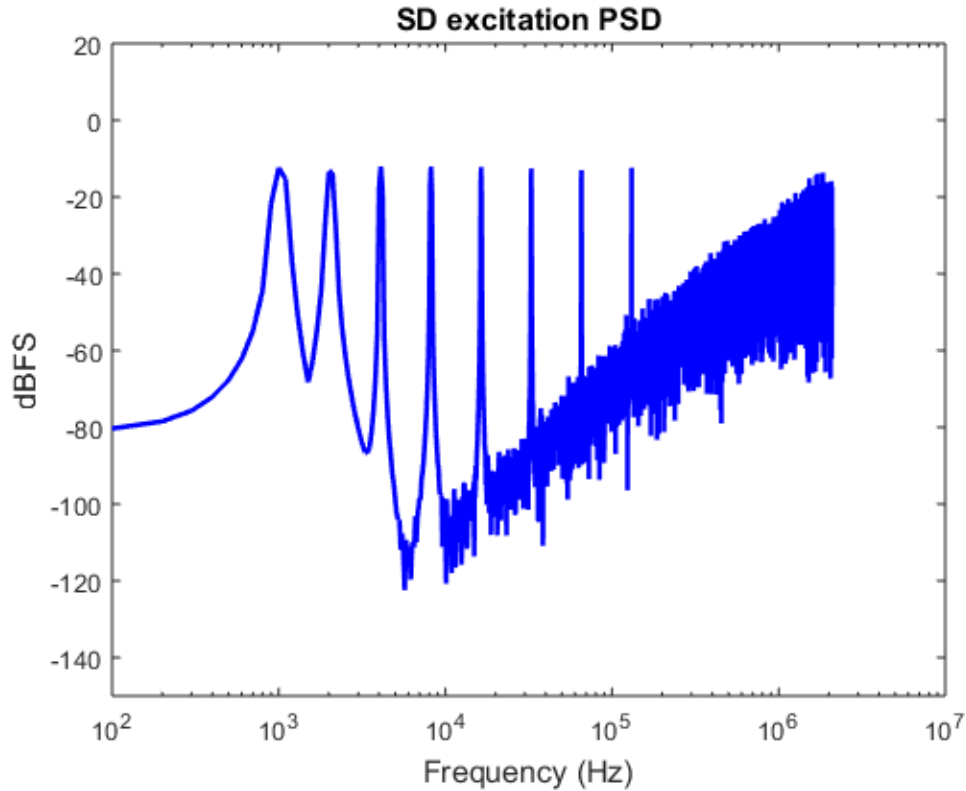


FIGURE 5.23: Frequency components of a classic sigma delta based multitone excitation

Frequency component (Hz)	Local SNR(dB)
1024	82.63
2048	81.64
4096	82.95
8192	82.43
16384	73.61
32768	60.98
65536	48.40
131072	34.20

TABLE 5.2: local SNR's for a classic sigma delta excitation

Therefore, we need to ensure that the noise shaping is optimal. One solution consists in customizing the transfer function of the loop filter $H(z)$.

For a second order sigma delta modulator, the loop filter transfer function can be written in the s domain as follows:

$$H(s) = \frac{K}{1 + \frac{s}{Q\omega_c} + \frac{s^2}{\omega_c^2}} \quad (5.31)$$

With K being the filter gain, Q the quality factor of the filter and ω_c its cut-off frequency. This 2^{nd} low pass filter can exhibit a resonant peak in the vicinity of the cut-off frequency. In fact, the quality factor Q determines the height and

narrowness of the resonance around the cut-off frequency. The higher the value of Q the more high and narrow is the resonance peak.

The proposed approach consists in exploiting this resonance property of the filter in order to enhance the SNR of the highest frequency components of the excitation band.

The filter transfer function at different frequency regions can be written as:

$$\begin{aligned}\omega \ll \omega_c &\longrightarrow H(s) = K \\ \omega = \omega_c &\longrightarrow H(s) = -j.K.Q \\ \omega \gg \omega_c &\longrightarrow H(s) = 0\end{aligned}\tag{5.32}$$

We can observe that in the vicinity of the highest frequency of the band, which is the cut-off frequency of the filter, the filter transfer function is increased by a Q factor. Which means that in the vicinity of the highest frequencies, the signal transfer function gain is increased and the noise transfer function gain decreased.

Implementation results

In order to illustrate the previously detailed frequency operation of the loop filter, we defined the following transfer function:

$$H(s) = \frac{4}{1 + \frac{s}{2.(2.\pi.131 \text{ kHz})} + \frac{s^2}{(2.\pi.131 \text{ kHz})^2}}\tag{5.33}$$

The bode diagram of the filter transfer function is presented in figure 5.24. Figure 5.25 presents the Nyquist diagram of the transfer function.

As calculated previously, we can observe that at low frequencies the gain of the loop filter is $K = 12$ dB raising to $K.Q = 18$ dB towards the upper limit of the bandwidth. The Nyquist diagram shows that the system has two zeros at the origin and complex conjugated poles. As the poles are on the half-side of the Nyquist plan, the sigma delta modulator maintain its stability.

Figure 5.26 presents the bode diagram of the signal transfer function and figure 5.27 presents the bode diagram of the noise transfer function.

The simulation results validate the previously established calculations. We can clearly observe the effects of the peak resonance of the loop filter on the STF and NTF.

For the signal transfer function, at low frequencies the filter gain K helps the STF gain to approach unity, and therefore minimizes the attenuation of the in-band low frequency components. At the vicinity of the cut-off frequency, the gain of the STF is increased, thus bringing more gain to the in-band high frequency components.

For the noise transfer function, at low frequencies the filter gain K decreases the NTF gain and therefore lowers the quantization noise spectral density for the in-band low frequency components. At the vicinity of the cut-off frequency, the introduced resonance helps decrease further the gain of the NTF, thus making the SNR of the in-band high frequency components bigger. Right after the cut-off frequency, the NTF gain increases sharply, redistributing the quantization noise to higher frequencies.

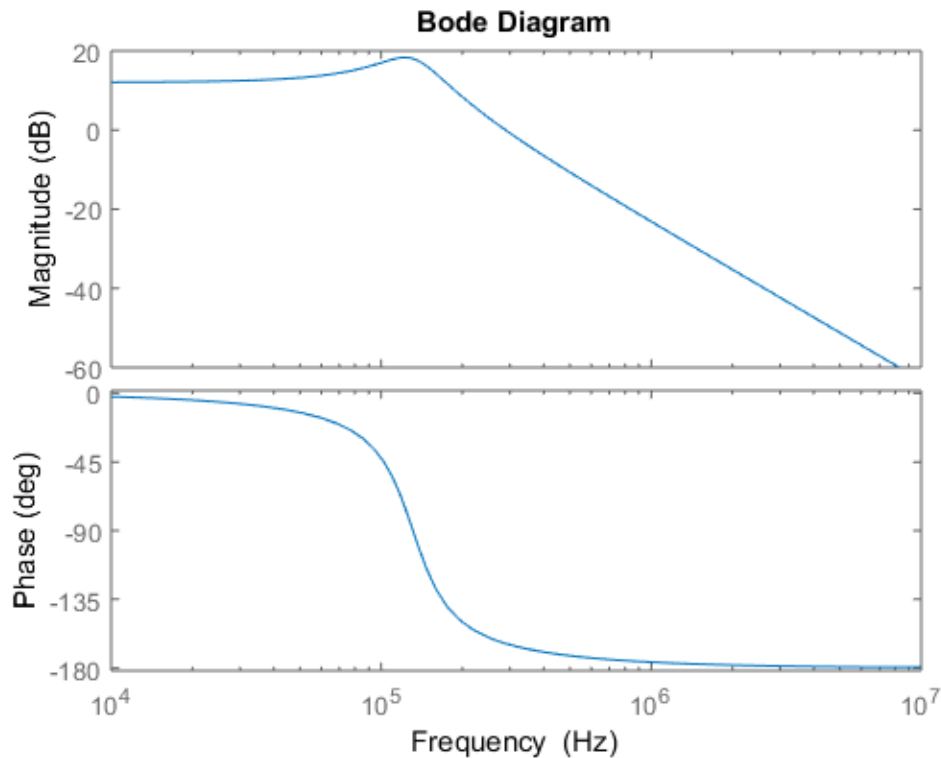


FIGURE 5.24: Customized loop filter bode diagram

Figure 5.28 shows the power spectral density of the proposed excitation frequency components. Figure 5.29 presents the power spectral density of the proposed excitation frequency components after the high frequency quantization noise has been filtered by the multitone architecture filter. Table 5.3 shows the local SNR's of the frequency components of interest.

The simulation results show that with the customized loop filter, we are able to maintain a steady quantization noise floor for the in-band frequency components even though the OSR is limited. Comparing the results to the BMS excitation, the proposed excitation shows better results. In fact, the local SNR's are several times higher than those of the BMS excitation, especially for the highest frequency components where the improvement is up to 42 dB.

Comparing this results to the standard sigma-delta modulation, the local SNR's are better for the higher components of the frequency band of interest (see table 5.3). Obviously, as the quantization noise remains the same, the price to pay is the increasing of the quantization noise spectral density for lower frequencies. However, at low frequencies, the impedance magnitudes are the highest. This means, that rebalancing the quantization noise by lowering the SNR of the low frequency components and increasing it for the high frequency components is an efficient way to improve the overall SNR of the whole impedance spectrum measurement.

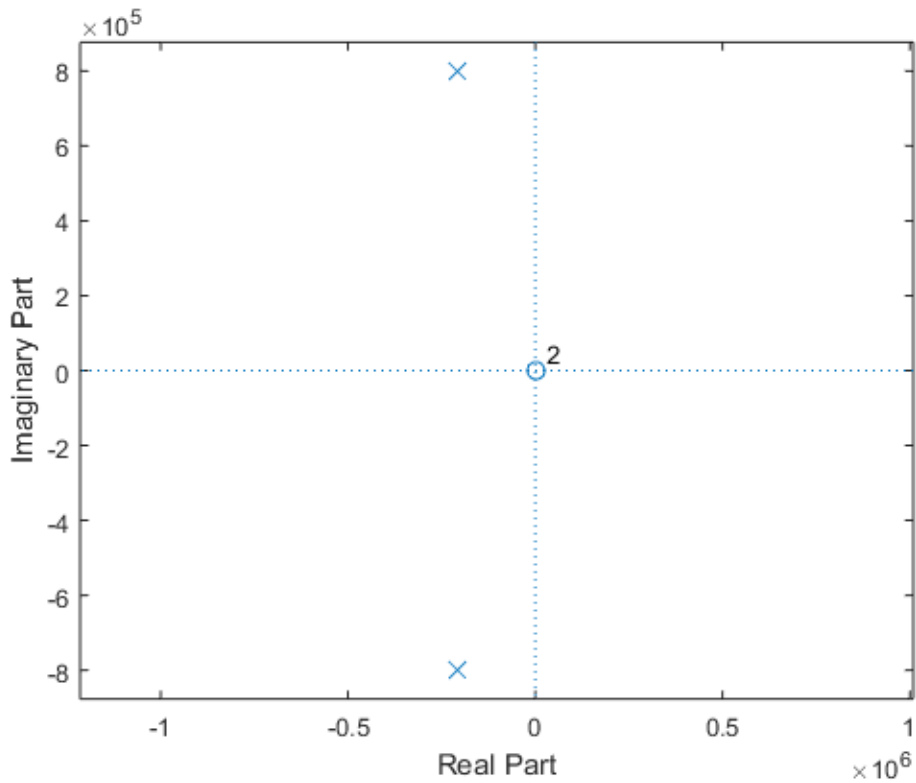


FIGURE 5.25: Nyquist diagram of the customized transfer function

Frequency component (Hz)	Local SNR(dB)
1024	53.03
2048	52.03
4096	48.4
8192	47.46
16384	48.71
32768	47.38
65536	53.04
131072	52.91

TABLE 5.3: local SNR's for the proposed excitation

5.3.5 Conclusion

The main goal of this section was to find the most efficient excitation stimuli for exploratory applications of bioimpedance spectroscopy. After defining the metrics defining the stimuli signal quality, several composite excitation signals have been compared and discussed. Finally, a novel multitone excitation based on sigma-delta modulation and optimized for bioimpedance spectroscopy measurements has been presented and simulated. By reshaping the quantization noise, we have been able to increase the SNR of the high frequency components even though the OSR is limited. The presented results show that the proposed excitation stimulus has a better local SNR's compared to the other excitation

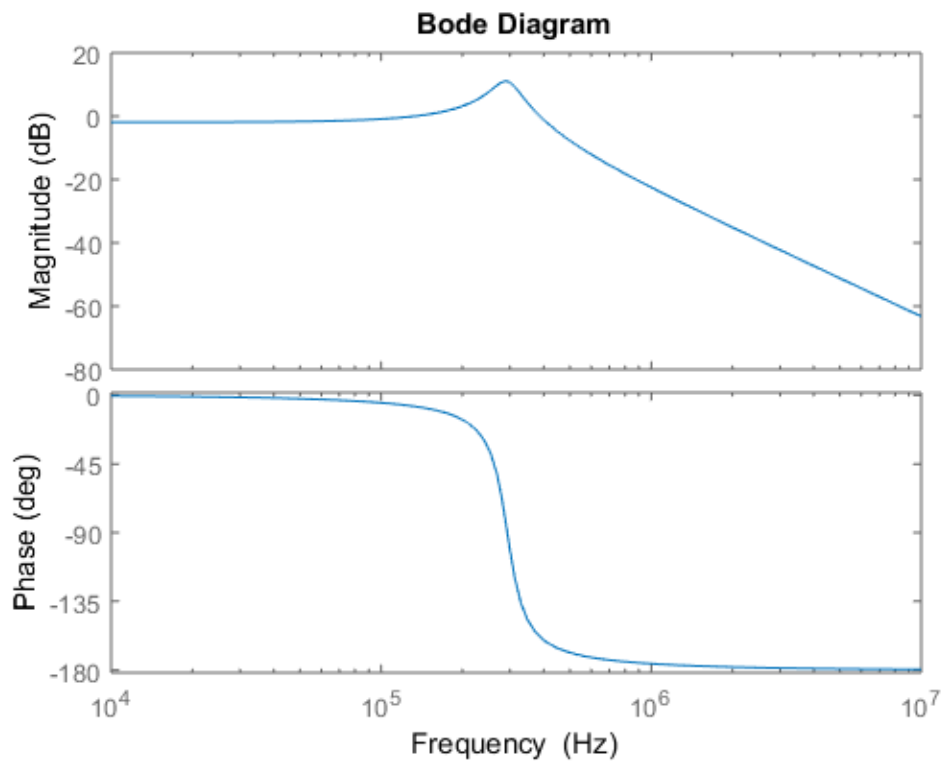


FIGURE 5.26: Signal transfer function of the proposed excitation

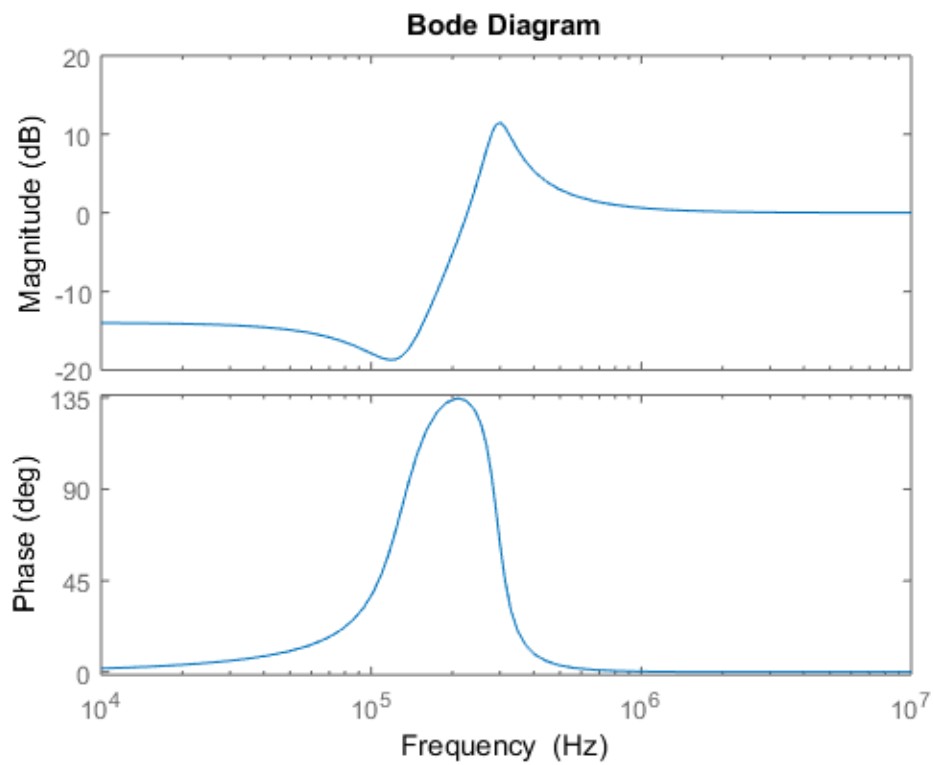


FIGURE 5.27: Noise transfer function of the proposed excitation

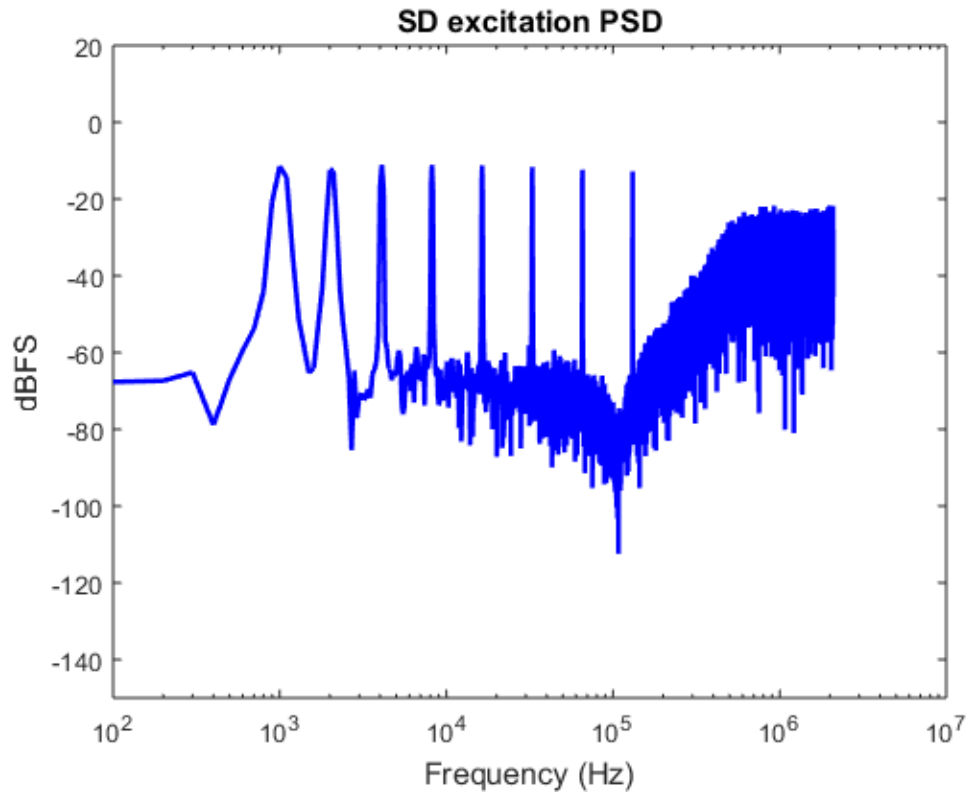


FIGURE 5.28: Frequency components of the proposed excitation

methods, especially for the high frequency components of the frequency band of interest where the improvement is up to 42 dB.

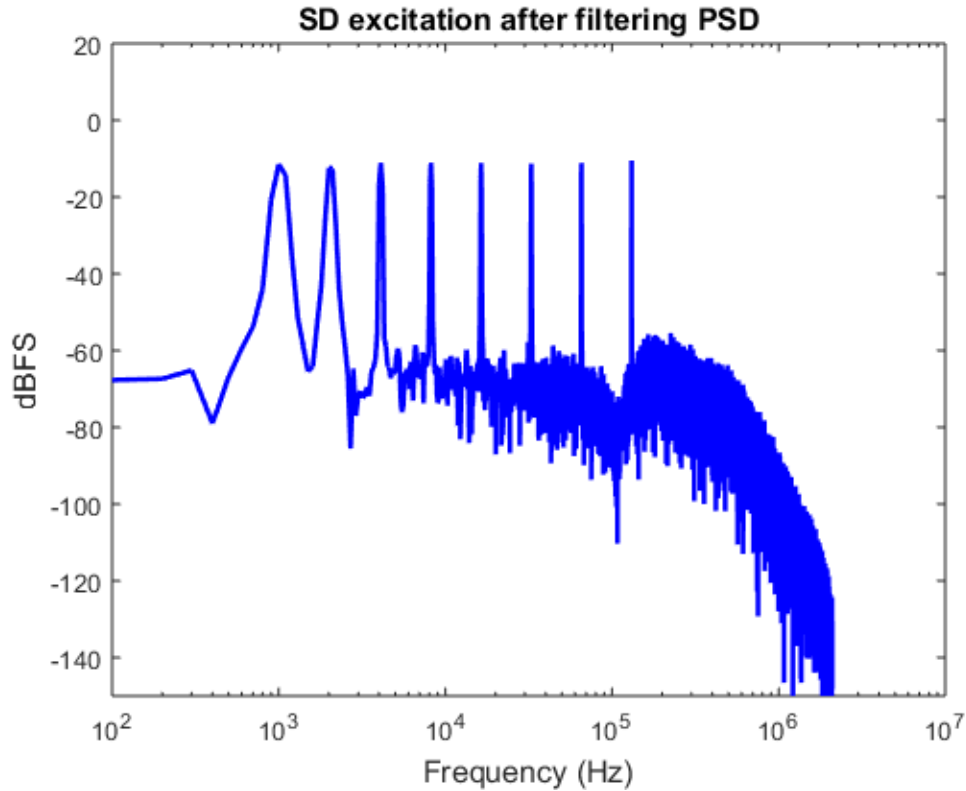


FIGURE 5.29: Frequency components of the proposed excitation after filtering

5.4 Chapter conclusion

This chapter deals with the stimuli generation block of the previously defined integrated circuit architecture. The main objective was the optimization of the stimuli generation for the two excitation scenarios, the frequency sweep and the simultaneous excitations.

In the first part of the chapter, sine-wave construction for the sweep excitation has been discussed. In order to lower the design complexity, we exploited the idea of generating sine wave signals by summing digital signals. By adjusting the parameters of the square-wave signals, the goal was to cancel low-order harmonics and therefore enhance the generated signal quality. To do this, we first compared the two main approaches. Then, we have analytically proven that for a given number of square-wave signals, using uniform phase shifts and adjusting the amplitudes of the square signals allows to cancel a higher number of harmonic while less constraining the design in terms of the generation clock frequency. Concerning the implementation of this approach, we proposed a solution to matching issues using a continued fraction development of ratios.

In the second part of the chapter, composite excitations has been studied. In order to decrease the risk of integrating different sources of errors related to the measurement environment and configuration, we exploited the idea of exciting the biological tissue with simultaneous frequencies, which enables the shortening of measurement durations. To do this, we first defined the signal quality metrics, and based on them we compared the main simultaneous wideband excitation

techniques. We then proposed a multitone excitation based on sigma delta modulation and optimized for exploratory bioimpedance measurements. by reshaping the quantization noise, we have been able to increase the SNR of the high frequency components even though the OSR is limited. The presented results show that the proposed excitation stimulus has a better SNR compared to the other excitation methods, especially for the high frequency components of the frequency band of interest where the improvement is up to 42 dB.

This two signal generation scenarios have a common block, which is the current driver of the architecture. The current driver transforms the voltage stimuli discussed in this chapter to a proportional current signal. The next chapter will present the topology and the design optimization of this block.

Chapter 6

Current driver for BioImpedance Spectroscopy

6.1 Introduction

The main objective of this thesis is to design an integrated bioimpedance measurement system capable of measuring a wide range of biomarkers for long periods of time. In the previous chapters, we presented the design challenges on a system-level and proposed an hybrid architecture suitable for a wide exploration of physiological variables of biological tissue. The second part of this research work focuses on the design and optimization of the stimuli signal generator block of the architecture. As presented before, this block is composed of waveform generators that produce different voltage stimuli depending on the frequency band of operation and a current driver that produces a current signal proportional to the voltage at its inputs.

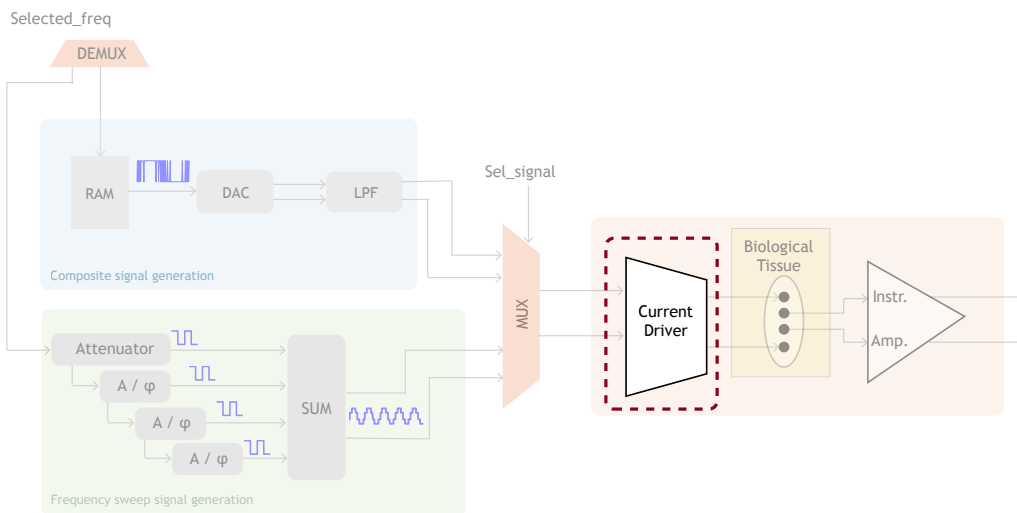


FIGURE 6.1: Current driver position in the integrated circuit architecture

In order to measure bioimpedance it has been decided to use current stimulation. Thus, a current containing a single or multiple frequencies is injected into the tissue via electrodes. The bio-modulated response voltage is then measured to determine the impedance transfer function. The current driver is a

critical block of bioimpedance spectroscopy architectures and its performance will influence the performance of the entire system.

A key parameter of a current source is the output impedance. The output impedance determines not only the frequency range of operation but also the range of load impedance in which the current source is able to maintain the constant output current. Another key parameter is the output voltage swing as it determines the range of load impedance in which the current source is able to maintain its linearity performances. Due to low voltage supply specifications and the need for high output current amplitudes necessary to ease the response analysis, maximizing the voltage swing is more and more critical.

From this perspective, this chapter presents the design and simulation of a current driver architecture providing high output impedance in the α and β frequency ranges. The output voltage swing is maximized, making it suitable for integrated design operating at low supply voltage. After beginning by describing the design constraints of current drivers for bioimpedance spectroscopy in section 6.2, a state of the art of existing current sources is presented in section 6.3. Section 6.4.1 presents the proposed current driver topology as well as the design methodology. Simulation results and comparison with existing architectures are presented in Section 6.5. In order to assess the performance of the current driver, simulation results were compared to load impedances retrieved from experimental measurements on bluefin tuna. Finally Section 6.6 concludes the chapter.

6.2 Design constraints of current drivers for BIS

As previously demonstrated in chapter 2, the complex impedance needs to be analyzed over a large range of frequencies for a rigorous characterization of the biological tissue composition. In fact, each tissue molecule has a different response to a given frequency. The electrical permittivity of biological tissues decreases in three main steps corresponding to three dispersions: the α dispersion (10 Hz to 10 kHz), the β dispersion (10 kHz to 10 MHz) and the γ dispersion (≥ 10 MHz). However, in medical and healthcare applications in general, and in the context of tissue composition assessment in particular, the most interesting dispersions are the α and β dispersions, since they are associated with relevant parameters related to changes in tissue composition, as well as changes between healthy and pathological tissue. The reader may refer to section 2.3.4 in the second chapter which presents the main electrical dispersion regions of biological tissue and their respective contributing elements.

As the current driver is a common block to the frequency sweep and the multi-frequency simultaneous excitation architectures (see Chapter 4). It must therefore operate in the already defined frequency region ranging from 8 Hz to 8 MHz.

This frequency range specification brings essentially two challenges. First, the voltage to current conversion transfer function must have a bandwidth of at least 8 MHz in order to maintain the linearity performance.

Second, the current should have a constant amplitude over this frequency range. This is achieved by having a large output impedance compared to the

load (see figure 6.2) which consists in both the biological tissue and electrode-tissue impedance. However, this is a relevant challenge regarding the size of the targeted operating frequency range and the potential maximum impedance load.

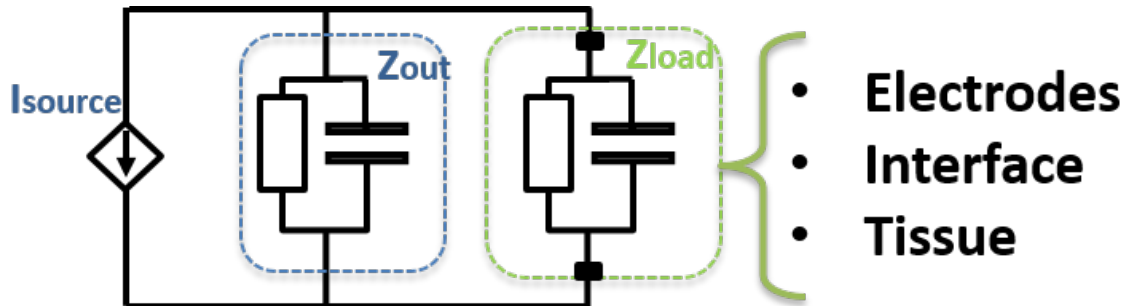


FIGURE 6.2: current source model

In fact, at lower frequencies, the sum of the electrodes-interface and tissue impedances have the highest magnitudes. Therefore, the output impedance of the current driver must be greater by several orders of magnitude at these frequencies. Whereas at higher frequencies, stray capacitance represents the biggest challenge since it shunts the output resistance of the current driver which reduces its value (see figure 6.3).

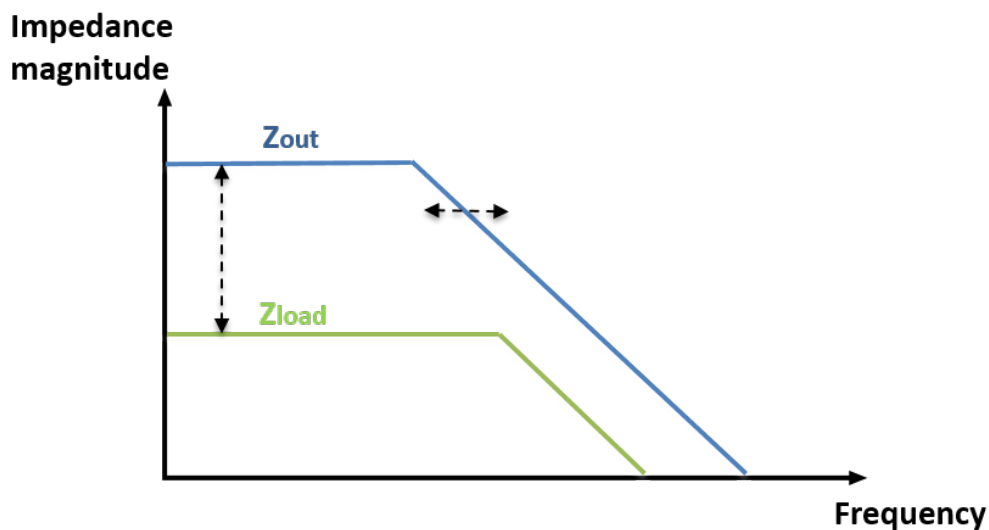


FIGURE 6.3: Output impedance vs load impedance illustration

Another important design constraint of the current drivers for bioimpedance spectroscopy concerns the output voltage swing. In fact, due to low voltage supply specifications and the need for high output current amplitudes necessary to ease the response analysis, the output voltage swing is a critical parameter for the current driver (see figure 6.4). Also, in implanted measurements applications, the electrode-interface impedance may increase due to biological effects such as fibrosis. Thus, care must be taken to ensure a maximal output voltage swing.

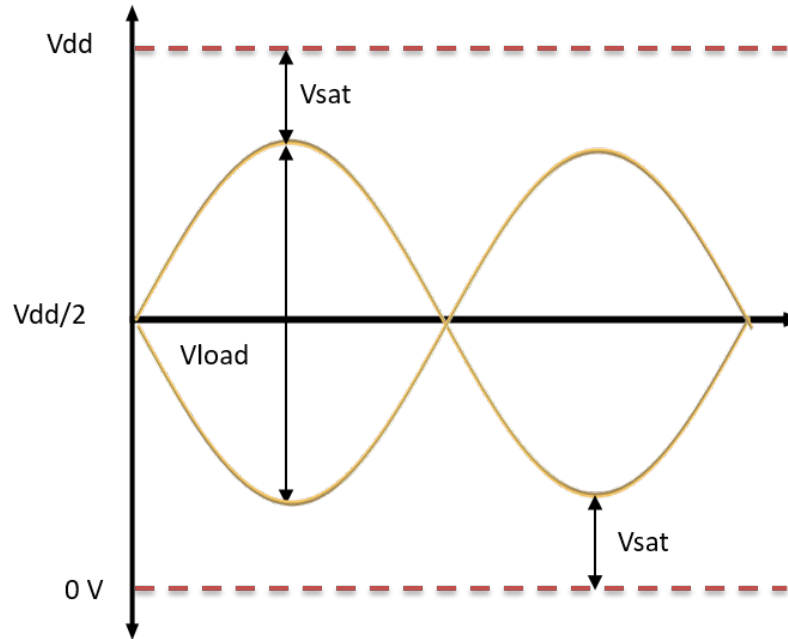


FIGURE 6.4: Saturation voltage illustration

6.3 State of the art of current drivers for BIS

For Bioimpedance measurements, numerous current driver circuits have been presented in the literature (Bertemes-Filho, Brown, and Wilson, 2000; Rafiei-Naeini and McCann, 2008; Hong et al., 2009; Frounchi, Dehkhoda, and Zarifi, 2009; Tucker et al., 2012; Bertemes-Filho et al., 2012; Constantinou et al., 2014; Langlois, Neshatvar, and Demosthenous, 2014). The Howland current driver is the most widely used circuit especially in discrete architectures. The *Howland* current driver is capable of providing high output impedance. However, the output impedance and stability of the *Howland* current source are dependent on the accurate matching of the resistors in the positive and negative feedback Tucker et al., 2012, which makes it more suitable for discrete designs than for integrated ones.

An alternative option is to use Operational Transconductance Amplifier (OTA) based current drivers (Hong et al., 2010; Demosthenous et al., 2011; Demosthenous, Constantinou, and Demosthenous, 2013; Constantinou et al., 2014; Constantinou, Bayford, and Demosthenous, 2015), which are well suited for applications requiring a fully integrated circuit.

The integrated current driver needs to have a large bandwidth to cover at least the first two frequency dispersions. The output impedance should be maximized especially in low frequencies in order to be insensitive to the variation of the relatively high electrode-tissue interface impedances. A current driver architecture providing high output impedance has been introduced in (Hong et al., 2010) and an improved version of this topology has been described in (Constantinou, Bayford, and Demosthenous, 2015). It is able to provide high output impedance using negative feedback that senses and regulates the output current. However, the design is complex and for a current of 200 μA , output impedance is limited to 665 $\text{K}\Omega$ at 100 kHz decreasing to 62 $\text{K}\Omega$ at 1 MHz.

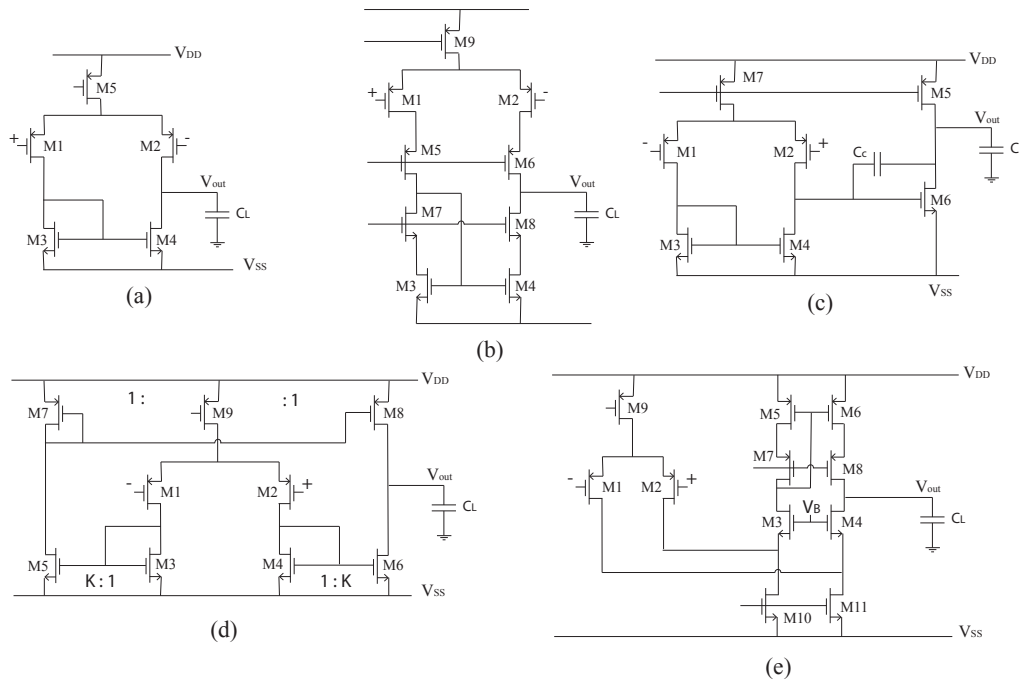


FIGURE 6.5: OTA architectures : (a) Simple OTA (b) Telescopic OTA (c) Miller OTA (d) Symmetrical OTA (e) Folded cascode OTA

Therefore, the following sections will deal with the design and simulation of a current driver based on an OTA architecture. Its output impedance must meet the requirements for a 0.1% accuracy. Its output voltage swing must be maximized making it suitable for integrated designs operating with low supply voltage.

6.4 Optimization of the Current driver's architecture

6.4.1 Proposed architecture

OTA-based current drivers are the most suitable solutions for integrated circuit measurement systems. In order to address the design constraints enumerated previously, a well optimized current driver architecture must be define.

Global architecture choices

Different OTA topologies have been introduced throughout the history of analog integrated circuit development (Sansen, 2006). Nevertheless, OTA's can be categorized into a limited number of important mainly used families. Examples of this categories are the symmetrical and the folded cascode OTA, which are extensively used. The main objective of this section is to review the main categories of OTA's, in order to choose the one with the best performances trade-off for our research context.

The OTA circuit topologies are presented in figure 6.5. The simple OTA is the most basic topology. Its biggest advantage is its ability to operate at high frequencies due to its simplicity. On the other hand, the output impedance of this circuit is limited since the output stage consists of a simple current mirror.

The telescopic OTA adds cascode in series with the input devices, which improves the output impedance while the power consumption remains the same. Its biggest drawback is its output voltage swing which is rather small.

The miller OTA has an enhanced voltage gain, but, obviously, it is out of the scope since its output impedance is the same as that of the simple OTA.

The symmetrical OTA is one of the most used OTA's. Due to its symmetry, matching is improved which provides better performances in terms of offset and Common Mode Rejection Ration(CMRR). The differential pair is loaded with two equal current mirrors which can provide a current gain. Another advantage of this configuration is that the output voltage swing is maximal. The symmetrical OTA has a small output impedance but could easily be improved by using cascodes in the output stage.

The folded cascode consists of a differential pair, two cascodes and a current mirror. It is also a symmetrical configuration, which provides the same advantages as the symmetrical OTA. It has a relatively good output impedance thanks to cascode topology. Its main drawbacks are the output voltage swing, which is smaller than that of the symmetrical OTA and its relatively high power consumption in comparison with other configurations.

OTA architecture	I_{total}	Z_{Out}	Output swing
Single stage	low	small	average
Symmetrical	average	small	maximal
Telescopic	low	high	small
Folded cascode	high	high	average
Miller 2-stage	high	small	maximal

TABLE 6.1: Comparison of amplifier architectures

Table 6.1 presents a comparison of the OTA configurations discussed before. We can observe that folded cascode presents a good compromise. However, the symmetrical OTA is the best configuration as it offers the maximal output swing while having a lower power consumption than the folded cascode. Also, by using cascodes in the output stage, the output impedance is increased. In this context, we chose to use the symmetrical OTA topology for our current driver.

Current drivers for bioimpedance spectroscopy applications can be single-ended or fully-differential. Fully differential current drivers offer several advantages. The first one is their immunity to common mode noise as it is canceled in this configuration. Another significant advantage of these structures is related to the output voltage swing. In fact, fully differential current drivers have twice

the output voltage swing compared with the single-ended one. This is very convenient for systems operating at low supply voltages since it enables to double the range of measurable impedances without introducing harmonic distortions.

Input differential pair

The current across the differential pair branches has been set in order to have a bandwidth of operation covering the α and β frequency dispersions.

One of the main drawbacks of an OTA is its limited linear input voltage range. The linearity of a transconductance amplifier is defined by its ability to maintain a constant slope for the voltage to current transfer function. Due to low supply voltage specifications, and the need for a high transconductance, the voltage input range of an OTA is low. Therefore, we need to increase the input voltage range and to linearize the OTA.

There are three types of linearization techniques for OTA (Sanchez-Sinencio and Silva-Martinez, 2000): attenuation, source degeneration, and canceling non-linear terms. In order to enhance the linearity of the current driver, a degeneration resistance R is added to the M1 differential pair transistors. The resulting transconductance is defined by following the equation:

$$G_m = \frac{G'_m}{1 + G'_m R} \quad (6.1)$$

With G'_m being the DC transconductance of the differential pair without the degeneration resistance.

Note that the transistor transconductance g_m is a function of the drain to source current I_{ds} :

$$g_m = \sqrt{2\mu C_{ox} \frac{W}{L} I_{ds}} \quad (6.2)$$

With μC_{ox} being a parameter of the technology linked to mobility and oxide capacitance. Because g_m is a function of drain current I_{ds} , the voltage gain will vary with current signal swing. When the degeneration resistance is added, we can observe that the voltage across it does not change with the signal swing, the overall voltage gain is then stabilized and is more linear. The bigger the degeneration resistance, the more linear is the transfer function. When $R \gg \frac{1}{G'_m} \rightarrow G_m = \frac{1}{R}$ the degeneration resistance becomes the major contributor to the voltage to current conversion.

By using this configuration, it has been demonstrated that the third harmonic distortion is decreased following the equation (Sanchez-Sinencio and Silva-Martinez, 2000):

$$HD_3 = \left(\frac{1}{1+N}\right)^2 HD'_3 \quad (6.3)$$

Considering $N = G'_m R$, HD'_3 the third harmonic distortion of the differential pair without source degeneration and HD_3 the third harmonic distortion of the degenerated differential pair. The input range is increased by a factor of $(1+N)$.

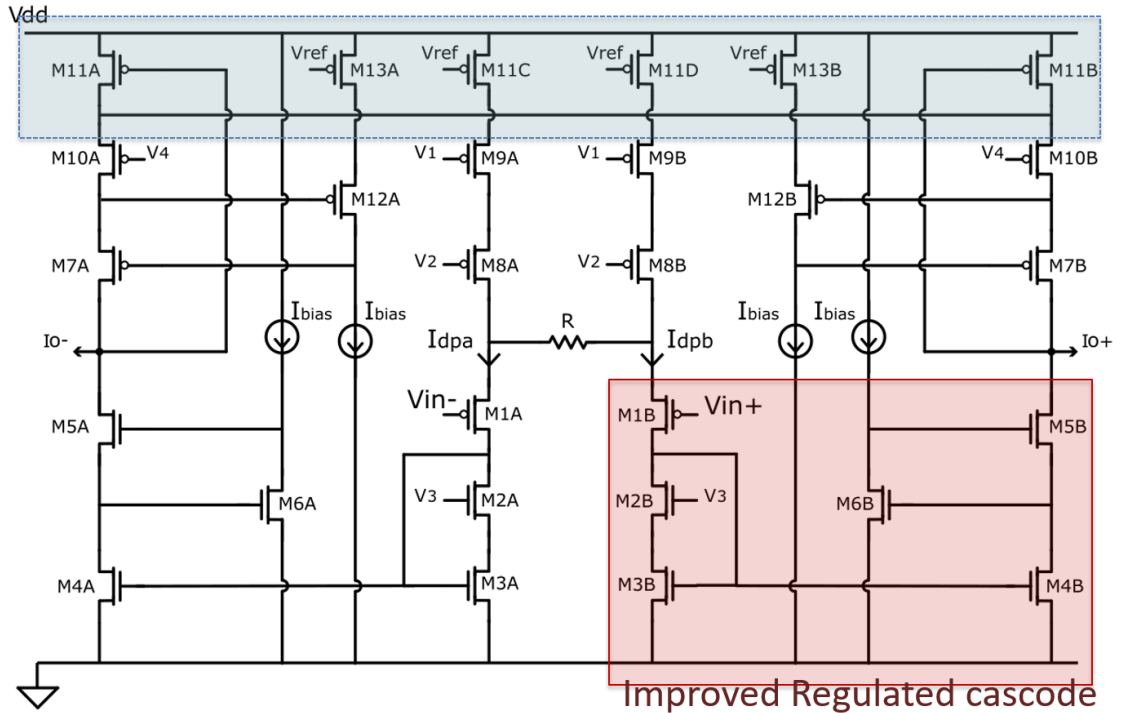


FIGURE 6.6: Current driver architecture

The input transistors are PMOS devices. Using PMOS devices enables to cancel the body effect by connecting the bulk to the source of the transistor. Moreover, a PMOS input pair has better matching performances.

Proposed architecture

Based on the global architectures parameters discussed previously, we defined the architecture of the current driver which is represented in Fig.6.6. It is a symmetrical fully-differential OTA. The first stage of the OTA consists of a degenerated differential pair.

The output stage is a critical part of the current driver structure. It needs to provide a high output impedance while enabling a maximum output swing. The proposed architecture uses an improved regulated cascode current mirror that provides the best compromise between a high output resistance and the lowest output voltage. The output stage design is detailed in section 6.4.2.

Since the OTA is fully-differential, a common-mode feedback (CMFB) loop is implemented to stabilize the common-mode output voltage at half supply (Sansen, 2006). Due to low supply voltage specifications and in order to compensate for process variations, the output DC level is tunable using an independent reference voltage (V_{ref}). The common mode feedback block will be detailed in section 6.4.3.

6.4.2 Output impedance increasing

The output stage of the current driver is critical. It has to provide an output current proportional to the input current at the high impedance output

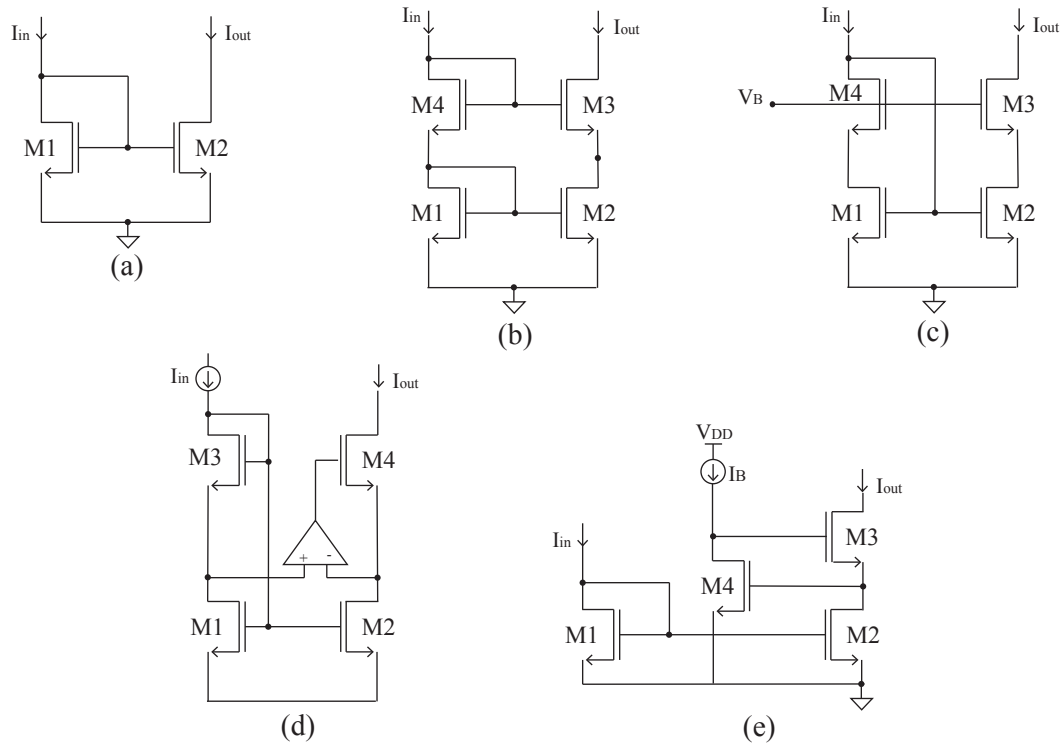


FIGURE 6.7: Current mirror structures: (a) Simple current mirror (b) cascode (c) high swing cascode (d) gain boosted cascode (e) regulated cascode

node. The output current amplitude needs to be constant regardless of loading. Therefore, the important factors defining the performance of the output stage are:

- **Accuracy:** which is achieved by the equality of the drain to source voltages of the current mirror transistors.
- **Output impedance:** a high output impedance will make the output current amplitude constant regardless of loading.
- **Minimum output voltage:** a low minimum output voltage will help maximize the output voltage swing of the current driver.

Figure 6.7 presents the structure of several well adopted current mirrors. Their performances are summarized in table 6.2.

Bandwidth specifications imposed by the application (bioimpedance spectroscopy) require the use of short channel MOSFETs. A size reduction of the transistors leads to a decrease in the output resistance. Simple current mirror blocks or basic cascode structures are unable to provide an acceptable output resistance 6.2, especially at low frequencies where the load (electrode-tissue interface impedance) displays the highest impedance magnitudes.

From that perspective, the boosted gain cascode and the regulated cascode are the best candidates, as they offer the highest output impedances. The biggest drawback of the boosted gain cascode is its complexity, as an op-amp

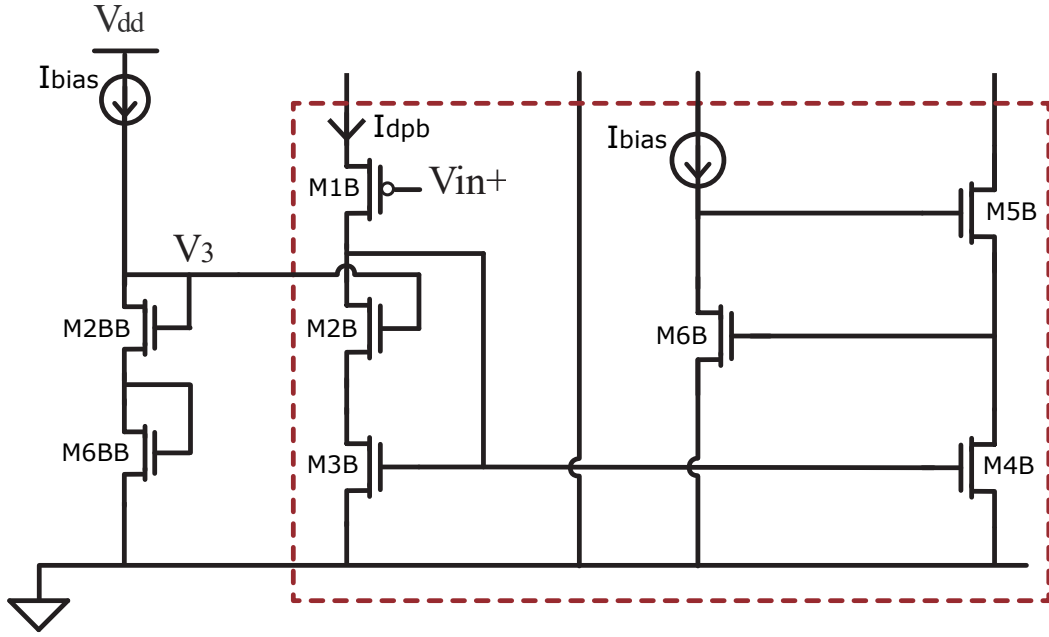


FIGURE 6.8: Improved regulated cascode architecture

needs to be designed. Since we are using a fully-differential architecture, four op-amps must be used, which enlarges the silicon surface of the circuit. On the other hand, the regulated cascode has a high output impedance but its minimum output voltage is high and its mirroring accuracy is low. Therefore, improved output stage structures must be used for higher performances. To do so, we improved the regulated cascode in order to overcome its weaknesses.

CM Structure	Accuracy	Z_{Out}	$V_{out_{min}}$
Simple CM	poor	R_{ds}	V_{eff}
cascode	good	$g_m R_{ds}^2$	$V_{th} + 2V_{eff}$
High swing cascode	good	$g_m R_{ds}^2$	$2V_{eff}$
boosted gain cascode	high	$R_{ds} A g_m R_{ds}$	$V_{cm_{min}}$
Regulated cascode	low	$g_m^2 R_{ds}^3$	$V_{th} + 2V_{eff}$

TABLE 6.2: Current mirror performances comparison

Regulated cascode current mirror have a high output impedance compared to the other structures. It uses negative feedback in order to enhance the output impedance.

The improved regulated cascode shown in Fig.6.8 is the basic block of the output stage. In order to minimize loading effects, the transistor M_{6B} is used to enhance the output impedance by a $g_m * r_o$ factor compared to basic cascode structures. The output impedance of the improved regulated cascode can be written as:

$$R_{out} = r_{oM_4} * r_{oM_6} * g_{mM_6} * r_{oM_5} * g_{mM_5} \quad (6.4)$$

The main drawback of the regulated cascode is the output minimum voltage, which is equal to $V_{th} + 2V_{eff}$. This could be improved to around $2V_{eff}$ by using the M_6 transistors in weak inversion. Although the matching of the M_6 transistors will be affected when operating in weak inversion, the loop gain of the structure is so important that the matching errors are negligible.

In order to enhance the accuracy of the current mirror, the drain to source voltages of M_{3B} and M_{4B} should be equalized. Since the V_{ds} of M_{4B} is imposed by the gate voltage of M_{6B} , the proposed solution consists in using in a mesh an M_{6BB} transistor of similar size as M_{6B} biased with the same current, together with an M_{2BB} transistor of similar V_{gs} as M_{2B} :

$$V_{ds_{M_{4B}}} = V_{gs_{M_{6B}}} \quad (6.5)$$

$$V_{gs_{M_{6B}}} = V_{gs_{M_{6BB}}} \quad (6.6)$$

$$V_{ds_{M_{3B}}} = V_{gs_{M_{2BB}}} - V_{gs_{M_{2B}}} + V_{gs_{M_{6BB}}} \quad (6.7)$$

$$V_{ds_{M_{3B}}} = V_{gs_{M_{6BB}}} = V_{ds_{M_{4B}}} \quad (6.8)$$

6.4.3 Maximization of the output voltage swing

Due to the low voltage supply specifications and the need for high output current amplitudes in order to ease the response analysis, the output voltage swing is a critical parameter of the current driver. Moreover, in implanted measurement applications, the electrode-tissue interface impedance may increase over time due to biological effects such as fibrosis. To avoid saturation errors, the output voltage swing should be maximized.

In order to maximize the output swing voltage, the architecture of the OTA should be carefully chosen. The symmetrical architecture offers the highest output swing voltage compared with the folded cascode or the telescopic topology (Sansen, 2006). OTA-based current drivers could be single-ended or fully-differential. Fully-differential current driver have twice the output voltage swing compared to the single-ended architectures, which has the advantage to allow for doubling the range of impedances that can be measured.

The common-mode feedback is implemented using M_{11} transistors as follows: output voltages are measured by M_{11A} and M_{11B} transistors, then the drains of the M_{11A} and M_{11B} transistors are connected to cancel the differential signal and the loop is closed. The gate voltages of M_{11C} and M_{11D} are controlled by an independent reference voltage. If the gate voltages of M_{11C} and M_{11D} are set to the half supply voltage, by matching $M_{11A} - M_{11B}$ to $M_{11C} - M_{11D}$ the output voltages are set to half supply voltage.

Another solution consists in using M_{11A}/M_{11B} transistors in their triode region without using a reference voltage as in (Constantinou, Bayford, and Demosthenous, 2015). However this solution is subject to process variations. In low supply voltage driven designs, the output common mode voltage should be accurately set to half supply voltage. In order to compensate for process variations, the M_{11C}/M_{11D} gates are driven by an adjustable reference voltage that consists of a multilevel digitally controlled voltage divider.

For an optimal design, the common mode transistors (M_{11}) channel length need to be small enough so their gate to source capacitance C_{gs} does not decrease the output impedance. On the other hand, their $\frac{W}{L}$ ratio need to be sized for a large V_{gs} (half supply) and a small V_{ds} in order to not loose a larger voltage drop. Furthermore, as the CMFB transistors are in their linear region, they will provide a linear cancellation of the differential signal.

6.5 Simulation Results

The current driver was designed in a $0.18\ \mu\text{m}$ AMS CMOS process operating at $1.8\ \text{V}$ power supply. The current driver is capable of providing currents up to $600\ \mu\text{A}$ peak to peak. The circuit design, simulations and layout were developed with Cadence suite using the toolkit provided by the foundry.

Figure 6.9 shows the layout of the circuit, the current driver occupies an area of $0.26\ \text{mm}^2$. In order to have a compact-sized layout, we used as much as possible transistor folding. In order to improve matching of the input differential pair and the different current mirrors of the structure, cross-chip gradients need to be minimized. For this purpose, we set-up pairs or groups of transistors with common-centroid.

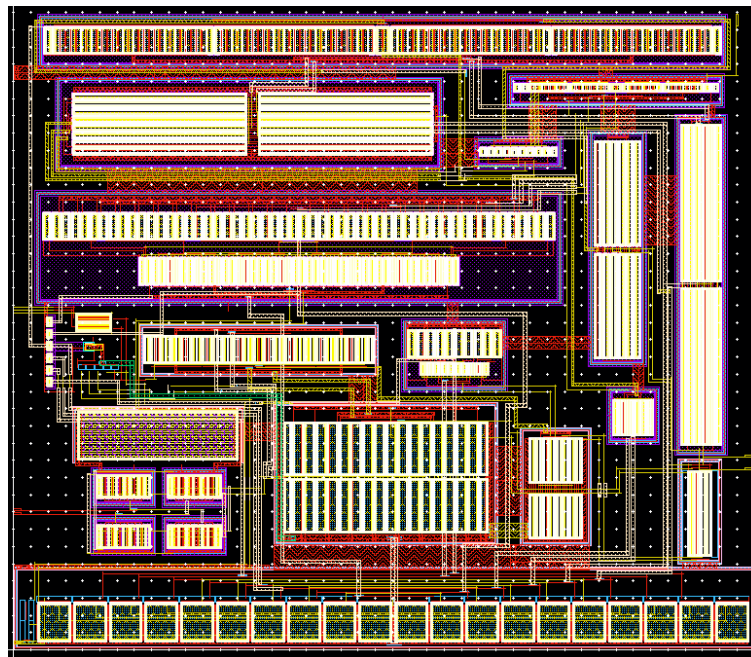


FIGURE 6.9: Layout of the current drive

The frequency response of the current driver transconductance is presented in Fig.6.10. It has a transconductance of $860\ \mu\text{S}$ up to $4\ \text{MHz}$ decreasing to $854\ \mu\text{S}$ at $8\ \text{MHz}$. The cut-off frequency is located at $67\ \text{MHz}$. The current driver was loaded with a $1\ \text{k}\Omega$ resistor with only its intrinsic stray capacitance in order to measure its intrinsic performances in terms of bandwidth.

Total Harmonic Distortion (THD) was computed for a $400\ \mu\text{A}$ peak to peak output current. The simulation results have showed a THD below 0.3% at low frequencies increasing to 0.6% at $8\ \text{MHz}$.

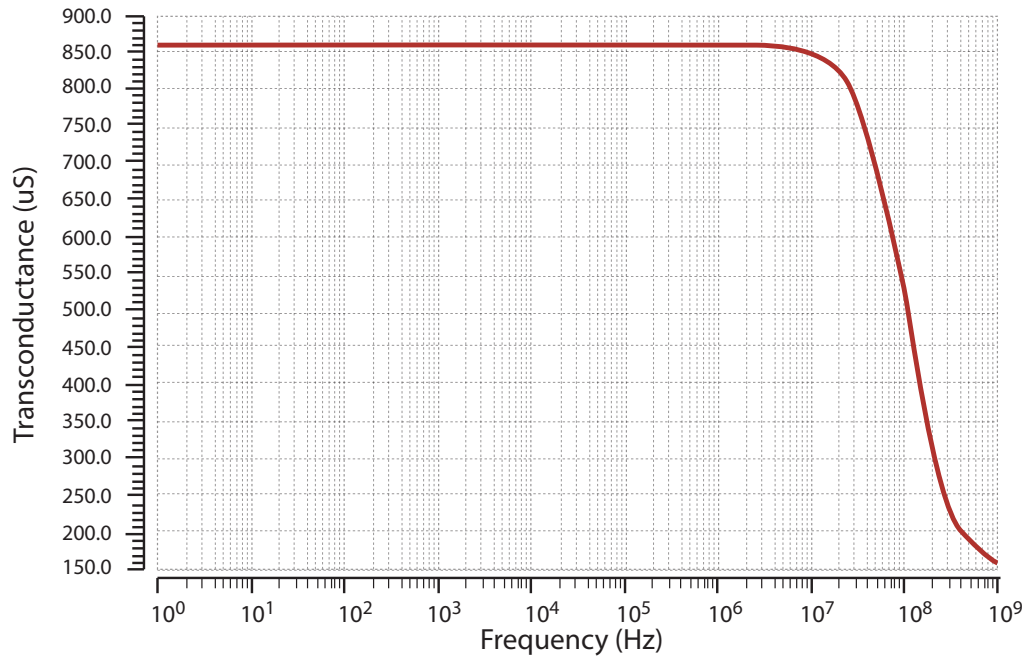


FIGURE 6.10: Current driver bandwidth

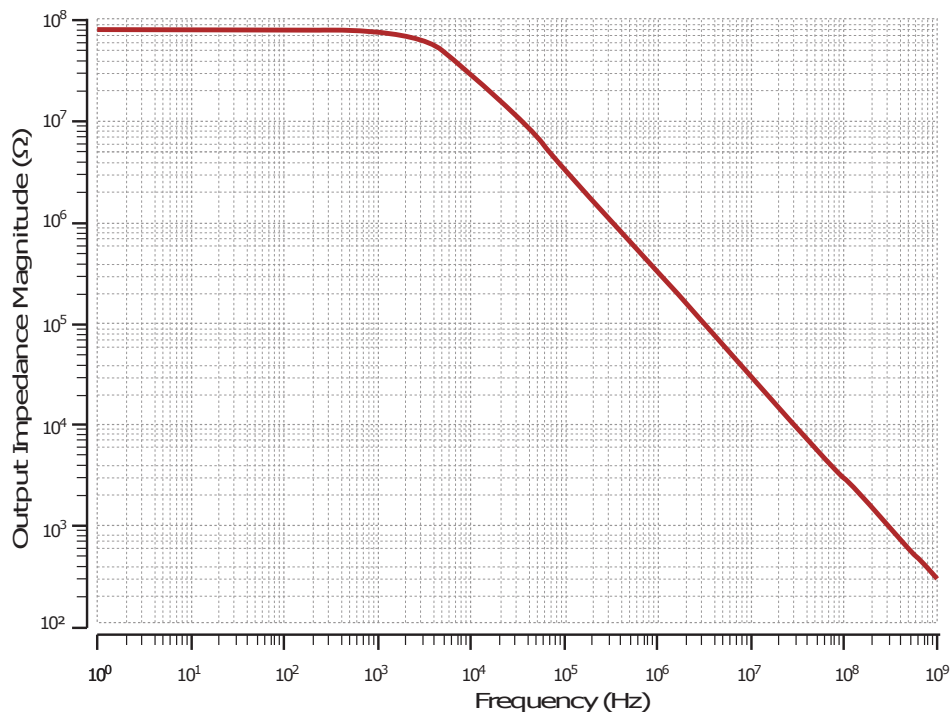


FIGURE 6.11: Output impedance of the current driver

6.5.1 Output impedance

First, the stability of the improved regulated cascode has been checked for the NMOS and PMOS versions. The open loop gain and phase of the NMOS version of the cascode are presented in figure 6.12. We observe that the phase margin is equal to approximately 65 degrees. Therefore, the improved regulated cascode

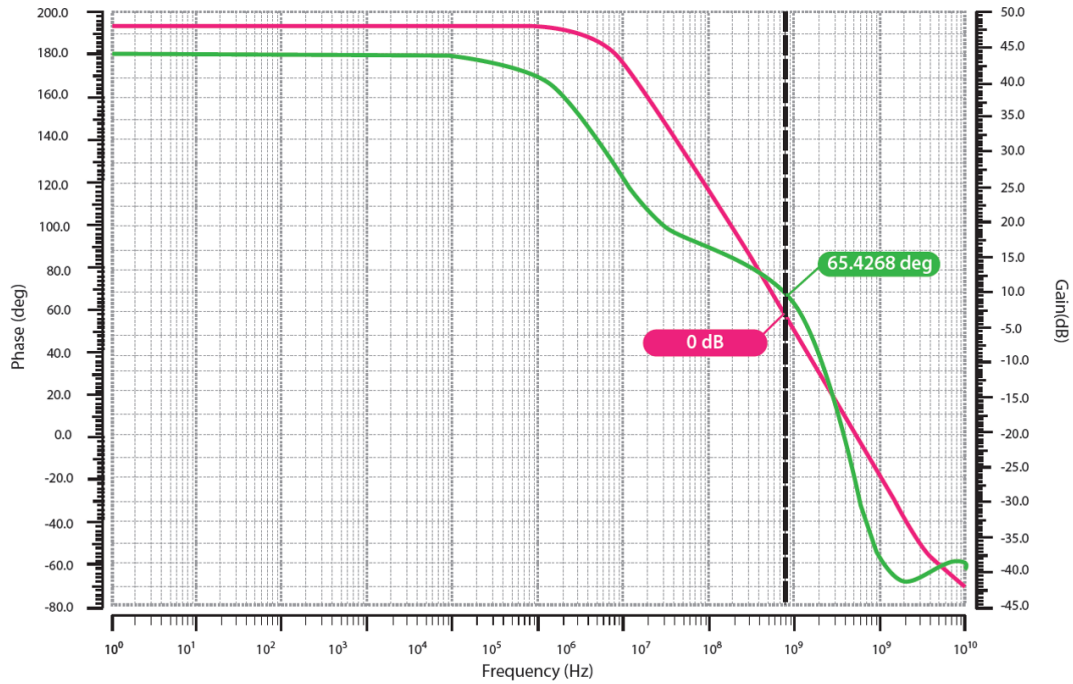


FIGURE 6.12: Improved regulated cascode (NMOS) stability check

is stable.

The frequency response of the output impedance of the current driver is presented in Fig.6.11. The output impedance is equal to $79\text{ M}\Omega$ from DC to 1 kHz. It decreases to $3.6\text{ M}\Omega$ at 100 kHz, and to $324\text{ k}\Omega$ at 1 MHz. The low frequency output impedance magnitudes are suitable for exploring the physiological processes occurring in the α region. At higher frequencies, the output impedance values are several orders of magnitude higher than the electrode-tissue impedance, since it is expected to decrease in the β region.

A research presented in (Rahal et al., 2009) shows a comparison of the impedance magnitudes of several Ag/AgCl commercial electrodes in the frequency range: 10 Hz-1 MHz. The average electrode-tissue impedance magnitudes were higher than $10\text{ k}\Omega$ for frequencies below 10 kHz, equal to $5\text{ k}\Omega$ at 10 kHz and equal to $337\text{ }\Omega$ at 1 MHz. The current driver output impedance results compared to the electrode-tissue magnitudes presented in (Rahal et al., 2009) show that it is capable of providing measurements with an error below 0.02% at 10 kHz and 0.1% at 1 MHz.

The output impedance was also compared with the requirements in our case study. Indeed, measurement were performed on bluefin tuna using the MFIA Analyzer and the flexible electrodes described in section 3.2. The impedance magnitude of the electrode-tissue-interface in 2 electrodes configuration have been measured from 10 Hz to 5 MHz. The results are presented in figure 6.13. The current driver output impedance results compared to the bluefin tuna electrode-tissue magnitudes show that it is capable of providing measurements with an error below 0.02% at low frequencies and approximately 0.6% at 1 MHz.

Obviously, the low frequency measurement errors enumerated previously are not realistic, since they only take into consideration the loading effects.

In reality other sources of errors such as the flicker noise may increase the error percentage. However, the biggest advantage of the proposed architecture is its ability to maintain measurement errors below the 0.1% mark at higher frequencies, where other architectures present measurement errors up to 0.6%.

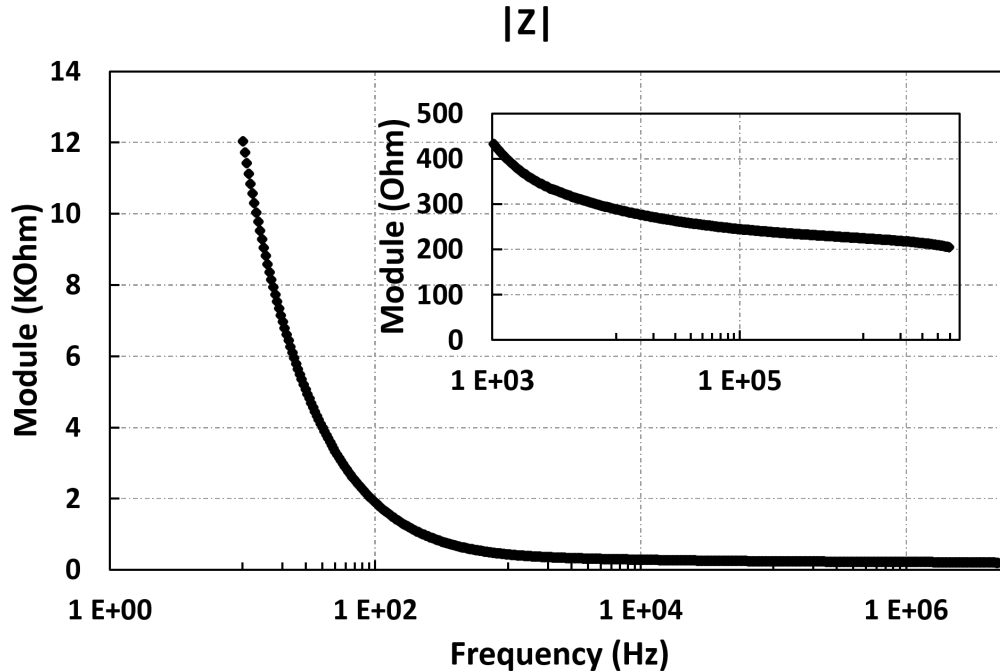


FIGURE 6.13: Impedance magnitude of the electrode-tissue-interface of bluefin tuna in a 2 electrodes configuration

6.5.2 Output voltage swing

Fig.6.14 shows the output current versus the output voltage characteristic of the NMOS improved regulated cascode presented in section 6.4.1 compared with the characteristics of the high swing cascode and the classic regulated cascode. For the high swing cascode, output resistance is low compared to the other structures. While the classic regulated cascode provides high output resistance, the output current is not accurate, and the output minimum voltage is maximal (around 0.55 V). The improved regulated cascode presented in section 6.4.2 provides high output impedance, high accuracy and low minimum output voltage (0.4 V).

The common mode transistors (M_{11}) were designed for a V_{eff} of 50 mV. A Monte-Carlo simulation (process and mismatch) of the DC output level (cf. figure 6.15) showed a mean value of 901 mV with a standard deviation of 9.91 mV.

Therefore, the overall output voltage swing is around 0.95 V from a supply voltage of 1.8 V.

6.5.3 Comparison table with existing architectures

Table 6.3 presents a performance comparison with existing discrete design current driver architectures (Bertemes-Filho, Brown, and Wilson, 2000) (Casas

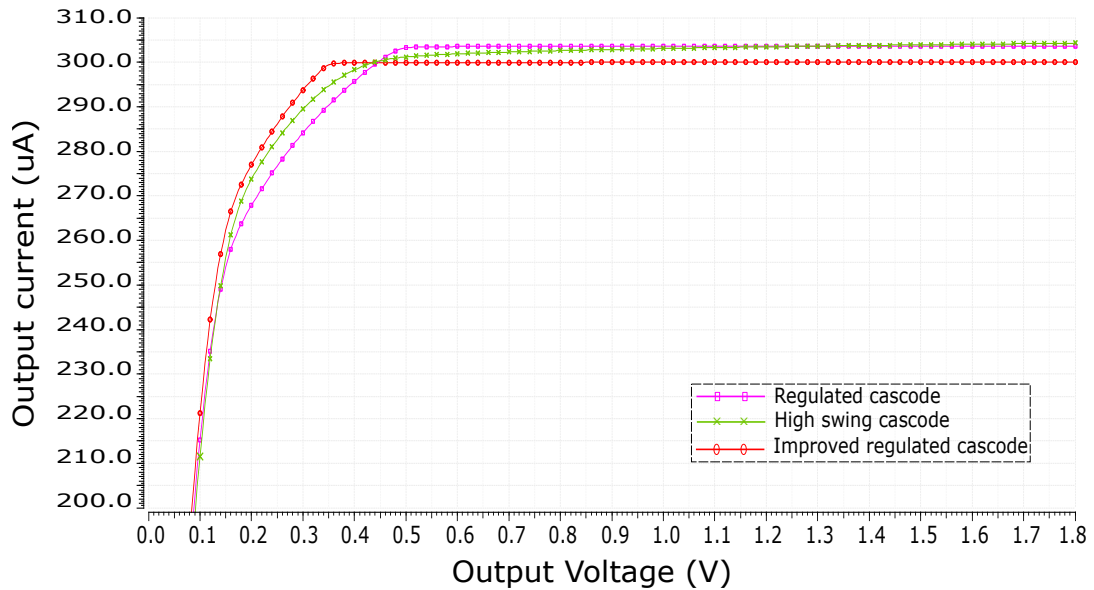


FIGURE 6.14: Output current vs output voltage characteristic of the high swing cascode, the regulated cascode and the improved regulated cascode for an input current of $300\ \mu\text{A}$

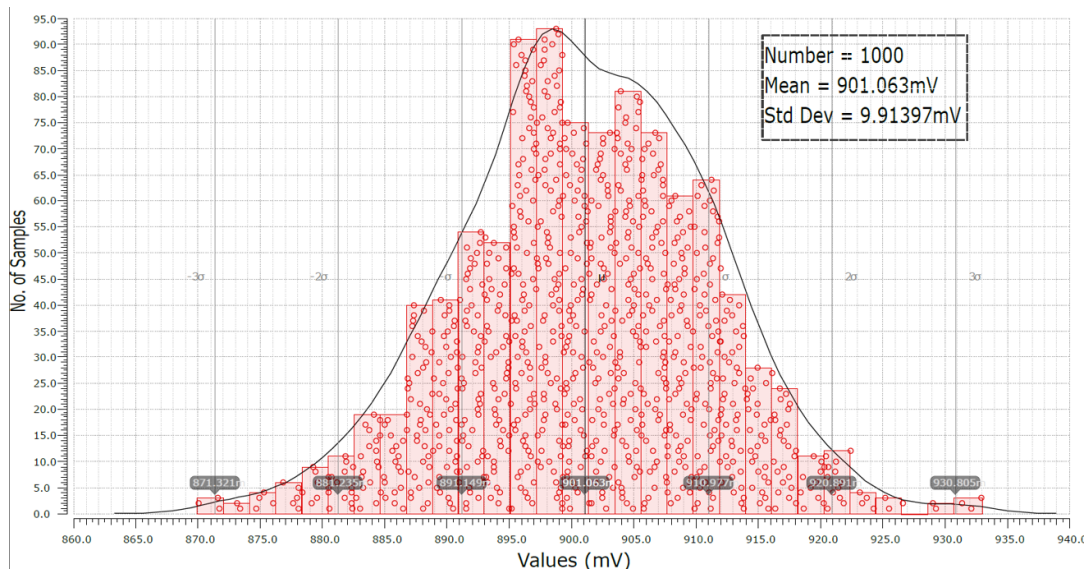


FIGURE 6.15: monte carlo simulation of the DC output level

et al., 1996) as well as integrated current driver architectures (Hong, Lee, and Ha, 2015) (Constantinou, Bayford, and Demosthenous, 2015) for bioimpedance measurement application. However, only simulation results are available for the proposed architecture whereas the cited architectures present measurement results. For a fair comparison with the integrated current driver architectures, the output impedance magnitudes are simulated for a $400\ \mu\text{A}$ peak to peak output current as in (Constantinou, Bayford, and Demosthenous, 2015) and (Hong, Lee, and Ha, 2015). Regarding the constraints induced by the need for bioimpedance measurement over a wide frequency range, the comparison table shows that our proposed architecture provides the highest output impedance magnitudes over the widest frequency range.

Architectures	(Bertemes-Filho, Brown, and Wilson, 2000)	(Casas et al., 1996)	(Hong, Lee, and Ha, 2015)	(Constantinou, Bayford, and Demosthenous, 2015)	Our work
Bandwidth	1KHz - 1MHz	10KHz-250KHz	100Hz-100KHz	>500KHz	10Hz-10MHz
Output impedance	670 k Ω @ 100kHz 330 k Ω @ 300KHz	149 k Ω @ 100KHz 30 k Ω @ 500KHz	100 k Ω @ 100KHz	665 k Ω @ 100kHz 372 k Ω @ 500kHz 64 k Ω @ 1MHz	79 M Ω @ 100Hz 3.24 M Ω @ 100KHz 324 k Ω @ 1MHz
THD	-	0.45% @ 1 mA _{pp}	0.2% @ 200 μ A _{pp}	0.53% @ 2 mA _{pp}	0.3% @ 400 μ A _{pp}
Output swing	-	-	0.4V	15V	0.95V
Supply voltage	-	30V	1.8V	18V	1.8V
Process	Discrete	Discrete	0.18 μ m 1P6M	0.6 μ m X-FAB	0.18 μ m AMS

TABLE 6.3: Results comparison with existing architectures

6.6 Conclusion

A current driver architecture optimized for bioimpedance measurements has been presented in this chapter. It uses an improved regulated cascode to enhance the output impedance, enabling accurate measurements of transfer impedances at low and high frequencies. The current driver uses a common-mode feedback compensation technique capable of accurately setting the output common mode voltage independently of process variations. The proposed architecture offers a high output swing for a given supply voltage. A circuit implementing the design methodology was designed and simulated in a 0.18 μm CMOS AMS process. It occupies an area of 0.26 mm^2 .

Conclusion

The research described in this report is in the research field called biologging. Biologging relies on the use of miniaturized electronic systems, attached on animals to collect, store and transfer data on their environment, which are used to infer information about their biology and ecology. The majority of sensors used provide information about the physical environment of animals (temperature, salinity. . .) or its movement (Global Positioning System, light level geolocation, Inertial Measurement Unit . . .). Despite a large amount of significant contributions, there is a lack of data on the biological or physiological characteristics of the tagged animals. Such information can be related to major processes such as feeding, spawning or migrations, which can have important applied consequences for instance within the context of fisheries stock assessment (e.g. bluefin tuna).

In this context, the present work aimed at designing an integrated measurement system capable of analyzing biological tissue composition. The few physiological sensors used for fish biologging cannot be deployed on large wild animals whose area of distribution encompass the Mediterranean and Atlantic ocean such as bluefin tuna. This is the first time, in the context of biologging, that a sensor is developed for analyzing biological tissue composition jointly with the fish geolocation. In addition the measurement system is also designed for exploratory applications where a wide range of biomarkers could be monitored.

The research presented throughout this thesis is part of the POP-up Satellite Tag for Advancing Research in marine ecology (POPSTAR) project which aims to develop an innovative generation of electronic tags for large pelagics. Beyond tissue composition analysis, the final objective of such a long-term project is to tag a large number of fish to provide inference at the population level about feeding and spawning areas in space and time.

As mentioned earlier, this is the first time that such a sensor is developed for biologging. The lack of a strong body of research warranted to start from the very beginning. As a consequence, **my first contribution was the choice of the sensing technique**. A state-of-the-art of commonly used biological tissue composition analysis techniques has been presented in the first part taking into consideration the integration constraints. As a result of this comparison, the bioimpedance spectroscopy has been chosen. A theoretical background for the concept of bioimpedance spectroscopy analysis has then been presented. From the dielectric properties of a single cell to the methods used for the correlation of biological variables with the bioimpedance measurement parameters. This theoretical study sought to bring a detailed understanding of the key principles of bioimpedance spectroscopy that will be used for the design of the integrated measurement system.

After the selection process of the sensing technique, **my second contribution consisted in identifying the design challenges related to the integration of this technique.** The design challenges have been defined using an in-depth literature review of the existing bioimpedance measurement systems as well as the bioimpedance theoretical concepts. Because design challenges are very application dependent, constraints related to the measurement environment and configuration were also accounted for. Given that in the literature the majority of bioimpedance measurements that were done on fish use single frequency, we have carried out several bioimpedance spectroscopy experiments on fish species such as bluefin tuna, sardine or sea bass in order to assess the missing parameters. Following this methodology, it was possible to identify as precisely as possible the integrated circuit specifications, which laid the foundation for the integrated circuit design guidelines.

Based on the design constraints definition related to the case study, **my third contribution was the definition of the integrated system architecture.** At first, the constraints on the design of the measurement system have been categorized regarding the frequency band of measurement. In order to break the trade-off between short measurement duration and precision, I have decided to use the wideband simultaneous excitation approach for the low and the nominal frequency bands, and the frequency sweep excitation for the high frequency band. A hybrid architecture providing fast measurements while maximizing precision has therefore been proposed. It has been defined for the POPSTAR project as a special research context, and for biological tissue electrical properties exploration over a wide frequency range as a general research context.

As the signal generation blocks are critical and their performances affect the whole architecture performances. **My fourth contribution was the design and optimization of the signal generation part of the architecture which is composed of stimuli generation blocks and a current driver that transforms the voltage stimuli to an excitation current.** For the stimuli generation block of the integrated circuit architecture, the main objective was the optimization of the stimuli generation for the two excitation scenarios, the frequency sweep and the wideband simultaneous excitations. For each excitation type, I have proposed solutions that enhance the generated signal quality while keeping the on-chip generation resources minimal.

In the first part of this study, sine-wave construction for the sweep excitation has been discussed. In order to lower the design complexity, I have exploited the idea of generating sine-wave signals by summing digital signals. By adjusting the parameters of the square-wave signals, the goal was to cancel low-order harmonics and therefore enhance the generated signal quality. To do this, I have first compared the most used approaches in literature. Then, I have analytically proven that for a given number of square-wave signals, using uniform phase shifts and adjusting the amplitudes of the square signals allows to cancel a higher number of harmonics while less constraining the design in terms of the generation clock frequency. Concerning the implementation of this approach, I have proposed a solution to matching issues using a continued fraction development of ratios.

In the second part of this study, simultaneous wideband excitation has been studied. In order to decrease the risk of integrating different sources of errors related to the measurement environment and configuration, I have exploited the idea of exciting the biological tissue with a multi-frequency composite signal, which enables the reduction of measurement durations. To do this, the main simultaneous wideband excitation techniques have been compared. Then I proposed a multitone excitation based on sigma-delta modulation and optimized for exploratory bioimpedance measurements. The proposed excitation can be used on top of a low complexity implementation. The results show that the proposed excitation stimulus has a better Signal-to-Noise Ratio compared to the other excitation methods, especially for the high frequency components of the frequency band of interest.

These two signal generation approaches have a common block, which is the current driver of the architecture. The current driver transforms the optimized voltage stimuli to a proportional current signal. **My fifth contribution is the design of the current driver optimized for bioimpedance measurements.** It uses an improved regulated cascode to enhance the output impedance, enabling accurate measurements of transfer impedances at low and high frequencies. The current driver uses a common-mode feedback compensation technique capable of accurately setting the output common mode voltage independently to process variations. The proposed architecture therefore offers a high output swing for a given supply voltage. A circuit implementing the design methodology was designed and simulated in a 0.18 μm CMOS AMS process. It occupies an area of 0.26 mm^2 .

The first chip prototype implementing the critical blocks of the bioimpedance integrated measurement architecture has been designed and simulated in a 0.18 μm CMOS AMS process. The chip was sent to fabrication and the delivery is expected for the last quarter of 2018. Therefore, we have not been able to validate the first chip prototype during the thesis period.

It goes without saying that the next steps of this work consists in validating the operation of the implemented critical blocks of the architecture. Using a Field-Programmable Gate Array (FPGA) and minimal discrete electronics circuitry, the missing blocks of the architecture could be added, and the first wideband bioimpedance spectroscopy measurements could be performed in-vivo on fish in particular for the POPSTAR project. This would open up new possibilities of extracting new insightful data that couldn't be done using available tools such as the handheld measurement system. In the long run, the ultimate goal is to embed all the different blocks of the defined architecture on a single implantable device composed of the chip and the electrodes.

Bibliography

- 1 MSPS, 12-Bit Impedance Converter, Network Analyzer (2005). AD5933. Rev. F. Analog Devices.
- Aberg, P. et al. (2004). “Skin cancer identification using multifrequency electrical impedance—a potential screening tool”. In: *IEEE Transactions on Biomedical Engineering* 51.12, pp. 2097–2102. ISSN: 0018-9294. DOI: [10.1109/TBME.2004.836523](https://doi.org/10.1109/TBME.2004.836523).
- AFE4300 Low-Cost, Integrated Analog Front-End for Weight-Scale and Body Composition Measurement (2017). AFE4300. Rev. C. Texas Instruments.
- Aluthwala, P. et al. (2014). “A simple digital architecture for a harmonic-cancelling sine-wave synthesizer”. In: *2014 IEEE International Symposium on Circuits and Systems (ISCAS)*, pp. 2113–2116. DOI: [10.1109/ISCAS.2014.6865584](https://doi.org/10.1109/ISCAS.2014.6865584).
- Barragan, Manuel J. et al. (2015). “On-chip sinusoidal signal generation with harmonic cancelation for analog and mixed-signal BIST applications”. In: *Analog Integrated Circuits and Signal Processing* 82.1, pp. 67–79. ISSN: 1573-1979. DOI: [10.1007/s10470-014-0456-0](https://doi.org/10.1007/s10470-014-0456-0). URL: <http://dx.doi.org/10.1007/s10470-014-0456-0>.
- Bertemes-Filho, P, B H Brown, and a J Wilson (2000). “A comparison of modified Howland circuits as current generators with current mirror type circuits.” In: *Physiological measurement* 21.1, pp. 1–6. ISSN: 0967-3334. DOI: [10.1088/0967-3334/21/1/301](https://doi.org/10.1088/0967-3334/21/1/301).
- Bertemes-Filho, Pedro et al. (2012). “Low power current sources for bioimpedance measurements: A comparison between Howland and integrated CMOS OTA circuits”. In: *Journal of Electrical Bioimpedance* 3.1, pp. 66–73. ISSN: 1891-5469. DOI: [10.5617/jeb.380](https://doi.org/10.5617/jeb.380).
- Bozkurt A., Onaral B. (2004). “Safety assessment of near infrared light emitting diodes for diffuse optical measurements”. In: *BioMedical Engineering Online*.
- Breitenstein, Darryl S. and Chris C. Shaw (1998). “Comparison of three tissue composition measurement techniques using digital mammograms — A signal-to-noise study”. In: *Journal of Digital Imaging* 11.3, p. 137. DOI: [10.1007/BF03168737](https://doi.org/10.1007/BF03168737). URL: <https://doi.org/10.1007/BF03168737>.
- Burger, Edward (2000). *Exploring the Number Jungle: A Journey into Diophantine Analysis*.
- Casas, O et al. (1996). “A parallel broadband real-time system for electrical impedance tomography.” In: *Physiological measurement* 17 Suppl 4, A1–A6. ISSN: 0967-3334. DOI: [10.1088/0967-3334/17/4A/002](https://doi.org/10.1088/0967-3334/17/4A/002).
- Chen, T. et al. (2017). “Novel 10-Bit Impedance-to-Digital Converter for Electrochemical Impedance Spectroscopy Measurements”. In: *IEEE Transactions on Biomedical Circuits and Systems* 11.2, pp. 370–379. ISSN: 1932-4545. DOI: [10.1109/TBCAS.2016.2592511](https://doi.org/10.1109/TBCAS.2016.2592511).

- Clerjon, S (2007). “Modelling the Radiation of a Commercial Sensor, the Fish Fat Meter, in a Multilayer Biological Material”. In: *proceedings of the comsol users conference*.
- Constantinou, Loucas, Richard Bayford, and Andreas Demosthenous (2015). “A Wideband Low Distortion CMOS Current Driver for Tissue Impedance Analysis”. In: *IEEE Transactions on Circuits and Systems II: Express Briefs* c, pp. 1–1. ISSN: 1549-7747. DOI: [10.1109/TCSII.2014.2387632](https://doi.org/10.1109/TCSII.2014.2387632).
- Constantinou, Loucas et al. (2014). “High-power CMOS current driver with accurate transconductance for electrical impedance tomography”. In: *IEEE Transactions on Biomedical Circuits and Systems* 8.4, pp. 575–583. ISSN: 19324545. DOI: [10.1109/TBCAS.2013.2285481](https://doi.org/10.1109/TBCAS.2013.2285481).
- Cox, M Keith and Kyle J Hartman (2005). “Nonlethal estimation of proximate composition in fish”. In: *Canadian Journal of Fisheries and Aquatic Sciences* 62.2, pp. 269–275. DOI: [10.1139/f04-180](https://doi.org/10.1139/f04-180).
- Creason, Sam C. and Donald E. Smith (1972). “Fourier transform faradaic admittance measurements II. Ultra-rapid, high precision acquisition of the frequency response profile”. In: *Journal of Electroanalytical Chemistry and Interfacial Electrochemistry* 40.1, A1 –A5. ISSN: 0022-0728. DOI: [https://doi.org/10.1016/S0022-0728\(72\)80146-3](https://doi.org/10.1016/S0022-0728(72)80146-3). URL: <http://www.sciencedirect.com/science/article/pii/S0022072872801463>.
- Dai, T. and A. Adler (2009). “In Vivo Blood Characterization From Bioimpedance Spectroscopy of Blood Pooling”. In: *IEEE Transactions on Instrumentation and Measurement* 58.11, pp. 3831–3838. ISSN: 0018-9456. DOI: [10.1109/TIM.2009.2020836](https://doi.org/10.1109/TIM.2009.2020836).
- Demosthenous, Andreas, Loucas Constantinou, and Andreas Demosthenous (2013). “A Wideband CMOS Current Driver for Bioimpedance Applications With Output DC Regulation A Wideband CMOS Current Driver for Bioimpedance Applications With Output DC Regulation”. In: February 2014. DOI: [10.1109/BioCAS.2013.6679637](https://doi.org/10.1109/BioCAS.2013.6679637).
- Demosthenous, Andreas et al. (2011). “An improved CMOS current driver for electrical impedance tomography An Improved CMOS Current Driver for Electrical Impedance Tomography”. In: February 2014. DOI: [10.1109/ECCTD.2011.6043343](https://doi.org/10.1109/ECCTD.2011.6043343).
- Douirin C., Haffray P. Vallet J.L. Fauconneau B (1998). “Détermination de la teneur en lipides des filets de truite arc-en-ciel *Oncorhynchus mykiss* par le Torry Fish Fat Meter”. In: *Sciences des Aliments* 18, pp. 527–535.
- Duncan, M. et al. (2007). “Bioimpedance assessment of body composition in cobia *Rachycentron canadum* (L. 1766)”. In: *Aquaculture* 271.1, pp. 432 – 438. ISSN: 0044-8486. DOI: <https://doi.org/10.1016/j.aquaculture.2007.06.002>. URL: <http://www.sciencedirect.com/science/article/pii/S0044848607004772>.
- Elsayed, M. M. and E. Sanchez-Sinencio (2010). “A Low THD, Low Power, High Output-Swing Time-Mode-Based Tunable Oscillator Via Digital Harmonic-Cancellation Technique”. In: *IEEE Journal of Solid-State Circuits* 45.5, pp. 1061–1071. ISSN: 0018-9200. DOI: [10.1109/JSSC.2010.2043885](https://doi.org/10.1109/JSSC.2010.2043885).

- Fricke, Hugo (1924). "A Mathematical Treatment of the Electric Conductivity and Capacity of Disperse Systems I. The Electric Conductivity of a Suspension of Homogeneous Spheroids". In: *Phys. Rev.* 24 (5), pp. 575–587. DOI: [10.1103/PhysRev.24.575](https://doi.org/10.1103/PhysRev.24.575). URL: <https://link.aps.org/doi/10.1103/PhysRev.24.575>.
- Fricke, Hugo and Sterne Morse (1925). "THE ELECTRIC RESISTANCE AND CAPACITY OF BLOOD FOR FREQUENCIES BETWEEN 800 AND 4½ MILLION CYCLES". In: *The Journal of General Physiology* 9.2, pp. 153–167. ISSN: 0022-1295. URL: <http://www.ncbi.nlm.nih.gov/pmc/articles/PMC2140800/>.
- Frounchi, Javad, F Dekhoda, and M H Zarifi (2009). "A Low-Distortion Wide-band Integrated Current Source for Tomography Applications". In: *European Journal of Scientific Research* 27.1, pp. 56–65. ISSN: 1450216X.
- Gabrielli, C., F. Huet, and M. Keddam (1992). "Comparison of sine wave and white noise analysis for electrochemical impedance measurements". In: *Journal of Electroanalytical Chemistry* 335.1. An International Journal Devoted to all Aspects of Electrode Kinetics, Interfacial Structure, Properties of Electrolytes, Colloid and Biological Electrochemistry, pp. 33–53. ISSN: 1572-6657. DOI: [https://doi.org/10.1016/0022-0728\(92\)80230-2](https://doi.org/10.1016/0022-0728(92)80230-2). URL: <http://www.sciencedirect.com/science/article/pii/S0022072892802302>.
- Grimnes, Sverre and Orjan G. Martinsen (2014). *Bioimpedance and Bioelectricity Basics*. Academic Press.
- HACHIM, MOUNIBOUDINE (2017). "Evaluation de la bio-impédance en fonction de l'état métabolique des tissus chez la dorade royale, Sparus aurata." MA thesis. 80222 POITIERS: UNIVERSITÉ DE POITIERS : UFR SCIENCES FONDAMENTALES ET 1 APPLIQUÉES.
- Hong, Hongwei et al. (2009). "Comparison of a new integrated current source with the modified Howland circuit for EIT applications". In: *Physiological Measurement* 30.10, pp. 999–1007. ISSN: 0967-3334. DOI: [10.1088/0967-3334/30/10/001](https://doi.org/10.1088/0967-3334/30/10/001). URL: <http://stacks.iop.org/0967-3334/30/i=10/a=001?key=crossref.b41d01341c122436d502c8ddf5df3abf>.
- Hong, Hongwei et al. (2010). "A high output impedance CMOS current driver for bioimpedance measurements". In: *2010 IEEE Biomedical Circuits and Systems Conference, BioCAS 2010*, pp. 230–233. DOI: [10.1109/biocas.2010.5709613](https://doi.org/10.1109/biocas.2010.5709613).
- Hong, Sunjoo, Kwonjoon Lee, and Unsoo Ha (2015). "A 4 . 9 m Ω -Sensitivity Mobile Electrical Impedance Tomography IC for Early Breast-Cancer Detection System". In: *IEEE Journal of Solid-State Circuits* 50.1, pp. 245–257.
- Ichise, Mitsunojo, Yutaka Nagayanagi, and Tsugio Kojima (1974). "Application of pseudo-random signals and cross-correlation techniques in electroanalytical chemistry". In: *Journal of Electroanalytical Chemistry and Interfacial Electrochemistry* 49.2, pp. 187–198. ISSN: 0022-0728. DOI: [https://doi.org/10.1016/S0022-0728\(74\)80226-3](https://doi.org/10.1016/S0022-0728(74)80226-3). URL: <http://www.sciencedirect.com/science/article/pii/S0022072874802263>.
- Jacek Ryl, Lukasz Gawel, Mateusz Cieslik, Husnu Gerengi, Grzegorz Lentka and Pawel Slepiski (2017). "Instantaneous Impedance Analysis of Non-Stationary

- Corrosion Process: a Case Study of Carbon Steel in 1M HCl". In: *International Journal of Electrochemical Science*, pp. 6908–6919. DOI: [10.20964/2017.07.15](https://doi.org/10.20964/2017.07.15). URL: <https://doi.org/10.20964/2017.07.15>.
- Jaffrin, M. Y. et al. (1997). "Extra-and intracellular volume monitoring by impedance during haemodialysis using Cole-Cole extrapolation". In: *Medical and Biological Engineering and Computing* 35.3, pp. 266–270. ISSN: 1741-0444. DOI: [10.1007/BF02530048](https://doi.org/10.1007/BF02530048). URL: <https://doi.org/10.1007/BF02530048>.
- Janssen, Erwin and Arthur van Roermund (2011). "Basics of Sigma-Delta Modulation". In: *Look-Ahead Based Sigma-Delta Modulation*. Dordrecht: Springer Netherlands, pp. 5–28. ISBN: 978-94-007-1387-1. DOI: [10.1007/978-94-007-1387-1_2](https://doi.org/10.1007/978-94-007-1387-1_2). URL: https://doi.org/10.1007/978-94-007-1387-1_2.
- Johansson J Gudtafsson M, Delsing J (2006). "Ultra low-power transmit/receive ASIC for battery operated ultrasound measurement systems". In: *Sensors and Actuators A: Physical* 125, pp. 317–328.
- Kanai, Hiroshi, Katsuyuki Sakamoto, and Makoto Haeno (1983). "Electrical Measurement of Fluid Distribution in Human Legs: Estimation of Extra- and intra-Cellular Fluid Volume". In: *Journal of Microwave Power* 18.3, pp. 233–243. DOI: [10.1080/16070658.1983.11689328](https://doi.org/10.1080/16070658.1983.11689328). URL: <https://doi.org/10.1080/16070658.1983.11689328>.
- Kassanos, P. and I. F. Triantis (2014). "A CMOS multi-sine signal generator for multi-frequency bioimpedance measurements". In: *2014 IEEE International Symposium on Circuits and Systems (ISCAS)*, pp. 249–252. DOI: [10.1109/ISCAS.2014.6865112](https://doi.org/10.1109/ISCAS.2014.6865112).
- Kassanos, P. et al. (2014). "An Integrated Analog Readout for Multi-Frequency Bioimpedance Measurements". In: *IEEE Sensors Journal* 14.8, pp. 2792–2800. ISSN: 1530-437X. DOI: [10.1109/JSEN.2014.2315963](https://doi.org/10.1109/JSEN.2014.2315963).
- Kent, M (1990). "Hand held instrument for fat/water determination in whole fish". In: *Food Control*, 47–53.
- Land, Raul et al. (2011). "Improvements in design of spectra of multisine and binary excitation signals for multi-frequency bioimpedance measurement". In: *Proceedings of the Annual International Conference of the IEEE Engineering in Medicine and Biology Society, EMBS*, pp. 4038–4041. ISSN: 1557170X. DOI: [10.1109/IEMBS.2011.6091003](https://doi.org/10.1109/IEMBS.2011.6091003).
- Langlois, Peter J, Nazanin Neshatvar, and Andreas Demosthenous (2014). "A Sinusoidal Current Driver With an Extended Frequency Range and Multifrequency Operation for Bioimpedance Applications." In: *IEEE Trans. Biomed. Circuits Syst.* 9.3, pp. 1–11. ISSN: 1940-9990. DOI: [10.1109/TBCAS.2014.2332136](https://doi.org/10.1109/TBCAS.2014.2332136).
- Lee, Seon Yeong and Dympna Gallagher (2008). "Assessment methods in human body composition". In: *Current opinion in clinical nutrition and metabolic care* 11.5, pp. 566–572. ISSN: 1363-1950. DOI: [10.1097/MCO.0b013e32830b5f23](https://doi.org/10.1097/MCO.0b013e32830b5f23). URL: <http://www.ncbi.nlm.nih.gov/pmc/articles/PMC2741386/>.
- Lin Ling Li Gang, Wang Yan qiu Xiang Shao xia Katsuyuki Yamamoto (2001). "In Vivo Determination of the Optical Properties of Human Fat and Muscle Tissues". In: *Journal of Optoelectronics. laser* 12.

- Lukaski, H C (1987). “Methods for the assessment of human body composition: traditional and new”. In: *The American Journal of Clinical Nutrition* 46.4, pp. 537–556. DOI: [10.1093/ajcn/46.4.537](https://doi.org/10.1093/ajcn/46.4.537). URL: <http://dx.doi.org/10.1093/ajcn/46.4.537>.
- Malloug, H. et al. (2016). “Mostly-digital design of sinusoidal signal generators for mixed-signal BIST applications using harmonic cancellation”. In: *2016 IEEE 21st International Mixed-Signal Testing Workshop (IMSTW)*, pp. 1–6. DOI: [10.1109/IMS3TW.2016.7524231](https://doi.org/10.1109/IMS3TW.2016.7524231).
- Malloug, H. et al. (2017). “Harmonic cancellation strategies for on-chip sinusoidal signal generation using digital resources”. In: *2017 IEEE 22nd International Mixed-Signal Testing Workshop (IMSTW)*.
- McKenzie, David (2011). “The energetics of Fish Swimming”. In: *Encyclopedia of Fish Physiology*. Elsevier Inc., San Diego: Academic Press/Elsevier, pp. 1075–1080.
- Mehta, Nilesh M et al. (2014). “Comparison of Body Composition Assessment Methods in Pediatric Intestinal Failure”. In: *Journal of pediatric gastroenterology and nutrition* 59.1, pp. 99–105. ISSN: 0277-2116. DOI: [10.1097/MPG.0000000000000364](https://doi.org/10.1097/MPG.0000000000000364). URL: <http://www.ncbi.nlm.nih.gov/pmc/articles/PMC4409423/>.
- MFIA User Manual* (2008). MFIA. Revision 5340. Zurich Instruments.
- Mohamadou, Youssoufa et al. (2012). “Performance evaluation of wideband bioimpedance spectroscopy using constant voltage source and constant current source”. In: *Measurement Science and Technology* 23.10, p. 105703. ISSN: 0957-0233. DOI: [10.1088/0957-0233/23/10/105703](https://doi.org/10.1088/0957-0233/23/10/105703).
- Nelson, M E et al. (1996). “Analysis of body-composition techniques and models for detecting change in soft tissue with strength training”. In: *The American Journal of Clinical Nutrition* 63.5, pp. 678–686. DOI: [10.1093/ajcn/63.5.678](https://doi.org/10.1093/ajcn/63.5.678). eprint: [/oup/backfile/content_public/journal/ajcn/63/5/10.1093_ajcn_63.5.678/3/678.pdf](http://oup/backfile/content_public/journal/ajcn/63/5/10.1093_ajcn_63.5.678/3/678.pdf). URL: <http://dx.doi.org/10.1093/ajcn/63.5.678>.
- Ojarand, J., M. Rist, and M. Min (2016). “Comparison of excitation signals and methods for a wideband bioimpedance measurement”. In: *Conference Record - IEEE Instrumentation and Measurement Technology Conference 2016-July*. ISSN: 10915281. DOI: [10.1109/I2MTC.2016.7520555](https://doi.org/10.1109/I2MTC.2016.7520555).
- Ojarand, Jaan, Raul Land, and Mart Min (2012). “Comparison of spectrally sparse excitation signals for fast bioimpedance spectroscopy: In the context of cytometry”. In: *MeMeA 2012 - 2012 IEEE Symposium on Medical Measurements and Applications, Proceedings*, pp. 214–218. DOI: [10.1109/MeMeA.2012.6226631](https://doi.org/10.1109/MeMeA.2012.6226631).
- Qureshi, T.R., Chris Chatwin, and Wei Wang (2013). “Bio-impedance Excitation System: A Comparison of Voltage Source and Current Source Designs”. In: *APCBEE Procedia* 7. The 3rd International Conference on Biomedical Engineering and Technology - ICBET 2013, pp. 42–47. ISSN: 2212-6708. DOI: <https://doi.org/10.1016/j.apcbee.2013.08.010>. URL: <http://www.sciencedirect.com/science/article/pii/S2212670813001127>.
- Rafiei-Naeini, M and H McCann (2008). “Low-noise current excitation subsystem for medical EIT”. In: *Physiological Measurement* 29.6, S173–S184.

- ISSN: 0967-3334. DOI: [10.1088/0967-3334/29/6/S15](https://doi.org/10.1088/0967-3334/29/6/S15). URL: <http://stacks.iop.org/0967-3334/29/i=6/a=S15?key=crossref.bfae5f2f9b4de61d3073c8ebd>
- Rahal, Mohamad et al. (2009). “A comparison study of electrodes for neonate electrical impedance tomography”. In: *Physiological Measurement* 30.6, S73. URL: <http://stacks.iop.org/0967-3334/30/i=6/a=S05>.
- Rairigh, D. et al. (2009). “Sinusoid signal generator for on-chip impedance spectroscopy”. In: *2009 IEEE International Symposium on Circuits and Systems*, pp. 1961–1964. DOI: [10.1109/ISCAS.2009.5118174](https://doi.org/10.1109/ISCAS.2009.5118174).
- Rodriguez, S. et al. (2016). “A Batteryless Sensor ASIC for Implantable Bio-Impedance Applications”. In: *IEEE Transactions on Biomedical Circuits and Systems* 10.3, pp. 533–544. ISSN: 1932-4545.
- Ropert-Coudert, Yan et al. (2010). “Diving into the world of biologging”. In: *Endangered Species Research* 10, pp. 21–27. DOI: [10.3354/esr00188](https://doi.org/10.3354/esr00188). URL: <https://hal.archives-ouvertes.fr/hal-00379474>.
- S. Cole, Kenneth and Robert H. Cole (1941). “Dispersion and Absorption in Dielectrics I. Alternating Current Characteristics”. In: 9, pp. 341–351.
- Sanchez, B. and R. Bragos (2010). “Multifrequency simultaneous bioimpedance measurements using multitone burst signals for dynamic tissue characterization”. In: *Journal of Physics: Conference Series* 224.1. ISSN: 17426596. DOI: [10.1088/1742-6596/224/1/012004](https://doi.org/10.1088/1742-6596/224/1/012004).
- Sanchez, B et al. (2012). “Basics of broadband impedance spectroscopy measurements using periodic excitations”. In: *Measurement Science and Technology* 23.10, p. 105501. URL: <http://stacks.iop.org/0957-0233/23/i=10/a=105501>.
- Sanchez-Sinencio, E. and J. Silva-Martinez (2000). “CMOS transconductance amplifiers, architectures and active filters: a tutorial”. In: *IEE Proceedings - Circuits, Devices and Systems* 147.1, pp. 3–12. ISSN: 1350-2409. DOI: [10.1049/ip-cds:20000055](https://doi.org/10.1049/ip-cds:20000055).
- Sansen, Willy M. C. (2006). *Analog Design Essentials*. Springer.
- Schreier, Richard, Shanthi Pavan, and Gabor C. Temes (2017). *Understanding Delta-Sigma Data Converters (IEEE Press Series on Microelectronic Systems)*. Wiley-IEEE Press. ISBN: 1119258278. URL: <https://www.amazon.com/Understanding-Delta-Sigma-Converters-Microelectronic-Systems/dp/1119258278?SubscriptionId=AKIAIOBINVZYXZQZ2U3A&tag=chimbori05-20&linkCode=xm2&camp=2025&creative=165953&creativeASIN=1119258278>.
- Schwan, H P. (1957). “Electrical properties of tissue and cell suspensions”. In: *Advances in Biological and Medical Physics* 5, pp. 147–209.
- Schwan, H. P. (1994). “Electrical properties of tissues and cell suspensions: mechanisms and models”. In: *Proceedings of 16th Annual International Conference of the IEEE Engineering in Medicine and Biology Society* 1, A70–A71 vol.1. DOI: [10.1109/IEMBS.1994.412155](https://doi.org/10.1109/IEMBS.1994.412155).
- Shi, C. and E. Sanchez-Sinencio (2015). “150-850 MHz High-Linearity Sine-wave Synthesizer Architecture Based on FIR Filter Approach and SFDR Optimization”. In: *IEEE Transactions on Circuits and Systems I: Regular Papers* 62.9, pp. 2227–2237. ISSN: 1549-8328. DOI: [10.1109/TCSI.2015.2459552](https://doi.org/10.1109/TCSI.2015.2459552).

- Shi, Congyin and Edgar Sanchez-Sinencio (2017). “On-Chip Two-Tone Synthesizer Based on a Mixing-FIR Architecture”. In: *IEEE Journal of Solid-State Circuits*.
- Smith, D., M. Johnson, and T. Nagy (2009). “Precision and accuracy of bioimpedance spectroscopy for determination of in vivo body composition in rats”. In: *International journal of body composition research* 7, pp. 21–26.
- Song, W. et al. (2009). “The System of Portable Fat Detector With Dual-Wavelength Near-Infrared Light”. In: *2009 3rd International Conference on Bioinformatics and Biomedical Engineering*, pp. 1–4. DOI: [10.1109/ICBBE.2009.5163675](https://doi.org/10.1109/ICBBE.2009.5163675).
- Sun, Tao et al. (2007). “High speed multi-frequency impedance analysis of single particles in a microfluidic cytometer using maximum length sequences”. In: *Lab Chip* 7 (8), pp. 1034–1040. DOI: [10.1039/B703546B](https://doi.org/10.1039/B703546B). URL: <http://dx.doi.org/10.1039/B703546B>.
- Tronstad, Christian and Are Pripp (2014). “Statistical methods for bioimpedance analysis”. In: *Journal of Electrical Bioimpedance* 5.1.
- Tucker, Aaron S et al. (2012). “Biocompatible, High Precision, Wideband, Improved Howland Current Source With Lead-Lag Compensation”. In: pp. 1–8.
- Ultrasonic Sensors, NDK Portal Site of. *Basix principle of medical ultrasonic probes*. URL: <http://www.ndk.com/en/sensor/ultrasonic/index.html>.
- Van Ingelgem, Yves et al. (2009). “Advantages of Odd Random Phase Multisine Electrochemical Impedance Measurements”. In: *Electroanalysis* 21.6, pp. 730–739. DOI: [10.1002/elan.200804471](https://doi.org/10.1002/elan.200804471). eprint: <https://onlinelibrary.wiley.com/doi/pdf/10.1002/elan.200804471>. URL: <https://onlinelibrary.wiley.com/doi/abs/10.1002/elan.200804471>.
- Vasan, B. Karthik et al. (2013). “Low-Distortion Sine Wave Generation Using a Novel Harmonic Cancellation Technique”. In: *IEEE Transactions on Circuits and Systems I: Regular Papers* 60.5, pp. 1122–1134. ISSN: 1549-8328. DOI: [10.1109/TCSI.2013.2249178](https://doi.org/10.1109/TCSI.2013.2249178).
- Wagner, Dale R. and Vivian H. Heyward (1999). “Techniques of Body Composition Assessment: A Review of Laboratory and Field Methods”. In: *Research Quarterly for Exercise and Sport* 70.2. PMID: 10380245, pp. 135–149. DOI: [10.1080/02701367.1999.10608031](https://doi.org/10.1080/02701367.1999.10608031).
- Weijun S, Song Z ; Yimn Y ; Lin Y (2009). “The System of Portable Fat Detector With Dual-wavelength Near-infrared Light”. In: *3rd International Conference on Bioinformatics and Biomedical Engineering*.
- Willis, Jay and Alistair J. Hobday (2008). “Application of bioelectrical impedance analysis as a method for estimating composition and metabolic condition of southern bluefin tuna (*Thunnus maccoyii*) during conventional tagging”. In: *Fisheries Research* 93, pp. 64–71. ISSN: 01657836. DOI: [10.1016/j.fishres.2008.02.010](https://doi.org/10.1016/j.fishres.2008.02.010).
- Xu, J. et al. (2015). “A low power configurable bio-impedance spectroscopy (BIS) ASIC with simultaneous ECG and respiration recording functionality”. In: *ESSCIRC Conference 2015 - 41st European Solid-State Circuits Conference (ESSCIRC)*, pp. 396–399. DOI: [10.1109/ESSCIRC.2015.7313911](https://doi.org/10.1109/ESSCIRC.2015.7313911).

- Yamamoto T., Yamamoto Y. (1981). “Non-linear electrical properties of skin in the low frequency range”. In: *Medical and Biological Engineering and Computing* 19 (3), pp. 302–310.
- Yang, C. et al. (2009). “Compact Low-Power Impedance-to-Digital Converter for Sensor Array Microsystems”. In: *IEEE Journal of Solid-State Circuits* 44.10, pp. 2844–2855. ISSN: 0018-9200. DOI: [10.1109/JSSC.2009.2028054](https://doi.org/10.1109/JSSC.2009.2028054).
- Yoo, Pil Joong et al. (2010). “Wideband bio-impedance spectroscopy using voltage source and tetra-polar electrode configuration”. In: *Journal of Physics: Conference Series* 224.1, p. 012160. URL: <http://stacks.iop.org/1742-6596/224/i=1/a=012160>.
- Yufera, A. et al. (2005). “A tissue impedance measurement chip for myocardial ischemia detection”. In: *IEEE Transactions on Circuits and Systems I: Regular Papers* 52.12, pp. 2620–2628. ISSN: 1549-8328. DOI: [10.1109/TCSI.2005.857542](https://doi.org/10.1109/TCSI.2005.857542).

RÉSUMÉ

Les techniques d'évaluation de la composition tissulaire permettent de mieux comprendre les processus physiologiques et leur impact global sur l'état biologique des sujets expérimentaux. Le travail présenté dans ce manuscrit vise à concevoir un système de mesure intégré de spectroscopie de bioimpédance capable de mesurer un large champ de biomarqueurs sur de longues périodes (jusqu'à un an). Le système de mesure présenté peut être utilisé pour des applications de suivi à long terme de variables physiologiques en général. Néanmoins, les solutions présentées visent en particulier le poisson dans le cadre du projet POPSTAR qui vise à améliorer notre compréhension du comportement des poissons en analysant non seulement l'environnement dans lequel les poissons se déplacent et vivent mais aussi les poissons eux-mêmes. Après avoir identifié les défis de conception d'un système de mesure intégré par spectroscopie de bioimpédance, nous avons proposé une nouvelle architecture hybride permettant une spectroscopie rapide tout en maximisant la précision des mesures. Les blocs de génération du signal d'excitation sont critiques car leurs performances affectent l'ensemble des performances de l'architecture. La deuxième partie de cette recherche porte donc sur la conception et l'optimisation de la partie génération de l'architecture. En effet, nous avons amélioré la qualité des signaux de génération de stimuli pour les excitations mono-fréquentielle et multi-fréquentielle tout en proposant pour cela des implémentations sur puce de basse complexité. Dans la dernière partie de notre travail, la source de courant analogique qui transforme les stimuli en un courant d'excitation est discuté. Pour ce bloc, nous avons proposé une nouvelle topologie analogique utilisant une version améliorée du cascode régulé et une compensation de rétroaction du mode commun indépendante des variations du processus. Le premier prototype de puce intégrée embarquant les blocs critiques de l'architecture de mesure de bioimpédance a été conçu et simulé avec un process CMOS 0.18 μm de AMS fonctionnant sous une tension d'alimentation de 1.8 V.

— \diamond —

Tissue composition assessment techniques are used to help better comprehend physiological processes and their overall impact on the biological state of the experiments subjects. The research presented in this manuscript aims to design a bioimpedance spectroscopy integrated measurement system capable of measuring a wide range of biomarkers over long periods of time (up to one year). The presented measurement system can be used for physiological variables long time monitoring applications in general. Nevertheless, the presented solutions target in particular fish species in the context of the POPSTAR project which aims to enhance our understanding of fish behavior by analyzing not only the environment in which fish travel and live but also the fish themselves. After identifying the design challenges of a bioimpedance spectroscopy integrated measurement system, we have proposed a novel hybrid architecture providing fast bioimpedance spectroscopy while maximizing the measurement precision. As the signal generation blocks are critical and their performances affect the whole architecture performances. The second part of this research focuses on the design and optimization of the signal generation part of the architecture. Indeed, we have enhanced the stimuli generation signals quality for single tone and multitone excitations while proposing for this blocks low complexity on-chip implementations. In the last part of our work the current driver that transforms the voltage stimuli into an excitation current is discussed. A novel analog topology using an improved regulated cascode and a common-mode feedback compensation independent of process variations is presented. The first chip prototype implementing the critical blocks of the bioimpedance integrated measurement architecture has been designed and simulated in a 0.18 μm AMS (Austria MicroSystems) CMOS process operating at 1.8 V power supply.

